

# Information technology Applications

# APLIKÁCIE informačných technológií

2013

Information technology Applications / APLIKÁCIE informačných technológií 2-2013

INDUCTOR ENERGY  
VCO 1 0 DC 90  
L 1 2 200MH IC=0  
S 2 0 5 0 SMOD  
D 2 3 DMOD  
R 3 1 20  
VCONTROL 5 0 PULSE(10N 10MS 100MS)  
TRAN 1M 100MS 0 .1M 01C  
www.eurokodex.sk



voltage-controlled switch

control for switch  
ceiling time of 0.1 ms  
gives smooth traces

switch model, on  
resistance set to .001  
switch diode model

FOURIER COMPONENTS OF TRANSIENT RESPONSE I (A)					
NO	(HZ)	COMPONENT	NORMALIZED	PHASE	NORMALIZED
1	5.000E+01	1.213E+01	1.000E+00	4.115E+01	1.000E+00
2	1.000E+02	1.597E-01	1.718E-01	1.245E+02	-8.731E+01
3	1.500E+02	2.541E-01	7.803E-02	2.370E+02	1.645E+02
4	2.000E+02	2.553E-01	1.226E-02	3.390E+02	5.775E+02
5	2.500E+02	1.169E-01	1.146E-03	7.462E+02	1.146E+02
6	3.000E+02	1.097E-01	3.369E-02	6.577E+02	-2.562E+02
7	3.500E+02	4.927E-02	1.513E-02	-1.406E+02	-1.005E+02
8	4.000E+02	1.302E-02	1.014E-02	3.191E+01	8.240E+00
9	4.500E+02	1.292E-02	1.206E-02	-8.990E+01	-4.976E+01
TOTAL HARMONIC DISTORTION = 2.450103E + 01 PERCENT					







Občianske združenie VZDELÁVANIE-VEDA-VÝSKUM

Civil Association EDUCATION-SCIENCE-RESEARCH

Некоммерческая организация ОБРАЗОВАНИЕ-НАУКА-ИССЛЕДОВАНИЕ

Andrusovova 5, 851 01 Bratislava, Slovakia

[www.v-v-v.sk](http://www.v-v-v.sk)



*Published with support from Stephan Verbovec Foundation*

## Information Technology Applications / Scientific Journal – 2/2013

### Design:

EUROKÓDEX s.r.o. ([www.eurokodex.sk](http://www.eurokodex.sk))

### Print: POLYGRAFICKÉ CENTRUM

Polygrafické centrum  
Tomášikova 26  
821 01 Bratislava  
[ba@polygrafcentrum.sk](mailto:ba@polygrafcentrum.sk)  
[www.polygrafcentrum.sk](http://www.polygrafcentrum.sk)

### Address of the Editorial Office:

Civil Association  
Education-Science-Research  
Andrusovova 5  
851 01 Bratislava  
Slovakia  
[vvv.esr@gmail.com](mailto:vvv.esr@gmail.com)

**The journal is published four times a year.**

**The Magazine is Reviewed, volume 2/II.**

### Subscription:

Subscription orders must be sent to the editorial Office.

The price is 20 EUR a year. It is possible to order older issues only until present supplies are exhausted (15 EUR an issue).

**Published by:** Pan-European University, Tomášiková 20, 821 02 Bratislava, Slovakia,  
IČO: 36077429 in collaboration with the Civil Association EDUCATION-SCIENCE-  
RESEARCH Andrusovova 5, 851 01 Bratislava, Slovakia, IČO: 42255180

**Number of copies:** 120 pieces, **ISSN:** 1338-6468 (print version), **EAN** 9771338646000 10

**Registration No.:** EV 4528/12

**Electronic version of Journal:** <http://www.v-v-v.sk>

**Delivered to the press:** October 2013

# Editorial Board List

---

## ► **Predseda redakčnej rady/ Chief editor:**

doc. Ing. Martin Šperka, PhD. .... Faculty of Informatics,  
Faculty of Informatics, Paneuropean University  
in Bratislava

## ► **Redakčná rada / Editorial board:**

prof. Mikhail A. Basarab, DSc., .... Bauman Moscow State Technical University,  
Moscow, Russian Federation

prof. Ing. Ivan Brežina, CSc., .... Faculty of Economic Informatics,  
The University of Economics in Bratislava

Dr. prof. Buchaev Yakhua Gamidovich, .... Dagestan State Institute of National Economy  
(DGINH), Russian Federation

doc. RNDr. Andrej Ferko, PhD., .... Faculty of Mathematics Physics and Informatics,  
Comenius University in Bratislava

doc. Ing. Beáta Gavurová, PhD. MBA, .... Faculty of Economics,  
The Technical University of Košice

Ing. Michal Grell, PhD., .... Civil Association EDUCATION-SCIENCE  
-RESEARCH in Bratislava

doc. Ing. Ladislav Hudec, CSc., .... Faculty of Informatics and Information Technologies,  
Slovak University of Technology in Bratislava

prof. RNDr. Jozef Kelemen, DrSc., .... Faculty of Philosophy and Science,  
Silesian University in Opava

Dr. Ing. Jaroslav Kultán, PhD., .... Faculty of Economic Informatics,  
The University of Economics in Bratislava

prof. V.I. Kolesnikov, .... Russian Academy of Science, Russian Federation

Ing. Eva Mihalíková, PhD., .... Faculty of Public Administration,  
Pavol Jozef Šafárik University in Košice

doc. RNDr. Eugen Ružický, PhD., .... Faculty of Informatics,  
Paneuropean University in Bratislava

doc. RNDr. Frank Schindler, PhD., .... Faculty of Informatics,  
Paneuropean University in Bratislava

doc. Ing. Anna Čepelová, PhD., .... Faculty of Public Administration,  
Pavol Jozef Šafárik University in Košice

prof. Ing. Jiří Voříšek, CSc., .... Faculty of Informatics and Statistics,  
University of Economics in Prague

prof. Vladimir Zuev, .... Institute for Social and Human Knowledge,  
Kazan, Russian Federation

## ► **Výkonný redaktor /Managing editor**

Ing. Ivana Černáková, PhD. .... Civil Association EDUCATION-SCIENCE-  
RESEARCH in Bratislava

# Obsah / Contents

---

## Predslov / Editorial

## Vedecké články / Research papers

- ▶ **Singular Point of Curves – Structure, Visualization and Application in Geometric Modeling.....** 5  
*Martina Bátorová, Pavel Chalmovianský, Barbora Pokorná, Miroslava Valíková*
- ▶ **Modeling Several Fluids with Preserved Volume on An Octree Data Structure.....** 23  
*Roman Ďurikovič*
- ▶ **Validation of the Virtual Gonio-Spectrophotometer Based on the Real Measurements..** 32  
*Andrej Mihálik, Roman Ďurikovič*
- ▶ **Spinklar-3D: Motion Capture, Interaction and Cooperation Between People and Avatars in 3D Augmented Reality and Virtual Reality.....** 46  
*Stanislav Stanek, Andrej Ferko, Zuzana Černeková, Elena Šikudová, Róbert Bohdal, Peter Borovský, Martin Florek, Lukáš Tencer, Ján Žižka, Matej Hudák, Zuzana Haladová, Martin Madaras, Jana Dadová, Palo Fabo, Ivka Varhaníková, Daniela Onačilová, and Tomáš Kovačovský*
- ▶ **Towards the Tabletop Interaction with Fingers and Hand .....** 54  
*Pavol Fabo, Roman Ďurikovič*
- ▶ **Why and How to Search for Best Views .....** 59  
*Ivana Varhaníková*
- ▶ **Selected Methods of Semantics Extraction .....** 67  
*Zuzana Černeková, Zuzana Haladová, Júlia Kučerová, Elena Šikudová*
- ▶ **Use of Cellular Automaton in Crowd Animation.....** 79  
*Jana Dadová, Roman Franta, Petra Gottlieberová, Dominik Kapišinský, Ján Rupalovský*
- ▶ **Muvis: A Public Participatory Urban Planning and Multidimensional Visualization Online System.....** 85  
*Matej Novotný, David Behal, Peter Borovský, Zuzana Černeková, Andrej Ferko, Martin Florek, Ján Lacko, Martin Samuelčík, Stanislav Stanek, and Elena Šikudová*

## Informácie / Information

- ▶ **Instructions for Authors.....** 101



This special ITA journal issue is a selection of papers from visual computing research at Comenius University in Bratislava – top research group in the field of visual computing in Slovakia. This group has a close connection to the Faculty of Informatics at the Paneuropean University (FI PEVŠ) and several professors were and are still involved in the common activities. One of them is organization of the Spring Conference on Computer Graphics (SCCG) conferences, the oldest annual computer graphics event in Central Europe. Approaching the celebration of 30th anniversary soon, in 2014, it was established by an initiative of ITA Editorial board member Eugen Ružický (now dean of FI PEVŠ) and Peter Mederly in mid 80s. Thanks to computer graphics boom in recent decades the group attracted tens of excellent students, among whom are now many internationally recognized scientists and successful software specialists. Three group members succeeded to publish even at ACM SIGGRAPH, the world leading conference in the field: Miloš Šrámek (tutorial on volume rendering), Roman Ďurikovič (mouse embryo visualization), and Ján Žižka (CATRA system for eye disease diagnostics). The most popular initiatives of the group seem to be a Virtual Bratislava, growing in multiple projects, education of hundreds of students a year, international student conference Central European Seminar on Computer Graphics (CESCG), and, recently, a scientific exhibition Virtuálny svet (Virtual World) 2012.

We perceive reality and process information given by both media and our sensory system. Human visual system is not completely understood and the same holds for light distribution in the scene. Both computer vision and graphics research communities manage the problem solutions by employing approximations. However, any approximate solution involves an error. The intermediate goal of visual information processing is to keep the errors bounded. The papers represent recent results in all three phases of computer graphics and vision methodology: geometry processing, rendering, and application specific visual computing. One can see that the unifying idea of all papers can be formulated as discovering the tricky solutions between speeding-up and rendering quality criteria.

In geometry processing, the universal tool for data representation are curves, but there appear complications with their singular points. Selected novel methods how to deal with specific real and complex cases describes the paper SINGULAR POINT OF CURVES - STRUCTURE, VISUALIZATION AND APPLICATION IN GEOMETRIC MODELING, co-authored by Martina Bátorová, Pavel Chalmovianský, Barbora Pokorná, and Miroslava Valíková.

For rendering research, there are two contributions. MODELING SEVERAL FLUIDS WITH PRESERVED VOLUME ON AN OCTREE DATA STRUCTURE, written by Roman Ďurikovič reports on a study of Volume-of-Fluid (VOF). Values of VOF are actually used to tract the fluid surface for visualization purposes and to calculate the surface tension forces acting on the fluid interfaces. This works well for multiple mixed fluids. In the second rendering paper VALIDATION OF THE VIRTUAL GONIO-SPECTROPHOTOMETER BASED ON THE REAL MEASUREMENTS, Andrej Mihalik and Roman Ďurikovič propose and implement a virtual gonio-spectrophotometer, which can be customized to allow measurements obeying industrial standards. The contribution is verified by a set of validation experiments.

The application section is opened by a structured report by Stanislav Stanek et al. surveying a VEGA project named SPINKLAR-3D: Motion Capture, Interaction and Cooperation between People and Avatars in 3D Augmented reality and virtual reality.

The interaction research using near infrared light is presented by Pavel Fabo and Roman Ďuríkovič TOWARDS THE TABLETOP INTERACTION WITH FINGERS AND HAND. A SHORT INTRODUCTION INTO SEARCHING FOR BEST VIEWS for virtual heritage application wrote Ivana Varhaníková to discuss, finally, the importance of this approach to reduce authoring and visiting overload. A similar interest, addressed from the computer vision perspective, introduces a paper MODERN METHODS OF SEMANTICS EXTRACTION by Zuzana Černeková, Zuzana Haladová, Júlia Kučerová, Elena Šikudová. For making virtual space alive the CROWD SIMULATION PROBLEM EXAMPLES are described and evaluated by Jana Dadová, Roman Franta, Petra Gottlieberová, Dominik Kapišinský, and Ján Ruhalovský. Last but not least, Matej Novotný et al. co-authored a paper entitled MUVIS: A PUBLIC PARTICIPATORY URBAN PLANNING AND MULTIDIMENSIONAL VISUALIZATION ONLINE SYSTEM. This is currently a leading application project among Comenius University visual computing research achievements.

Combining geometric modeling, computer graphics, and computer vision methods develop the confluence of these research lines into a fertile research ground for contemporary visual computing

For conclusion, I have to recall the beautiful and clever words from Alexander Pasko, SCCG 2003 chair: "Dear ITA readers, this issue provides selected ideas and results, especially for those who are not only hypnotized by the visual quality of modern computer graphics works in modeling, rendering, and animation. We all know that such a work still requires tedious manual labor hampered by erroneous models and algorithms. Let us hope that the next spiral of development will make our work in computer graphics more close to a joyful mind game."

October 2013

---

**Martin Šperka**  
ITA Editor-in-chief





# Singular point of curves – structure, visualization and application in geometric modeling

Martina Bátorová, Pavel Chalmovianský,  
Barbora Pokorná, Miroslava Valíková

## Abstract:

During the computations of non-linear problems such as optimization, classification of varieties in algebraic geometry, analysis of complex functions, an occurrence of singular points in the area of interest plays a significant role. Singularities often appear during a qualitative change of the computed object. We consider them in case of real and complex curves as well as complex functions. We provide visualization of certain invariants arising during their description as well as elementary methods and tools used during their analysis. The covered areas form a necessary theoretical background of many application areas such as robotics, geometric modeling, computational geometry, numerical mathematics, approximation theory.

## Keywords:

isolated singularity, resolution, cable knots, Riemann surface, visualization of complex function, Minkowski space-like curves.

## ACM classification:

**G.1.2** [Numerical Analysis]: Approximation – Approximation of Surfaces and Contours; **G.1.5** [Numerical Analysis]: Roots of Nonlinear Equations; **I.3.5** [Computer Graphics]: Computational Geometry and Object Modeling – Curve, Surface, Solid and Object Representations; **J.6** [Computer-aided engineering]: Computer-aided design (CAD).

## 1. Introduction

The idea of *regularity* is spread throughout the whole mathematics and it is a key component of many so called generic algorithms. Such algorithms work if the data are “nice” and may not work in other cases. The situation, when the data, functions or some observed aspects are not stable under arbitrary small changes of the parameters, is called *singular* or *unstable*. We consider this idea in several applications and use the visualization techniques to introduce the results to non-experts as well. The topics include singularities of complex plane algebraic curves, singularities on complex valued functions and singularities gained via intersection of real curves in Minkowski space. Due to the vast amount of results in these areas, the written examples give only a flavor of the whole field of singularities.

Intuitively, the real singularities occur on a curve, when the curve cannot be locally

approximated well by a unique tangent line. This (often) inaccurate approach has been developed into a set of theoretical tools and extended to areas where the real numbers were changed with complex numbers or even a more exotic ring, and nowadays it is used to reach far deeper than the original methods were proposed to.

The first ideas and achievements in the area of plane algebraic curves and their singularities date back to ancient Greece. However, the true beginnings of their systematic study are attributed to Newton. It was not until the centuries after his lifetime, especially the 19th one, that the rigorous methods for the investigation of singularities of algebraic curves were developed.

Today, the area of singularities of algebraic curves is a meeting point of many mathematical disciplines, both theoretical and applied. The interactions and ideas of algebraic geometry, topology, robotics, approximation theory or scientific visualizations – to mention just a few – make the subject of the singularities of plane algebraic curves a very fruitful and exciting field of study.

Singular points introduce complications not only in theory, e.g. when computing an image of a curve in a suitable map, but also in practice e.g. in numerical and scientific computations, "division by zero" etc. We wish to eliminate, to *resolve* them, which means to pass by a suitable simplification process from a singular curve to such a curve that no longer has singularities and which is still in a close connection with the original curve.

The complex analysis is well established in many branches of mathematics, like number theory or applied mathematics as well as in physics, including thermodynamics, hydrodynamics and electrical engineering.

The understanding of the function properties might be difficult, because we need 4D Euclidean space to graph a complex function of a complex variable. Several methods to overcome the need of more dimensions were developed to ease the access of the human imagination to the true image of such a function. One of them is the domain colouring method, which describes one dimension using a spectrum of colours. We used this approach in our visualization of the complex function and extended it to the 3D space. When possible, we visualized the whole domain of the function.

Cable knots are special invariants of the isolated singularities of complex curves. We briefly sketch their construction. The detailed description is far longer than this paper can comprise.

In the last topic, we show how the singularities determine the global quality of a curve in Minkowski space. In [4, 14, 5] the conditions for the control points of a quadratic and cubic planar space-like Bézier curves are looked for. We sketch the fundamental idea how to find the conditions on one specific example.

## 2. Plane algebraic curves and their singularities

Let  $\mathbb{A}^2(\mathbb{C})$  be an affine plane over the field of complex numbers  $\mathbb{C}$  and let  $f \in \mathbb{C}[x, y]$ ,  $\deg f > 0$  be a non-constant square-free polynomial in indeterminates  $x, y$ . An *affine plane algebraic curve* is the set  $\mathcal{C} := \mathcal{V}(f) := \{(p_1, p_2) \in \mathbb{A}^2(\mathbb{C}) \mid f(p_1, p_2) = 0\}$ . The polynomial  $f \in \mathbb{C}[x, y]$  is called the *defining polynomial* of the curve  $\mathcal{C}$ . We define the *degree of the curve*  $\mathcal{C}$  to be the degree of its defining polynomial  $f$ , i.e.  $\deg \mathcal{C} := \deg f$ . Intuitively, we speak about the zeros or solutions of the equation  $f = 0$ .

The affine plane algebraic curve  $\mathcal{V}(f)$  is said to be *irreducible* iff  $f$  is irreducible, otherwise it is called *reducible*. Any reducible curve can be uniquely decomposed into a set of irreducible curves. Such a maximum irreducible algebraic subset of the curve is called an (*irreducible*) *component* of the curve.

The affine plane algebraic curve  $\mathcal{C} \subset \mathbb{A}^2(\mathbb{C})$  consists of two types of points. The point  $P \in \mathcal{C}$  is called a *singular point* of  $\mathcal{C}$ , if both partial derivatives  $\frac{\partial f}{\partial x}, \frac{\partial f}{\partial y}$  vanish at  $P = (p_1, p_2)$ . A point which is not singular is called *regular*. We say that the curve  $\mathcal{C}$  is *regular* if all its points



are regular, otherwise it is called *singular*.

We consider the point  $P = (0, 0)$ . Let  $f = \sum_{i=1}^d a_i f_i$ , where homogeneous  $f_i$  have  $\deg f_i = i$  and  $a_i \in \mathbb{C}$  for all  $i = 1, \dots, d$ . The set of tangents at singular point  $P \in \mathcal{V}(f)$ , the *tangent cone*, is given by the (linear) factorization of  $f_i(x, y)$  with  $a_i \neq 0$  and  $i$  being minimal possible. If the tangents of  $P$  are all distinct with multiplicity 1, the singularity is called *ordinary*, otherwise *non-ordinary*. Also,  $P$  is called an  $i$ -fold point - in particular, for  $i = 2$  a *double point*, for  $i = 3$  a *triple point* of given curve  $\mathcal{V}(f)$  (see fig. 1).

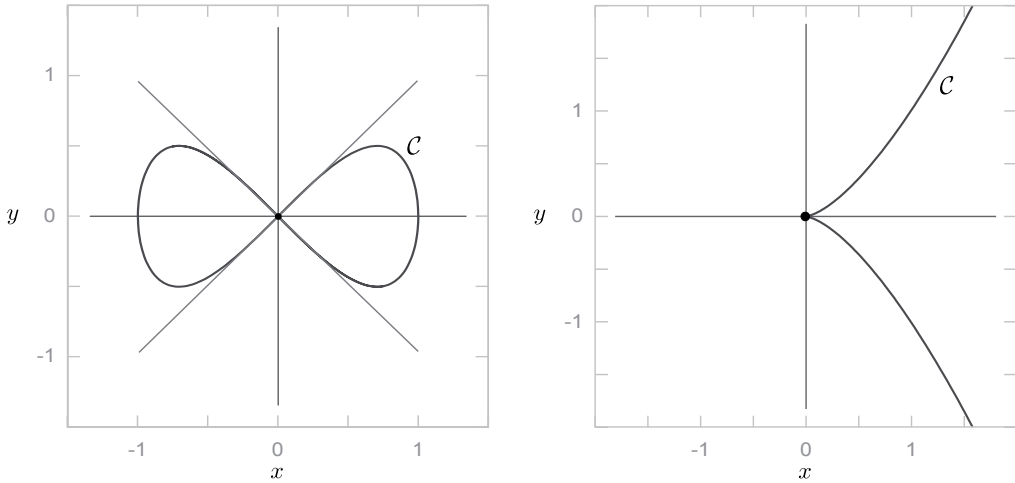


**Fig. 1.** Left: the origin is an ordinary double point of the Gerono lemniscate  $\mathcal{C} := \mathcal{V}(x^4 - x^2 + y^2)$ . The tangents at  $(0, 0)$  are defined by (linear) factors of  $f_2(x, y) = y^2 - x^2$ , i.e. as  $\mathcal{V}(y - x)$  and  $\mathcal{V}(y + x)$ . Right: the origin is a double point of the semicubical parabola  $\mathcal{C} := \mathcal{V}(y^2 - x^3)$ . The double tangent at  $(0, 0)$  is defined by  $f_2(x, y) = y^2$ , i.e. as  $\mathcal{V}(y)$ . (Note: the figure depicts only the real part of  $\mathcal{C}$ ).

It is convenient to consider a *projective plane algebraic curve* over the field of complex numbers i.e. the set  $\mathcal{V}(F) := \{(z_0 : z_1 : z_2) \in \mathbb{P}^2(\mathbb{C}) \mid F(z_0, z_1, z_2) = 0\}$ , where  $F \in \mathbb{C}[z_0, z_1, z_2]$  is a homogeneous polynomial of positive degree and  $\mathbb{P}^n(\mathbb{C})$  is the *projective space of dimension*  $n$  for  $n \in \mathbb{N}_0$ , with class of the vector  $(z_0, \dots, z_n) \in \mathbb{C}^{n+1}$  denoted by  $(z_0 : \dots : z_n)$ .

Let  $\mathcal{V}(f)$  be an affine curve and let  $F$  be the homogenization of  $f$ . The projective curve  $\mathcal{V}(F)$  is called the *projectivization* of  $\mathcal{V}(f)$  and  $\mathcal{V}(f)$  is the *affine part* of  $\mathcal{V}(F)$ . We define an *affine map*  $\mathcal{A}_i = \{(z_0 : z_1 : z_2) \in \mathbb{P}^2(\mathbb{C}) \mid z_i \neq 0\}$ . If we homogenize  $f$  by  $z_0$ , the points of  $\mathcal{V}(F)$  with  $z_0 \neq 0$  correspond precisely to the original affine curve  $\mathcal{V}(f)$  via  $(x, y) := (\frac{z_1}{z_0}, \frac{z_2}{z_0})$ . The points with  $z_0 = 0$  are called the *points at infinity* of  $\mathcal{V}(F)$ . We define affine part and points at infinity of  $\mathcal{V}(F)$  with respect to  $\mathcal{A}_1, \mathcal{A}_2$  in a similar fashion.

The singularity of a point at a curve is a local property. Hence, we always consider an appropriate affine chart of the projective space. However, the global properties (such as maximum number of singular points of certain type, genus of the curve, degree and so on) have to be considered globally.

## 2.1 Resolution of singularities of plane algebraic curves

The process of passing from a singular algebraic curve to a curve which no longer has singularities is called a *resolution of singularities*. One of the usual resolution techniques is known as *blowup*. It enables us to find a birationally equivalent curve, which is either regular, or is less singular in a certain way. In the latter case, we can repeat the process and obtain a regular curve

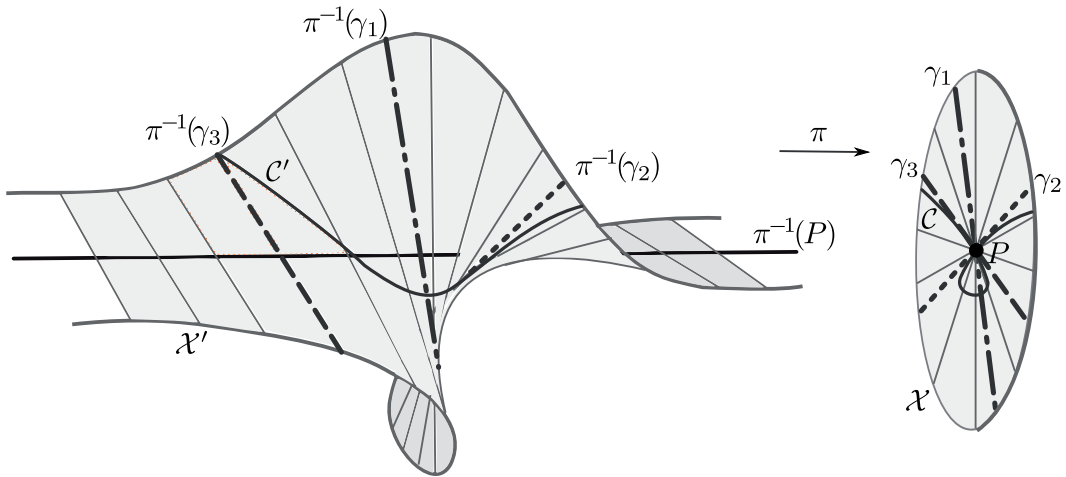


**Fig. 2.** The blowup of the surface  $\mathcal{X}$  is a regular surface  $\mathcal{X}'$ . The projection  $\pi: \mathcal{X}' \rightarrow \mathcal{X}$  is a homeomorphism of  $\mathcal{X} \setminus \{P\}$ , a proper mapping, and  $\pi^{-1}(P)$  is the projective line  $\mathbb{P}^1(\mathbb{C})$ .

after a finite number of steps (see [3, 16]). However, the final curve usually lies on an algebraic surface other than the plane.

The resolution of singularity itself can be defined in general terms, but we restrict ourselves to the constructing of a resolution  $\pi: \mathcal{C}' \rightarrow \mathcal{C}$  for which  $\mathcal{C}'$ ,  $\mathcal{C}$  are respectively a regular curve embedded in a regular surface  $\mathcal{X}'$  and a singular curve embedded in a regular surface  $\mathcal{X}$ ; we assume that  $\mathcal{X}$  lies in a projective space  $\mathbb{P}^n(\mathbb{C})$  of sufficient dimension. The map  $\pi$  should reflect embedding of  $\mathcal{C}'$  in  $\mathcal{X}'$  in such a way that it corresponds to the embedding of  $\mathcal{C}$  in  $\mathcal{X}$ , i.e. we want to construct such a curve  $\mathcal{C}'$ , that only the singular point  $P \in \mathcal{C}$  is affected. All the other points of the neighbourhood of  $P$  remain unchanged (up to a homeomorphism), and both the curves have the same local behaviour.

The simplest case happens when  $\mathcal{X} \equiv \mathbb{C}^2$  and  $P$  is an ordinary singularity of  $\mathcal{C}$  placed in the origin. The essence of the blowup process then consists of replacing the point  $P$  by the set of all lines passing through  $P$ . The surface  $\mathcal{X}'$  is then a ruled surface and we get a new curve  $\mathcal{C}'$  (see fig. 2; for technical details see [3, 16]).

However,  $\mathcal{C}$  being a planar curve is not a generic case. In general,  $\mathcal{X}$  is a two-dimensional variety in  $\mathbb{P}^n(\mathbb{C})$ . In this situation, we use the tangent plane to  $\mathcal{X}$  at  $P$  (denoted  $\mathcal{T}_P(\mathcal{X})$ ). We construct  $\mathcal{T}_P(\mathcal{X})$  by taking all tangents to curves lying on  $\mathcal{X}$  and passing through  $P$ , at the point  $P$  (for more see [6]). After this, we can use the algorithm above.

The blowup of  $\mathcal{X}$  is another non-singular surface  $\mathcal{X}'$ . Note that the fig. 2 may not give the right impression, as there is not a line through the point  $P$  but a one-dimensional projective space  $\mathbb{P}^1(\mathbb{C})$ , and hence (homeomorphically) a circle  $\mathbb{S}^1$ . The "spiral staircase" depicted is in fact an infinite Möbius strip.

In the case of complex curves, we may consider the curve as a real surface and the one we get after the resolution is a Riemann surface. We give a method of visualization for special cases of such curves in section 3..

## 2.2 Invariants of singularities

During the resolution, an  $r$ -fold point  $P$  is transformed into  $r$  regular points  $P_1, \dots, P_r$ . This process can be visualized in the form of a *resolution tree* as follows. In the root is the original  $r$ -fold singular point  $P$ . The vertices of the first level represent points  $P_{11}, \dots, P_{1k_1}$  arising from



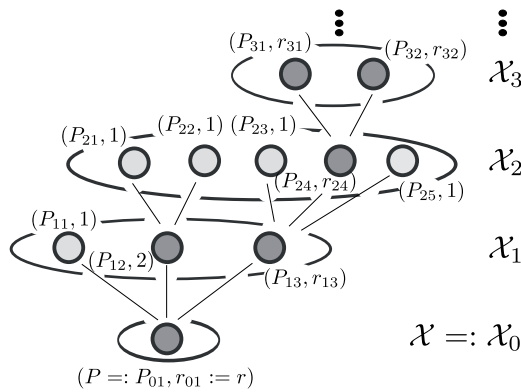


**Fig. 3.** An example of the resolution tree of singular curve  $\mathcal{C}$  with  $r_{ij} > 1$  for non-explicitly written values.

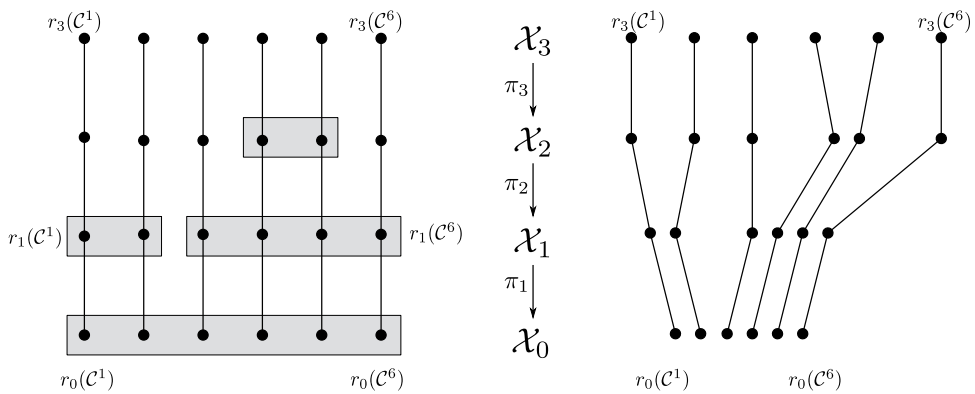


**Fig. 4.** A visualization of the multiplicity sequences in the case of reducible curve  $\mathcal{C} = \mathcal{C}^1 \cup \dots \cup \mathcal{C}^6$ , whose resolution was obtained in 3+1 blow up steps. The separation of branches on each level is depicted either by a grey rectangle (left) or by a closeness of corresponding points (right).

the first application of blowup, along with their multiplicities  $r_{11}, \dots, r_{1k_1}$ . In the second level, we blowup only singular points from the first level and depict them in a similar fashion. We continue until all arising singularities are resolved. Of course, the multiplicities at each level sum up to  $r$  (see fig. 3).

The iteration of blowups evokes subsequent changes in the internal structure of singularity. These can be reasonably encoded via the *multiplicity sequences* as follows. In the case of irreducible curves, we record the multiplicity of the point being resolved in each iteration of blowup, resulting in a finite sequence of positive integers. In the reducible case, each component is encoded in similar fashion, though we need to proceed more carefully – we write not only the multiplicities for each component, but also when the separations of branches occur. The details can be found in [3, 9, 16], for schematic depiction of multiplicity sequences see fig. 4.

The major drawback of the previous method is that we have to construct the entire resolution, which can be very tedious. Luckily, the internal structure of singularity can be characterized via *invariants*, integer values completely characterizing the structure of singularity.

The *Milnor number*  $\mu$  is one of the most important invariants. It may be defined in va-

rious ways, depending whether we wish to emphasize its topological, algebraic or geometric significance. In all cases, it is the key measure of the complexity of a singularity – it can be proven, that we can break up any (isolated) singularity into  $\mu$  distinct ones, each with  $\mu = 1$ . These singularities are very simple, each is a union of two smooth branches meeting transversely (for proofs see [16]). In case of a single branch  $\mathcal{C}$ , the Milnor number  $\mu(\mathcal{C})$  is even, if it is smooth,  $\mu(\mathcal{C}) = 0$ . Another example, the  $\delta$ -invariant of a curve, measures the number of double points of the curve.

Some numerical invariants are mutually tied, e.g. via the Plücker formulas. However, the most important result is that the topological type of  $\mathcal{C}$  is completely determined by, and it determines, the system of multiplicity sequences, see [16, 9]. Thus, we may choose any of the two presented methods to describe the singularity structure, depending on the usage and available data – if necessary, they are mutually convertible.

### 2.3 Deformations of singularities

The technique of deformations is a fundamental method of algebraic geometry. We may deform various objects, e.g. algebraic varieties or morphisms. In our case, we use the deformations for handling isolated singularities of algebraic curves.

Loosely speaking, the deformation is a "slight change" of the curve in the neighborhood of its singularity in such a way, that the newly created curve still carries enough information about the original one. The term "slight" can be on certain examples illustrated in Euclidean topology, however for general rings it cannot be presented visually. Hence, this condition is expressed via *flatness*. Therefore, a natural question arises: is it possible to deform the curves in such a way, that the internal structure of singularity is preserved? The answer is yes.

We distinguish different types of invariant-preserving deformations, the most important are the *equimultiple*, *equinormalizable* and *equisingular* deformations. They respectively preserve the multiplicity, the  $\delta$ -invariant and the Milnor number  $\mu$ . In this text, we do not proceed further, the interested reader may find more in [9].

## 3. Riemann surface of a complex function

A notion which is very tightly bound with a complex algebraic curve is the notion of Riemann surface – a regular real two-dimensional surface obtained from the curve using resolution of singularities provided the starting curve is singular. We show the case of a complex function since any algebraic curve can be locally parameterized by such a function.

We work with the standard definition of complex numbers, the interested reader can find more in [12]. We use the compactification of  $\mathbb{C}$  by a point  $\infty \notin \mathbb{C}$  and the result is called *closed complex plane*  $\Sigma = \mathbb{C} \cup \{\infty\}$  (see [12]). It is homeomorphic to  $\mathbb{S}^2$  via stereographic projection.

We get the visualization of the closed complex plane  $\Sigma$  by representing the complex numbers using the two dimensional unit sphere given as equation

$$\mathbb{S}^2 = \{(x_1, x_2, x_3) \in \mathbb{R}^3 \mid x_1^2 + x_2^2 + x_3^2 = 1\}. \quad (1)$$

Identifying the Gauss plane with a plane defined by equation  $x_3 = 0$  in  $\mathbb{R}^3$  provides the representation of every  $z = x + iy \in \mathbb{C}$  by a point with the coordinates  $(x, y, 0)$ . We plot the Gauss plane  $\mathbb{C}$  on the unit sphere using the stereographic projection  $P: \mathbb{C} \rightarrow \mathbb{S}^2$ , which assigns point  $Z = (x_1, x_2, x_3) \in \mathbb{S}^2$  to the point  $z = (x, y) \in \mathbb{C}$  (see [10]). Therefore, the closed complex plane  $\Sigma$  is often called the Riemann sphere.

In complex analysis, we often get multivalued functions. Such a function associates with every input more than one output value (e.g. logarithm, root function). The plotting of a graph of such a function brings some problems [13]. The often used domain coloring does not give us



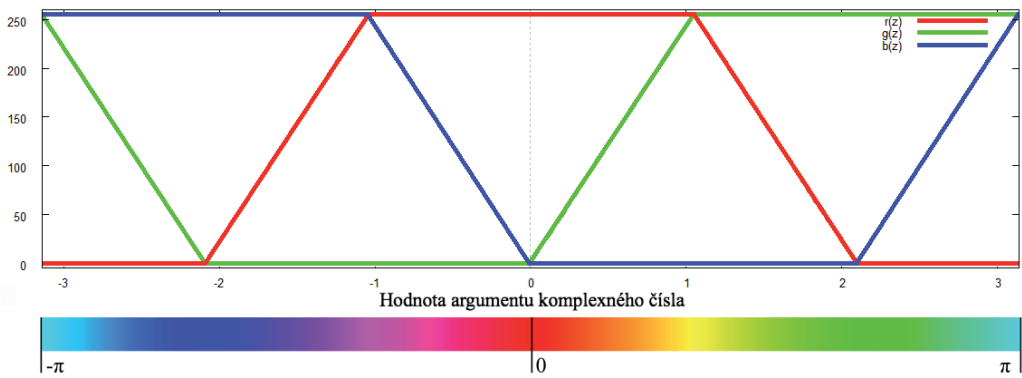


**Fig. 5.** The color gradient configuration used to visualize the value of the argument of a complex number in the range of  $[-\pi, \pi]$ . The colors changes from left to right in this order: cyan, blue, magenta, red, yellow, green, cyan. The red color shows, where the argument of the function is 0.

satisfactory results, because it plots only a part of the values of the function. Therefore, we used Riemann surface to visualize the whole family of single-valued functions which put together give the original multivalued one.

The Riemann surface is defined as a pair  $(X, \mathcal{S})$ , where  $X$  is a simple connected two-dimensional manifold and  $\mathcal{S}$  is a complex structure on  $X$ . This structure is needed to define unambiguously the complex function  $f(z)$ . That means that a multivalued complex function  $f(z)$  is single valued on this 2-dimensional manifold. If we take only one leaf of Riemann surface (a maximum connected subset on which the original function is uniquely defined), we get one branch of the multivalued function  $f(z)$ . One can find more about Riemann surfaces and their properties in [8].

### 3.1 Used tools and techniques

We created the visualizations using the free software Blender, see [2]. A user can create short scripts within the provided environment using a built-in scripting tool. The tool uses object oriented scripting language called Python, see [15].

In the visualization, the value of the argument is depicted via color gradient (see fig. 5). The distance of the semitransparent layer from the unit sphere is calculated using the absolute value of the function. From the definition of the absolute value, the values clearly lie in the interval  $[0, \infty)$ . In order to get a bounded graph, we transform the absolute value using the function  $\arctan(|z|)$  (other functions are possible as well). After this transformation, we get the values from the interval  $[0, \pi/2)$ . Such values are used to compute the mesh of the approximated Riemann surface as several functions (represented by semitransparent layers) over the Riemann sphere. These vertices are colored according to the argument of their values.

### 3.2 Power function visualization

We picked the function  $z^n$  to demonstrate the proposed method. The fig. 6 illustrates the results of the script for different values of the constant  $n \in \mathbb{Q}^+$ . It is enough to look at the cases of positive integers and their reciprocals. In the fig. 6, we can see that for integer  $n > 1$  the color gradient covers the whole Riemann sphere  $n$ -times. Hence, the values for this function of the argument are repeating. The semitransparent layer osculates with the Riemann sphere

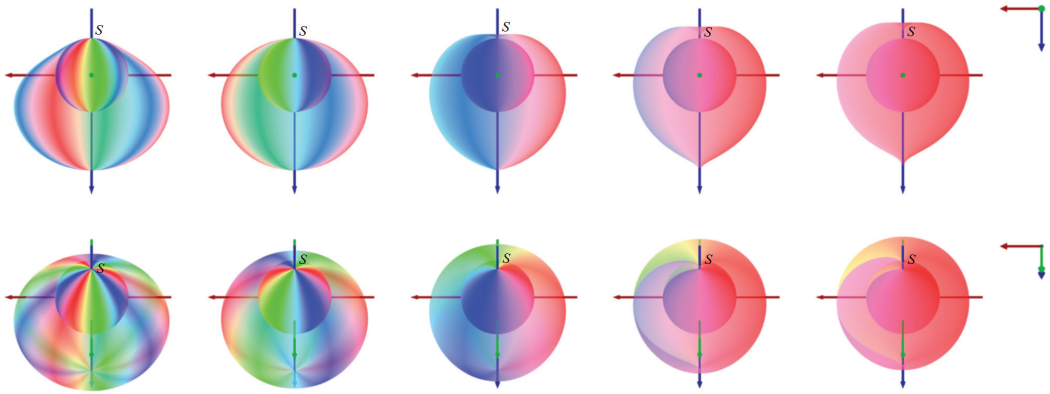


**Fig. 6.** The visualization of the function  $z \mapsto z^n$  for values  $n = 3, 2, 1, \frac{1}{2}, \frac{1}{3}$  is shown. The color gradient describes the argument of the complex number  $z^n$ . The distance of the semitransparent layer from the sphere is obtained by calculating the value of the function  $\arctan(|z^n|)$ . The semitransparent layer touches the Riemann sphere in the root of the polynomial.

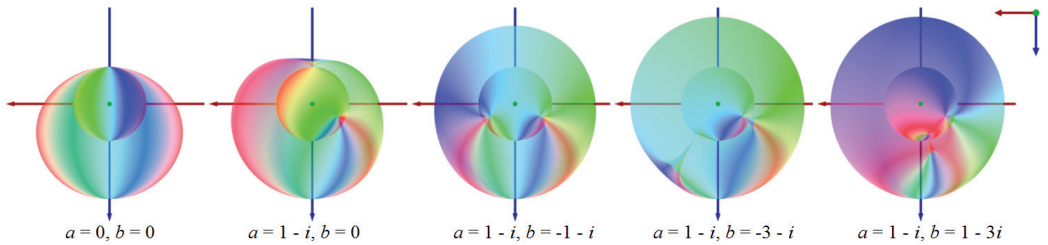


**Fig. 7.** In the picture, the visualization of the function  $f(z) = (z - a)(z - b)$  for different values of the constants  $a, b$  is shown. Notice, the cone structures pointing to the Riemann sphere in the neighbourhood of the root of the function.

in the point  $S$ , which is the projection of the point with coordinates  $(0, 0)$ . The examples show the absolute values in the neighborhood of the point  $S$  are growing slower for the higher values of the exponent  $n$  and faster for the smaller values of exponent  $n$ .

For  $n < 1$ , there are multiple values associated with the argument, so we can see only  $1/n$  of the color gradient on the Riemann sphere. This will be discussed in the subsection 3.4. In the neighbourhood of the point  $S$  the semitransparent layer has cone-like shape, which gets bigger for smaller exponent  $n$ . Hence, the absolute values of complex number are growing faster in the neighborhood of the point  $S$ .

### 3.3 Visualization of quadratic functions

We examined closer the function  $f(z) = (z - a)(z - b)$ , where  $a, b \in \mathbb{C}$ . In fig. 7, we see the examples for certain values of the constants  $a$  and  $b$ . Clearly, the visualization gives the graph of the function  $z^2$  for values  $a = 0, b = 0$ . For different values of the constants  $a, b$ , we get two cone-like shapes formed by the semitransparent layers. These are situated in neighbourhoods of the roots of the equation  $(z - a)(z - b) = 0$ . It is also apparent, that the values of argument

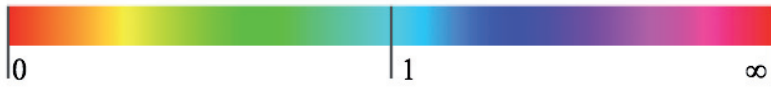


**Fig. 8.** The color gradient used to visualize the absolute value of the complex number. The colors change from left to right in following order: red, yellow, green, cyan, blue, magenta, red.

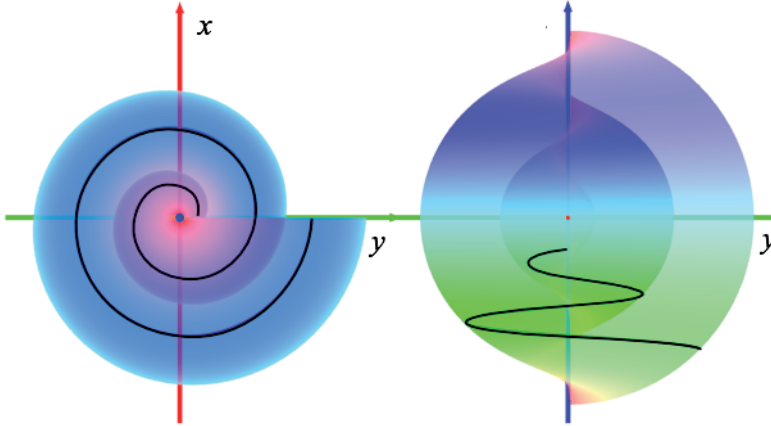


**Fig. 9.** The visualization of the function  $f(z) = \sqrt{z}$ . The viewpoint is aligned with the  $z$ -axis in the left part of the figure, the right viewpoint is aligned with the  $x$ -axis. The constant value of the modulus  $r \doteq 0,4$  is highlighted.

of the complex numbers concentrate near the values of the roots.

### 3.4 The visualization of the Riemann surface

For obtaining the visualizations of the multivalued function using the Riemann surface, we changed the procedure of creation of the model. In this case, the absolute value of the complex number is depicted by the color gradient (see fig. 8). From the color of the point on the semi-transparent layer, we get an approximate value of the absolute value of the complex number. We highlighted the specific absolute value to get a grip for our eyes.

The value of the argument of the complex number gives us the distance from the unit sphere with the centre in the origin. This sphere represents the Riemann sphere for  $\Sigma$ . Hence, we get a point on the unit sphere corresponding to the zero value of the argument. If the value of the argument is  $\pi$ , the distance of the corresponding point on the semitransparent layer from the unit sphere is also  $\pi$ . In the case of multivalued function, we scale this value properly. The argument of  $z = 0$  and  $z = \infty$  is not defined. Therefore, we get the limit value of the argument, if it exists.

### 3.5 Visualization of general root function

The figure 9 represents the Riemann surface of the function  $f(z) = \sqrt{z}$  using several viewpoints. In the case the viewpoint is aligned with the  $z$ -axis, the visualization produces a spiral-like shape. Therefore, the argument of the value of the function increases if we proceed counterclockwise on the circle around the branching point (a singularity).

If the viewpoint is aligned with the  $x$ -axis, the fact that the absolute value of the function increases. The graph does not contain any disruptions in the color gradient and this demonstrates the continuity of the absolute value of the function.



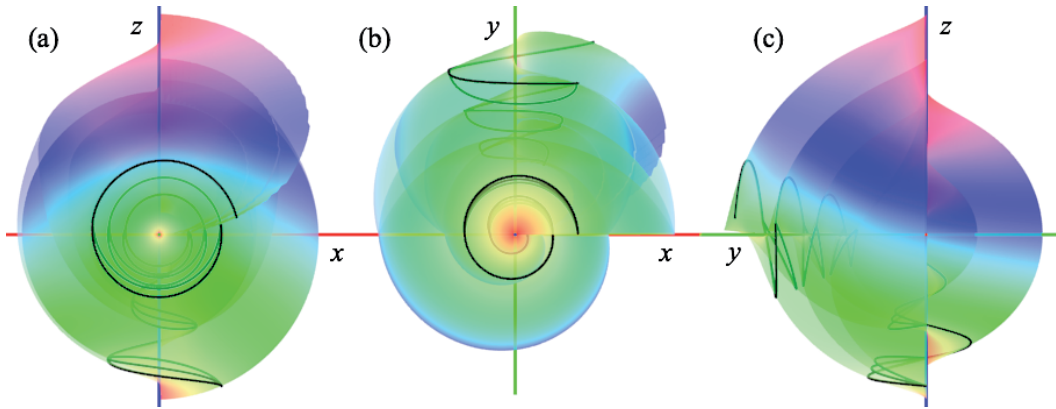


**Fig. 10.** Visualisation of the Riemann surface of the complex root  $f(z) = \sqrt{z} \sqrt[3]{z+i}$  a) the viewpoint is aligned with the  $y$ -axis, b) the viewpoint is aligned with the  $z$ -axis and c) the view point is aligned with the  $x$ -axis. The images of the circles with the centers lying in the branching points  $0, -i$  respectively and the radii of values  $r \doteq 0, 2$  respectively are depicted by the dark/black spirals. The layer intersections caused by the different degrees of the root are clearly visible in the c) subfigure.

The Riemann surface in the neighborhood of the points  $0$  and  $\infty$  is in the shape of the helical surface. Therefore, these two points are the branching points of the  $f(z) = \sqrt{z}$  function. The Riemann surface revolves twice around both branching points, hence the function has two branches.

A similar situation is in the case of  $f(z) = \sqrt[n]{z+a}$ , where the similar type of behaviour can be observed in the neighbourhood of the point  $-a$  and  $\infty$ .

### 3.6 Visualisation of product of roots

We illustrate the general case on the function  $f(z) = \sqrt[n]{z+a} \sqrt[n]{z+b}$  for  $a = 0, b = i$ ,  $m = 2, n = 3$ . The fig. 10 shows the Riemann surface of the  $f(z) = \sqrt{z} \sqrt[3]{z+i}$  function. Locally, the function is composed from two different degrees of root function. It is convenient to adapt the original function to contain only roots of the same degree, which is calculated as the least common multiple of the original degrees, resulting in the  $f(z) = \sqrt[6]{z^3(z+i)^2}$  function. The visualization depicts the sixth root, therefore the final Riemann surface contains six layers. In the fig. 10, we see three double spiral around the root  $0$  and two triple spiral around the root  $-i$ . We also see the intersection of the layers between the roots. These self-intersections are caused by the used projection of the Riemann surface to the 3 dimensional space. Notice, that the function has two branch cuts. One from the branching point  $0$  along the half-line  $l_0 = \{z \in \mathbb{R}; z \geq 0\}$  and the other from the branching point  $-i$  along the half-line  $l_{-i} = \{z \in \mathbb{C}; \Re(z) \geq 0, \Im(z) = -i\}$ .

## 4. Topological classification of an isolated singularity

Each isolated singularity has in its neighborhood a stable structure given by a special knot called a cable knot.

Points in the zero set  $Z(f)$ , where  $f(x, y) \in \mathbb{C}[x, y]$  is irreducible,  $f(0, 0) = 0$  and  $f(0, y) \neq 0$ , may be written as  $(t^m, g(t))$ ,  $t \in \mathbb{C}$ , where  $g \in \mathbb{C}\{z\}$  (the ring of complex series convergent in zero). Such a description can be considered as a parameterization of the curve using  $m$ -th root of  $x$  in a neighborhood of zero given by  $y = g(x^{\frac{1}{m}})$ . It is sometimes called the

*Puiseux expansion* of the polynomial  $f$ . The existence of such an expansion can be guaranteed using the finite algorithm via normalization process.

Minimum  $m$  allowing such a parameterization corresponds to the so called “good parameterization” of  $Z(f)$ . Then

$$f(x, y) = u(x, y) \prod_{j=1}^m (y - y(\xi^j x^{\frac{1}{m}})), \quad (2)$$

where  $\xi$  is a primitive  $m$ -th root of unity and  $u \in \mathbb{C}\{x, y\}$  is a unit.

We start with a Puiseux series with  $m$ th root of  $x$  and let  $E_{\mathbb{N}}$  be the set of denominators in the exponents of the Puiseux series in the terms with non-zero coefficients. Let  $(m; \beta_1, \dots, \beta_g)$  be a sequence of positive integers such that

$$\begin{aligned} \beta_1 &= \min\{k: a_k \in E_{\mathbb{N}}, m \nmid k\} \quad \text{and} \quad e_1 = \text{GCD}(m, \beta_1), \\ \beta_i &= \min\{k: a_k \in E_{\mathbb{N}}, e_{i-1} \nmid k\} \quad \text{and} \quad e_i = \text{GCD}(e_{i-1}, \beta_i) \end{aligned}$$

for  $i = 2, \dots, g$ , with  $e_g = 1$ , where GCD denotes the greatest common divisor. Let  $e_0 = m$ . This sequence is called the *Puiseux characteristics* and the sequence  $\{e_0; e_1, \dots, e_g\}$  is called the *associated Puiseux sequence*.

**Example:**  $f(x, y) = x^3 - y^2$  with parameterization  $x = t^2, y = t^3$  has the Puiseux characteristic  $(2; 3)$  with the associated Puiseux sequence  $(2; 1)$ .

## 4.1 Knot construction

A complex algebraic curve  $C \subset \mathbb{C}^2$  can be considered as a real surface in  $\mathbb{R}^4 = \mathbb{C}^2$ . The knot associated to a singularity is a intersection of such a surface and a small sphere around the singularity. It is known to be independent of the radius  $\epsilon$  for small enough  $\epsilon > 0$ .

Let  $K = C \cap \mathbb{S}_{\epsilon}^3$  be the knot associated with the singularity. A good parameterization can be obtained via projection on the cylinder  $Q = \{(x, y) \in \mathbb{C}^2 : |x| = \delta\} \equiv \mathbb{S}^1 \times \mathbb{C}$  for sufficiently small  $\delta > 0$ .

The knot equation has the form

$$x = t^m, y = a_1 t^{\beta_1} + a_2 t^{\beta_2} + \dots + a_g t^{\beta_g}, \quad (3)$$

where  $a_1, \dots, a_g \neq 0$  are properly picked.

By a mapping of  $m$  copies of circle with radius  $\sqrt[m]{\delta}$  for  $x$  and taking corresponding  $y$ , we get the image of the knot. For  $t = \sqrt[m]{\delta} e^{i\theta}$ ,  $\theta \in [0, 2\pi]$ , we get

$$x = \delta e^{im\theta}, y = a_1 \sqrt[m]{\delta} e^{i\beta_1\theta} + a_2 \sqrt[m]{\delta} e^{i\beta_2\theta} + \dots + a_g \sqrt[m]{\delta} e^{i\beta_g\theta} \quad (4)$$

**Example:** Continuing with the example of the cusp, we have the equation  $y^2 = x^3$  and its parameterization after a substitution of  $t = e^{i\theta}$  gives  $x = e^{i2\theta}, y = e^{i3\theta}$  for  $\theta \in [0, 2\pi]$ . The corresponding figure is in fig. 11.

In case of more complex singularities and their knots, one can use a sequence of steps for building the final knot. It can be considered as a sequence of wrapping around previously constructed knot (see the additive structure of the coordinate  $y$  in (3)).

Both coordinates are cyclic, hence it is convenient to graph them on a torus. The coordinate  $x$  is represented by parallels of the torus and the coordinate  $y$  by the meridians. In fig. 11, the meridian direction is wrapped three times while the parallel direction two times. This corresponds to the exponents in parameterization or in the Puiseux characteristic. Similarly, the meridian direction of the red knot is for the parameterization in fig 12(a) wrapped two times around the blue one while the parallel direction is wrapped 7 times. Composing together, it gives the 7 wraps around the meridians while 4 wraps around the parallel direction of the basic torus.

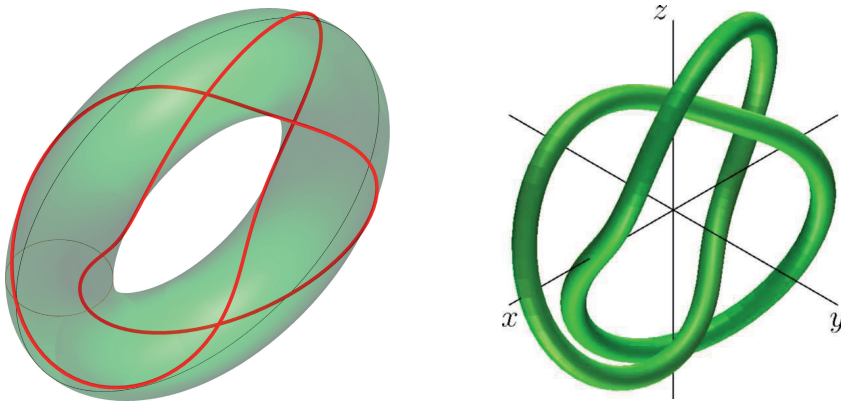


**Fig. 11.** The knot associated with the cusp at the curve given by the equation  $x^3 - y^2 = 0$ .

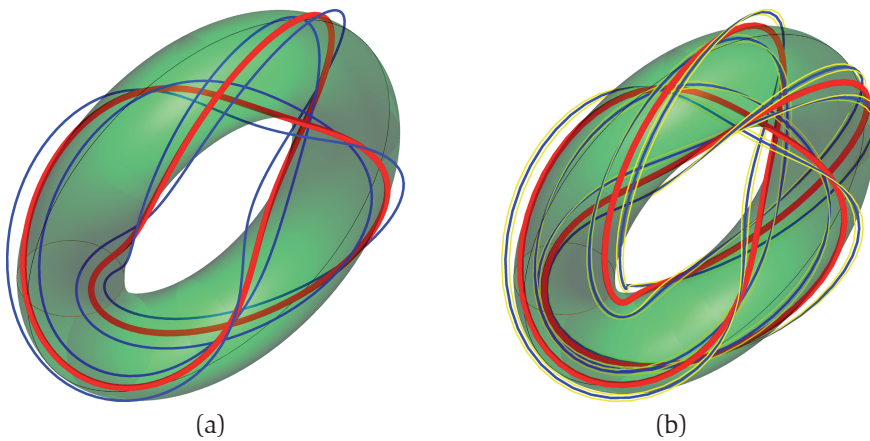


**Fig. 12.** Examples of more complex knots in singularities with local parameterization (a)  $x = e^{i4\theta}$ ,  $y = e^{i6\theta} + e^{i7\theta}$ , its Puiseux characteristic (4;6,7) and its associated Puiseux sequence (4;2,1); (b)  $x = e^{i12\theta}$ ,  $y = e^{i16\theta} + e^{i18\theta} + e^{i19\theta}$ , its Puiseux characteristic (12;16,18,19) and its associated Puiseux sequence (12;4,2,1).

In general, if  $T_k$  is a torus for the first  $k$  terms in (3), adding the next term produces the knot wrapping  $\frac{e_k}{e_{k+1}}$  in parallel direction and  $\frac{\beta_{k+1}}{e_{k+1}}$  times wrapping in the meridian direction. Using this information, one can generate a carousel (see fig. 13) for a construction of the knot at once. One pushes the largest circle around the torus once and the other are turning with relative speed given by the numbers in Puiseux characteristic. Hence, the knot can be generated “mechanically”.

## 5. Space-like Bézier quadratic curves in Minkowski space

The structure of real singularities is a bit more difficult to detect. We show its usage in the area of modeling in Minkowski space. Since affinely there is no difference to the Euclidean plane, the properties interesting in Minkowski space have to be determined by the (pseudo-)scalar product. We give a short overview.

*Pseudo-Euclidean space*, denoted by  $\mathbb{R}_p^n$ ,  $n \in \mathbb{N} = \{1, 2, 3, \dots\}$ ,  $p \in \mathbb{N}_0 = \{0, 1, 2, \dots\}$  is



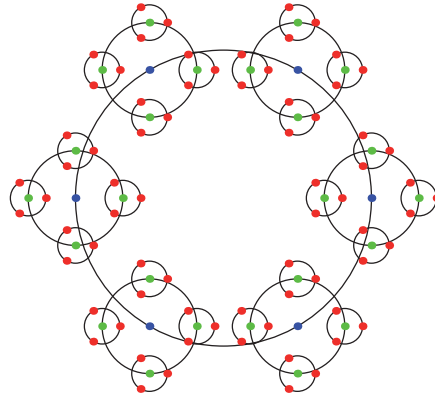


**Fig. 13.** Carousel and the corresponding knot for generating the characteristic knot of a singularity out of Puiseux characteristic  $(72; 42, 111, 160)$  and  $\mathbf{e} = (72; 6, 3, 1)$ .

an  $n$ -dimensional real vector space with a regular quadratic form  $\mathbf{q}: \mathbb{R}^n \rightarrow \mathbb{R}$ , where

$$\mathbf{q}(x_1, \dots, x_n) = \sum_{i=1}^{n-p} x_i^2 - \sum_{j=n-p+1}^n x_j^2$$

in a certain basis. For  $p = 1$ , it is called *Minkowski space*. For  $p = 0$ , we get *Euclidean space*. We use the notation  $\bar{x} = (x_1, \dots, x_n)^\top$  for the vectors in  $\mathbb{R}_p^n$ . More can be found in [1].

A quadratic form has an associated polar form  $P$ , which plays the role of scalar product. Hence, we call it the *pseudo-scalar product* since positive definiteness might not be satisfied. The vectors  $\bar{x}, \bar{y} \in \mathbb{R}_p^n$  are *pseudo-orthogonal* if  $P(\bar{x}, \bar{y}) = 0$ .

By a standard construction, we get an affine space with a *pseudo-Cartesian* coordinate system  $S(O, x_1, \dots, x_n)$ . Using the quadratic form, we classify the vectors in the pseudo-Euclidean space as follows. We call the vector  $\bar{x} \in \mathbb{R}_p^n$  *space-like* if  $\mathbf{q}(\bar{x}) > 0$ , *time-like* if  $\mathbf{q}(\bar{x}) < 0$  and *light-like* if  $\mathbf{q}(\bar{x}) = 0$ . All the vectors in  $\mathbf{q}^{-1}(0)$  are also called *isotropic*. The set of all light-like vectors forms an *isotropic cone*  $Q$  of the corresponding quadratic form  $\mathbf{q}$ .

A point  $x \in \mathbb{R}_p^n$  is space-like (time-like, light-like respectively) if its position vector  $\bar{x} = x - O$  is such. Note that this depends on the coordinate system.

Now, there are two possible ways, how to define a space-like curve. A differentiable curve  $p: I \rightarrow \mathbb{R}_p^n$  is called *tangentially space-like* if the tangent vector  $\dot{p}(t)$  is space-like for each  $t \in I$ . A curve  $p: I \rightarrow \mathbb{R}_p^n$  is called *point-wise space-like*, if it contains only space-like points, i.e. the vector  $\overline{p(t)} = p(t) - O$  is space-like for every  $t \in I$ . In our work, we use the definition of the point-wise space-like curve. One of the advantages is that the condition of differentiability is not required, although the curves we consider in this paper are polynomial.

Bézier curve in Minkowski space of degree  $n$  is the polynomial map  $b: [0, 1] \rightarrow \mathbb{R}_1^n$  that  $b(t) = \sum_{i=0}^n B_i^n(t) b_i$  for  $t \in [0, 1]$ . Points  $b_i \in \mathbb{R}_1^n$  are called control points,  $B_i^n(t) = \binom{n}{i} (1-t)^{n-i} t^i$  for  $i \in \{0, \dots, n\}$  are Bernstein polynomials of degree  $n$ . More properties can be found in [7, 11].

There is an alternative way of the Bézier curve definition. Instead of one control point, we determine one point of the curve and the tangent line to the curve at this point. For the curves of degree higher than 2, the definition may be ambiguous, but it allows us to define some useful maps.

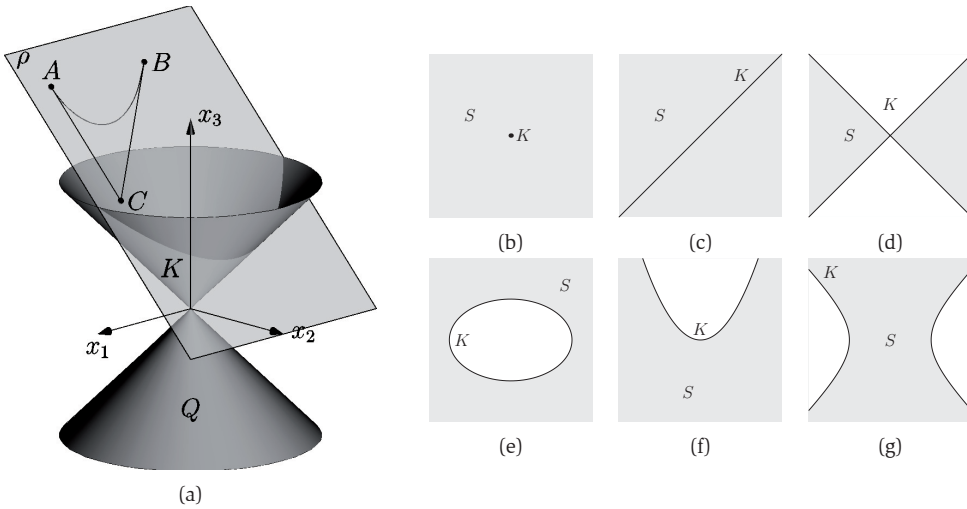


**Fig. 14.** (a) Plane  $\rho$  spans the points  $A, C, B$ . In the case of their non-collinearity, they generate  $\rho$  as their affine hull. The conic section  $K$  is an intersection of the light cone  $Q$  and the plane  $\rho$ .  
 (b-g) Let  $K \subset \rho$  be the conic section (point, double line, pair of lines, ellipse, parabola, hyperbola). The set  $S$  consists of all space-like points in the plane  $\rho$ .

## 5.1 Space-like conditions

Let us consider Minkowski space  $\mathbb{R}_1^3$  and a quadratic Bézier curve with the control points  $A, C, B$  in this order, denoted by  $b_{ACB}(t)$ . In order a Bézier curve to be space-like, each of its points has to be space-like. Let the points  $A = [a_1, a_2, a_3]$  and  $B = [b_1, b_2, b_3]$  be fixed. Since Bézier curve interpolates its endpoints, we have necessary and sufficient conditions

$$a_1^2 + a_2^2 - a_3^2 > 0, \quad (5)$$

$$b_1^2 + b_2^2 - b_3^2 > 0. \quad (6)$$

The quadratic Bézier curve is planar and it lies in the affine plane  $\rho \subset \mathbb{R}_1^3$ . Now, we fix the points  $A, B$ . In any case, the intersection of the light-cone  $Q$  and the plane  $\rho$  is a conic section  $K$  (see fig. 14(a)). The figures 14(b-g) show all cases of the set  $S$  of space-like points in any type of the plane  $\rho$ . The point-wise space-like Bézier curve  $b_{ACB}(t) \subset S$ . We solve the problem in the plane  $\rho$  for each type of conic section and the planar results can be put together to form the spatial result.

Let  $S_\rho(O, x, y)$  be any pseudo-Cartesian coordinate system in the plane  $\rho$ . Let  $A = [a_x, a_y], C = [c_x, c_y], B = [b_x, b_y]$  be the local affine coordinates of the control points in  $S_\rho(O, x, y)$ . From now on, the points  $A, B$  are arbitrary, but fixed, and they satisfy the conditions (5), (6).

Let  $V_\rho(A, B)$  be the set of points  $C \in \rho$  such that the curve  $b_{ACB}$  is space-like. Then, we say that  $V_\rho(A, B)$  is a *set of admissible solutions* in the plane  $\rho$  with respect to  $A, B$ . If no confusion arise, we say only the set of admissible solutions  $V$ .

By  $V_\rho^v(A, B)$ , we denote the set of points  $C \in \rho$  such that  $b_{ACB} \cap K = M$ , where  $X \in M$  is a point of contact of order 2 between  $b_{ACB}(t)$  and  $K$ . The set of points  $C \in \rho$  such that  $b_{ACB}$  and  $K$  have transversal intersection is denoted by  $V_\rho^t(A, B)$ . The union of disjoint sets  $V_\rho(A, B) \cup V_\rho^v(A, B) \cup V_\rho^t(A, B)$  gives the whole plane  $\rho$  for the given points  $A, B$ .

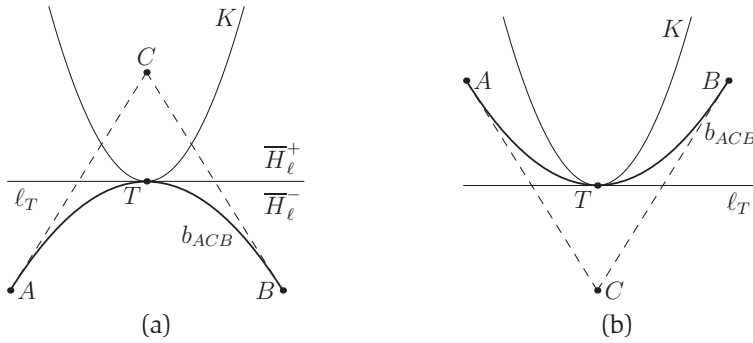


**Fig. 15.** Separation of the conic section  $K$  and the Bézier curve  $b_{ACB}(t)$  by the tangent line  $\ell_T$ : (a) exterior point of contact  $T$ , (b) interior point of contact  $T$ .

## 5.2 Set of admissible middle control points

We study the set  $V_\rho^v(A, B)$ . It is natural, because a "boundary" between the situation that two curves have no common points and the situation that one curve intersects the other curve is, that they touch each other in our setup.

We say that the set  $D \subset K$  is the *set of points of contact* between  $K$  and the set of all  $b_{ACB}$  if for any point  $X_0 = [x_0, y_0] \in D$  there is at least one point  $C_0$  such that  $C_0 \in V_\rho^v(A, B)$  and  $X_0 \in b_{AC_0B} \cap K$ .

We divide the points of contact into two groups. Points  $T \in D$  such that the Bézier curve and the conic section  $K$  are lying in the opposite half-planes with respect to their common tangent line  $\ell_T$  at the point  $T$  form the set of exterior points of contact  $D_{ext}$ . In the set of interior points of contact  $D_{in}$  are such points  $T \in D$  that the Bézier curve and conic section  $K$  are lying in the same half-plane with respect to their common tangent line  $\ell_T$  at the point  $T$  (see fig. 15). Clearly,  $D = D_{ext} \cup D_{in}$ .

Let us consider the situation that the conic section  $K$  is a unit circle and the points  $A, B$  are space-like as in fig. 16. As we proved in [14], the sets  $D_{ext}, D_{in}$  are considered with respect to the tangent lines from the points  $A, B$  to the conic section  $K$ . Let  $t_{1A}, t_{2A}, t_{1B}, t_{2B}$  be the tangent lines from the points  $A, B$  to  $K$  and the points  $T_{1A}, T_{2A}, T_{1B}, T_{2B} \in K$  be the corresponding points of contact.

The set  $D_{ext} = \widehat{T_{1A}T_{2A}} \cap \widehat{T_{1B}T_{2B}}$ , because it is the only arc on the  $K$  containing such points  $T$  that the corresponding tangent lines  $\ell_T$  separate the Bézier curve and the conic section  $K$ . We also proved that the set  $D_{in}$  is determined by the tangent lines from  $A, B$  to  $K$  that do not separate the segment  $AB$  and  $K$ . In our case, these are  $t_{2A}, t_{2B}$ . The set  $D_{in} \neq \emptyset$  iff  $t_{2A}, t_{2B}$  converge, therefore the point  $P = t_{2A} \cap t_{2B}$  lies in the same half-plane with respect to line  $\overleftrightarrow{AB}$  as the points  $t_{2A}, t_{2B}$ . In general, the set of interior points of contact is determined by the arc  $\widehat{T_{2A}T_{2B}}$ . In this case, the set  $D_{in}$  consists of two affiliated components  $\widehat{T_{2A}U_1} \cup \widehat{U_2T_{2B}} \cup \{U_1, U_2\}$ . The split of the arc is caused by the existence of the curve  $b_{AC_uB}$ , which has double contact with the conic section  $K$ . As one can see,  $b_{AC_uB} \cap K = \{U_1, U_2\}$ .

For the given points  $A, B, X \in D \subseteq K$  and the tangent line  $\ell_X$  at  $X$  to  $K$ , the Bézier curve  $b_{ACB}$  touching the conic section  $K$  is clearly identified. In order to find the middle control vertex  $C$ , we use the following map  $\sigma$ . The map  $\sigma : D \rightarrow \rho$  is called *boundary map* if for every  $X \in D$  holds  $\sigma(X) = C$ , for  $C$  from the definition of the set of contact points (see fig. 17). The boundary map has the form

$$\sigma(X) = \frac{b(t_0) - B_0^2(t_0)A - B_2^2(t_0)B}{B_1^2(t_0)}, \quad (7)$$



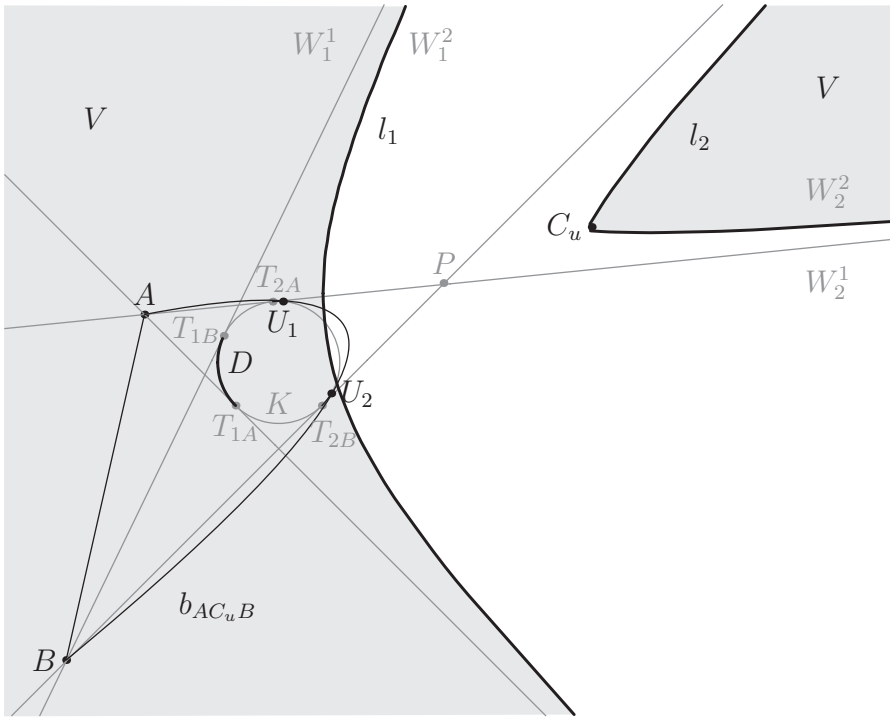


**Fig. 16.** Example of the set of admissible solutions  $V(A, B)$  for the conic section  $K$  being a unit circle.

where  $t_0 \in [0, 1]$  is a solution of the equation  $0 = \alpha t_0^2 + \beta t_0 + \gamma$  and for  $A = [a_x, a_y, 1]$ ,  $B = [b_x, b_y, 1]$ ,  $X = [x_0, y_0, 1]$  are

$$\alpha = (A - B)M_K X^\top,$$

$$\beta = 2(X - A)M_K X^\top,$$

$$\gamma = -\frac{\beta}{2}.$$

As we proved in [14], the set  $V_\rho^v(A, B)$  generated by the set  $D$  using the map  $\sigma$ , forms the boundary  $\partial V$  of the set of admissible solutions  $V(A, B)$ .

In our case, the set of points of contact  $D = D_{ext} \cup D_{in}$  generates the curves  $l_1, l_2$  such that  $l_1 \cup l_2 = \partial V_\rho(A, B)$ , see fig. 16. Because the curve  $l_1$  is generated by the exterior points of contact, the region  $W_1^1$  containing the points  $A, B$  is the subset  $W_1^1 \subset V_\rho(A, B)$ . The curve  $l_2$  is generated by the interior points of contact. It bounds the region  $W_2^2$  not containing the points  $A, B$  and  $W_2^2 \subset V_\rho(A, B)$  according to the theorem proved in [14]. The set of admissible solutions  $V_\rho(A, B) = W_1^1 \cup W_2^2$  consists of two regions.

However, there are some specific cases in the solution for other types of conic sections. For example, the two components of hyperbola are to be considered separately and the final result is obtained as intersection of the two partial results.

## 6. Conclusion

We have surveyed basic notions and selected new results in the research of algebraic curves and their singularities. We have presented multiple tools and methods for measuring and capturing the internal structure of given singularities, as well as techniques for their complete removal

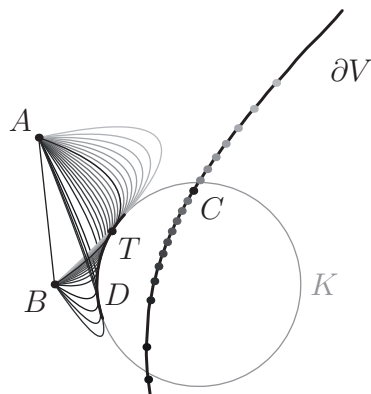


**Fig. 17.** The boundary map  $\sigma$  maps the points of the arc  $D$  to the points in  $\partial V$ . Clearly,  $\sigma(T) = C$ .

while preserving essential properties of the original curve. This has served as a preparation for the final topic of the text, the deformations of singularities, which enable us to study the singularities of algebraic curves and their internal structure from a different point of view.

We have also created visualizations of elementary functions over the Riemann sphere and described the generation of the Riemann surface of root functions and their product. Our approach enables to visualize all branches of a function over its domain.

A user may interact with the created 3D model, they can be edited and used for creation of animations. These features lead to a better understanding of the function behavior in both studying and tutoring sessions.

One of the aims is to use such functions for local parameterization of the algebraic curves. The isolated singularities of algebraic curves have a knot invariant describing completely the topological characteristic of the singularity. Hence, the knot can be composed out of knots of the parameterising functions.

In the future work, we want to use the deformations in order to clarify the structure of an isolated singularity and present its transition to a regular situation.

Finally, we also showed the usage of real singularities in classification of Bézier quadratic curves in Minkowski space. It is completely described in [14]. Currently, we work on the case of special higher degree Bézier curves. Some partial results are given in [5]. For example, we derive the form of the boundary map  $\sigma$  for cubic curves and we describe and study the problem of ambiguity of alternative definition of Bézier curve.

## References

- [1] M. BERGER. *Geometry I, II*. Universitext. Springer-Verlag, Berlin, 1987. Translated from the French by M. Cole and S. Levy.
- [2] Blender. <http://www.blender.org/>, 2012.
- [3] E. BRIESKORN and H. KNÖRRER. *Plane Algebraic Curves*. Birk-Häuser Verlag Basel, New York, 1986.
- [4] P. CHALMOVIANSKÝ and B. POKORNÁ. Quadratic space-like Bézier curves in the three dimensional Minkowski space. *Proceedings of Symposium on Computer Geometry*, 20:104–110, 2011.

- [5] P. CHALMOVIANSKÝ and B. POKORNÁ. Planar cubic space-like Bézier curves in the three dimensional Minkowski space. *Proceedings of Symposium on Computer Geometry*, 21:93–98, 2012.
- [6] M. P. DO CARMO. *Differential Geometry of Curves and Surfaces*. Prentice Hall Inc. Englewood Cliffs, New Jersey, 1976.
- [7] G. FARIN, J. HOSCHEK, and M.-S. KIM, editors. *Handbook of computer aided geometric design*. North-Holland, Amsterdam, 2002.
- [8] O. FORSTER. *Lectures on Riemann Surfaces (Graduate Texts in Mathematics)*. Springer, 1981.
- [9] G. M. GREUEL, CH. LOSSEN, and E. SHUSTIN. *Introduction to Singularities and Deformations*. Springer-Verlag New York Inc., New York, 2007.
- [10] G. A. JONES and D. SINGERMAN. *Complex functions: an algebraic and geometric view-point*. Press Syndicate of the University of Cambridge, Great Britain, 1987.
- [11] E. KUNZ. *Introduction to plane algebraic curves*. Birkhäuser Boston Inc., Boston, MA, 2005. Translated from the 1991 German edition by Richard G. Belshoff.
- [12] S. LANG. *Complex Analysis, Fourth Edition*. Springer, New York, USA, 1999.
- [13] K. POELKE and K. POLTHIER. Lifted domain coloring. *Computer Graphics Forum*, 28(3):735–742, 2009.
- [14] B. POKORNÁ. Quadratic space-like Bézier curves in three dimensional Minkowski space. Project of Dissertation Thesis, 2012.
- [15] Python. <http://www.python.org/>, 2012.
- [16] C. T. C. WALL. *Singular points of algebraic curves*. Cambridge University Press, New York, 2012.

.....

**RNDr. Martina Bátorová, PhD.**

Department of Algebra, Geometry and Didactics of Mathematics,  
Faculty of Mathematics, Physics and Informatics, Comenius University,  
Mlynská dolina, 842 48 Bratislava, Slovakia.  
[martina.batorova@fmph.uniba.sk](mailto:martina.batorova@fmph.uniba.sk)

**doc. RNDr. Pavel Chalmovianský, PhD.**

Department of Algebra, Geometry and Didactics of Mathematics,  
Faculty of Mathematics, Physics and Informatics, Comenius University,  
Mlynská dolina, 842 48 Bratislava, Slovakia.  
[pavel.chalmoviansky@fmph.uniba.sk](mailto:pavel.chalmoviansky@fmph.uniba.sk)

**RNDr. Barbora Pokorná**

Department of Algebra, Geometry and Didactics of Mathematics,  
Faculty of Mathematics, Physics and Informatics, Comenius University,  
Mlynská dolina, 842 48 Bratislava, Slovakia.  
[barbora.pokorna@fmph.uniba.sk](mailto:barbora.pokorna@fmph.uniba.sk)

**RNDr. Miroslava Valíková**

Department of Algebra, Geometry and Didactics of Mathematics,  
Faculty of Mathematics, Physics and Informatics, Comenius University,  
Mlynská dolina, 842 48 Bratislava, Slovakia.  
[miroslava.valikova@fmph.uniba.sk](mailto:miroslava.valikova@fmph.uniba.sk)





# **MODELING SEVERAL FLUIDS WITH PRESERVED VOLUME ON AN OCTREE DATA STRUCTURE**

**Roman Ďurikovič**  
**Comenius University**

## **Abstrakt**

V článku rozširujeme metódu Marker-and-Cell (MAC) simulácie kvapalín na bunkách. V každej bunke máme zaznamenanú hustotu a tlak v strede bunky, a rýchlosti kvapaliny na každej stene samostatne v 6 smeroch. Táto metóda štandardne pracuje len s jedným typom kvapaliny. Náš prístup rozširuje metódu simulácie na viac kvapalín súčasne a preto sme navrhli modifikáciu Volume-of-Fluid (VOF) metódy, ktorá sleduje povrch kvapalín v bunke. Hodnoty VOF metódy používame na presné sledovanie povrchu kvapaliny, nutnej pre výpočet povrchového napätia, a tiež na vizualizáciu povrchu kvapaliny. Ak sa v jednej bunke nachádzajú rôzne kvapaliny počítame simulácie s jednou kvapalinou, ktorej hustota a viskozita je konštantná v bunke ale mení sa mimo bunky.

**Keľúčové slová:** dynamika kvapalín, zachovanie objemu, plávajúce objekty, octree

## **Abstract**

We simulate a one-way solid fluid interaction (either solid influences the velocity of the fluid or fluid moves the solid) that requires having fine details in the colliding areas. To cope with this problem we use an octree data structure with adaptive mesh refinement technique to enable higher level of detail and solve Navier Stokes equations for multiple fluids. We propose the technique for discretizing the equations on the octree grid yielding to a symmetric positive definite linear system.

Our approach is an extension of a well known Marker-and-Cell (MAC) fluid simulation method, within each cell we define density and pressure in center and fluid velocities on the walls separately in each 6 directions. To simulate several fluids, we propose the modification of Volume-of-Fluid (VOF) method enabling us to track the fluid surface and integrate it into the multi phase-fluid approach. A mixture of fluids is treated as a single fluid having variable density and viscosity. This scheme allows two or more fluids having different densities and viscosities to be simulated simultaneously. Values of VOF are actually used to track the fluid surface for visualization purposes and to calculate the surface tension forces acting on the fluid interfaces.

**Keywords:** volume of fluid, fluid dynamics, one-way coupling, octree, Navier-Stokes, floating objects

**Classification:** Computer graphics:Animation:Procedural animation, Physical simulation

## **1 INTRODUCTION**

Interaction between fluid and solid is very common in real world and in computer graphics animation. Common interactions between fluid and solid object can be various objects falling into water, objects

floating on the surface or acting as unmoving obstacle for the flow of fluid.

First type of interaction is one-way solid-to-fluid coupling, where the motion of solid is predetermined and is not influenced by the velocity of fluid, but the solid influences the velocity of the fluid so it can splash the water as it falls into water or it can be an unmoving obstacle.

The second type of interaction is one-way fluid-to-solid coupling, where the fluid moves the solid without the solid affecting the fluid. This is the reason why the size of the solid can be from tiny to big object without affecting the motion of the fluid.

Most interesting in the way of simulation and visual effect is the two-way coupling of solids and fluid. It is the 'real world' way of interaction, where the properties of solid, like density, are taken in count. This type of coupling is mathematically a difficult problem.

## 2 PREVIOUS WORKS

The scope of this paper deals with the visual appealing fluid simulations and therefore we commonly refer to the computer graphics papers. The full three dimensional Navier-Stokes equations were solved by Foster and Metaxas [5] for both water and smoke in computer graphics community. Big steps in efficiency were made introducing the use of semi-Lagrangian numerical techniques by Stam 1999 [7]. Another improvement of fluid-solid interaction was the introduction of tangential movement of fluid along the obstacles presented by Foster and Fedkiw 2001 [3].

Foster and Metaxas 1996 [4] demonstrate one-way fluid-to-solid coupling, where solids are treated as massless particles that move freely on the fluid surface. Yngve et al. 2000 [11] demonstrated two-way coupling of breaking objects and compressible fluids in explosions, however their technique does not apply to incompressible fluids like water. Two-way coupling on regular grid was first presented by Takahashi et al. 2002 [9], they used rigid body solver and fluid solver to achieve solid-fluid coupling. Drawback of this techniques is neglecting the dynamic forces and torques of solid objects [8]. To approximate solid-to-fluid coupling they set zero Neumann boundary conditions for the pressure at these boundaries.

There are a few researches to handle interaction of two fluids, or fluid and solid objects in computer graphics. Tanaka et al. [10] used VOF and CIP techniques to create fluid animations. They also integrated rigid body simulation into their fluid simulator. Hong and Kim [6] used the VOF method to animate bubbles in a liquid.

Our paper follows the following simulation steps:

1. Setting the time step size  $\Delta t$ .
2. Move the VOF values according to the current velocity field.
3. Solving one-way solid fluid interaction and rigid dynamics of solids.
4. Set boundary velocities on faces of obstacle cells, similarly set Neumann boundary conditions for pressure on obstacle cells.
5. Calculate intermediate velocities using the Navier-Stokes equations without taking account of the pressure term, see Eqs. 1, 2.
6. Calculate pressure field from the intermediate velocity field.
7. Make the intermediate velocity field mass-conserving to get correct velocities.
8. To generate the animation frame construct fluid surface from the VOF values according to Eqs. 3, 4.

## 3 MOTION

The main contribution towards the goal of this research is to simulate mixtures of fluids, for example a gas and liquid. We represent each fluid by a VOF function, in other words the percentage occupation of a simulation cell. The VOF function designates volume fraction of a cell, where  $F_n = 1$  means that the cell is full of  $n$ -th fluid and  $F_n = 0$  means the cell does not contain the  $n$ -th fluid. Assuming

the fluids are incompressible, then the spatial distributions of fluids has the following relation:  $\langle F \rangle = \sum_n F_n = 1.0$ , where  $F_n$  is the VOF function of  $n$ th fluid, while fluid can have different densities and viscosities,  $\rho_n$  and  $\nu_n$ .

Each simulation cell has several VOF values, the interface between two fluids lies in cells which contain several nonzero VOF values. We treat a flow of a mixture of fluids as a flow of a single fluid which have variable density and viscosity. Then, the motion of the flow is calculated using density and viscosity weighted by VOF values  $\langle \rho \rangle = \sum_n (F_n \rho_n)$ ,  $\langle \nu \rangle = \sum_n (F_n \nu_n)$ .

In this case, there are two or more fluids, and they are treated as a fluid with variable density  $\langle \rho \rangle$  and viscosity  $\langle \nu \rangle$ . Fluid is expressed by velocity field  $\mathbf{u}$ , density field  $\rho$  and pressure field  $p$ . The Navier-Stokes equations describing the multiple flow conservation of momentum then will be

$$\frac{\partial \mathbf{u}}{\partial t} = -(\mathbf{u} \cdot \nabla) \mathbf{u} + \nabla \cdot (\langle \nu \rangle \nabla \mathbf{u}) - \frac{1}{\langle \rho \rangle} \nabla p + \frac{\mathbf{f}}{\langle \rho \rangle} \quad (1)$$

$$\nabla \cdot \mathbf{u} = 0, \quad (2)$$

Here the viscosity  $\langle \nu \rangle$  is placed inside the derivative. Left hand side of the equation is the unsteady acceleration. The first term on the right hand side of equation is the convective acceleration. The other terms following the acceleration are the forces such as the pressure gradient force, the viscosity force and other external forces  $\mathbf{f}$ . The conservation of mass, Eq. 2, can be written in the other way as

$$\nabla \cdot (\langle \rho \rangle \mathbf{u}) = -\frac{\partial \langle \rho \rangle}{\partial t}.$$

We can interpret the second equation such that the total of mass flow out of a small region is negative of mass change of the region.

### 3.1 Surface Tension from VOF

Accurate calculation of the surface tension effect needs well-defined fluid interfaces. Although our simulator does not consider actual shape of the interface, a model called continuum surface force (CSF) can be used to approximate the surface force without that information [1]. Method is based on volume force that converges to surface force as the grid size becomes smaller.

We propose the extension of this idea to multiple fluids as well. Surface force,  $\mathbf{f}_n^{sv}$ , exerted by fluid  $n$  based on the VOF value,  $F_n$ , is written as

$$\mathbf{f}_n^{sv} = \sigma_n \kappa_n \nabla F_n,$$

where  $\sigma_n$  is surface tension coefficient, and  $\kappa_n$  is curvature of the fluid surface. The normal and curvature of the surface can be calculated from VOF values as  $\mathbf{n}_n = \nabla F_n$ ,  $\kappa_n = -(\nabla \cdot \hat{\mathbf{n}}_n)$ , where  $\hat{\mathbf{n}}_n = \mathbf{n}_n / |\mathbf{n}_n|$  represents unit normal vector. Curvature  $\kappa_n$  is defined at center of a cell. However, as normal is a vector quantity, components of  $\hat{\mathbf{n}}_n$  are separately defined on faces of a grid cell, and they must be interpolated to obtain values at other positions. For example,  $x$ -component of a normal vector defined on center of right face on grid cell  $(i, j, k)$  with the cell size in  $x$  direction  $dx$  will be

$$n_{i+1/2,j,k}^{nx} = \frac{F_{n,i+1,j,k} - F_{n,i,j,k}}{dx},$$

and its  $y$ -component can not be calculated directly from VOF but by interpolation of known  $y$ -components normals at the neighboring parallel faces on a grid cell:  $n_{i+1/2,j,k}^{ny} = \frac{1}{4}(n_{i,j-1/2,k}^{ny} + n_{i+1,j-1/2,k}^{ny} + n_{i,j+1/2,k}^{ny} + n_{i+1,j+1/2,k}^{ny})$ . Now, we are almost ready to calculate the surface force  $\mathbf{f}_n^{sv}$  on each cell face. To get the curvature defined on a face between two cells we need to interpolate two cell-centered curvatures. Finally, surface forces for all fluids are accumulated and added to the external forces  $\mathbf{f}^{ext}$ :

$$\mathbf{f} = \sum_n \mathbf{f}_n^{sv} + \mathbf{f}^{ext}.$$

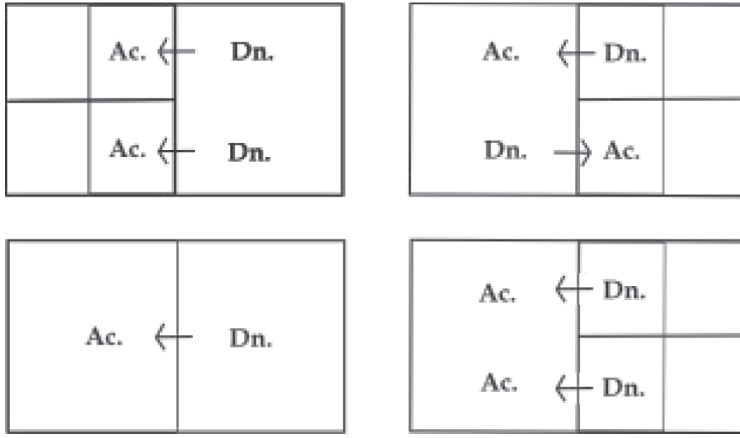


Fig. 1. Donor-Acceptor situations. Left column: donor cell is a single cell and the acceptor cells are on the left side. Right column: a single cell on the right serves as acceptor or has a double functionality donor/acceptor.

## 4 PROPOSED MULTIPLE FLUID VOF

As a method of surface tracking we choose VOF method based on step function  $F$ , presented by Durikovic, Numata [2]. Our previous surface tracking method worked primarily for a regular grid structure. The contribution of our work here is to extend the VOF method for multiple fluids on an adaptive octree cell structure consisting of different cell sizes. The problem we are facing here is that a single face of a bigger cell can touch two smaller cells in octree cell structure. Therefore we introduce the term of common surface area the smaller area of the two faces and calculate the fluid stream passing two smaller faces rather than one big face. Value  $F$  is changed by the velocity of fluid on cell faces, to compute it we use donor-acceptor schema. The approximation by finite differences would “blur” the surface of fluid so the sharp profile of surface detail is lost.

We outline the computing of VOF. Volume of stream that flows from donor to acceptor is  $|V_i| = u_i \Delta t \Delta S_{ss}$ , where  $u_i$  is the normal velocity on the face of cell  $i$  and the sign of velocity defines whether the cell is donor or acceptor. The  $\Delta S_{ss}$  is the common surface area between donor and acceptor, i.e. the smaller area of the two faces. Let us note  $F_{in}$  the fluid fraction of  $n$ -th fluid in cell  $i$ . Volume of fluid  $n$  that flows through face of the cell in time step  $\Delta t$  is

$$|V_n| = \min \{ F_{in}^{AD} |V_i| + CF_{in}, F_{in}^D |V_D| \}, \quad (3)$$

where

$$CF_{in} = \max \{ (1 - F_{in}^{AD}) |V_i| - \left( \sum_i F_{in}^D - F_{in}^D \right) |V_D|, 0 \}. \quad (4)$$

Indexes  $D$  and  $A$  denote donor and acceptor while double index  $AD$  denotes donor or acceptor by the orientation of interface in respect of direction of the flow. The minimum in Eq. 3 restrains the cell to give away more fluid it has and the maximum in Eq. 4 assures additive flow  $CF$  if volume that should be transferred is larger than accessible. Few examples of donor acceptor situations are shown in Figure 1. A single donor can donate the fluid to a single acceptor, Figure 1 left-bottom, or to two acceptor cells, Figure 1 left-top. Two smaller cells can serve as donor to a single acceptor cell, Figure 1 right-bottom. The mixed situation can happen when a large cell serves both as a donor and acceptor to two smaller neighboring cells, Figure 1 right-top.

It can happen that if some cell has the  $F_{in} > 0$  then we proportionally distribute excess fluid back to donor cells. The whole process runs for all cells in volume from top to bottom and should be repeated till no change in  $F_{in}$  values occurs.



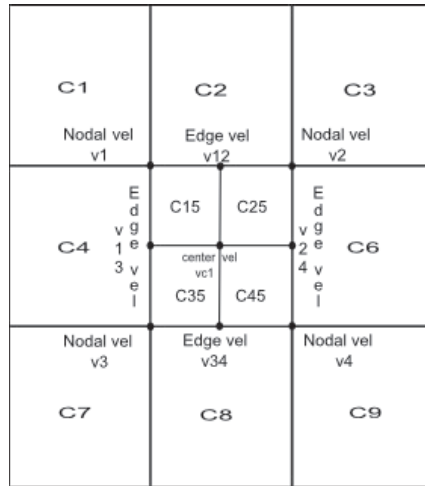


Fig. 2. Velocity computation by trilinear interpolation.

## 5 OCTREE GRID

In our simulation we propose to use the octree data structure. Advantages of this approach are less computational demands at preservation of level of details. We use the ability of adaptive mesh refinement (AMR) in visually pleasant sections. Disadvantage is the necessity of recomputing the velocity, density, pressure and VOF values when changing the level of octree.

### 5.1 Velocity Computation

We show the method of velocity re-computation at the center of  $C5$  on a 2D example in Figure 2. The cell  $C5$  was split by octree method into four equal sub-cells.

First, we compute the nodal velocities on  $C5$  which are  $v_1, \dots, v_4$ . Nodal velocity is an average of velocities on faces that are incident on the node. Next, we compute edge velocities  $v_{12}, v_{13}, v_{24}, v_{34}$  as an average of adjacent nodal velocities. Average of edge velocities gives us central velocity  $v_{c1}$  at face  $C5$ . The final velocities of new sub-faces of face  $C5$  are average of their nodal velocities:

$$c15 = \frac{v1 + v12 + vc1 + v13}{4}. \quad (5)$$

The remaining three sub-face velocities are computed similarly.

Other way around, when combining 4 faces into a single face by octree method we just average their velocities.

### 5.2 Density and Pressure

Pressure and density are constants defined at the cell center. When dividing a single cell into sub-cells we just set the respective values of sub-cell for pressure and density equal to the parent cell. When combining cells into a parent cell we set the pressure and density parameters as average of child cells.

### 5.3 VOF Computation

When combining child cells indexed  $i = 1, \dots, 8$  to a parent cell the final VOF value is given as the weighted average of child VOF values

$$F_n = \frac{\sum_{i=1}^8 F_{i_n} |V_i|}{|V|}. \quad (6)$$

Dividing of parent cell into cells indexed  $i = 1, \dots, 8$  is a little more complex problem because we need to be sure there won't be any holes within the fluid after cell dividing. The value of VOF of the child cell is

$$F_{i_n} = \min \left( 1.0, 8F_n \frac{\sum_{neigh(i)} F_{s_n}}{\sum_{j=1}^8 \left( \sum_{neigh(j)} F_{s_n} \right)} \right), \quad (7)$$

where  $n$  is the index of the fluid,  $i$  is the index of child cell and  $s$  is the index of neighbor of child cell. Neighbor of cell is every cell that has common face with child cell  $i$  and one neighbor cell with common node. None of these neighbors is another child cell.

## 6 IMPLEMENTATION

In our simulation, we simplify the movement of solid objects to translation and rotation of the centre of the mass  $CM$ , with position and orientation matrix saved as global variables. Due to the grid representation of fluid with known velocities at grid points we represent the floating object as a set of grid cells lying on the object surface.

First, we have to calculate the forces acting on our solid in a grid cell  $i$ . For floating objects, we have three possible types of forces which can act on the object: gravitation force, buoyancy force, and resistance force.

**Gravitation force** is computed by the following equation:  $F_{Gi} = M_s \cdot g$ , where  $M_s$  is the mass of the object  $s$  and  $g$  is the gravitational acceleration.

**Buoyancy force** is calculated as:  $F_{Bi} = gV_s D_f$ , where  $V_s$  is the volume of object  $s$ .  $D_f$  is temporary density computed every simulation step as

$$D_f = \frac{\sum_i d_i \cdot V_i}{\sum_i V_i}, \quad (8)$$

where  $i$  is the index of fluid cell that contains at least one of the points representing the floating object.  $V_i$  is the volume of the cell  $i$ , and the  $d_i$  is the density of the fluid cell.

**Resistance force** is calculated in the fluid cells that contain points representing the object from the velocities of fluid and object known from previous simulation step. Resistance force is  $F_{Ri} = \frac{1}{2} C S \rho v^2$ , where  $S$  is the surface of the floating object,  $C$  is the resistance constant depending on the shape of the object,  $\rho$  is the density of fluid in the cell  $i$ , and  $v$  is the relative velocity of the object to water. The relative velocity is the difference between the fluid velocity and the object velocity.

It is easy to find the vector from the point of force activity to the  $CM$ , because we save the  $CM$  position. The vectors of gravitation and buoyancy are contra-directional to that direction, while gravitation force acts downwards on the  $z$  axis, and buoyancy force acts upward on the  $z$  axis. We sum the forces to find the total force and torque. After solving the dynamics of the solid object, as explained in the previous section, we update the position of floating object and all of its surface reference points.

## 7 RESULTS

The results of our simulation are stored in series of xml files. One xml file for each simulation step and one PovRay [2] file, where the positions of obstacles are defined are combined to form the scene

file that is rendered by PovRay raytracing program. Figure 3 shows interaction of two fluids air and water with static obstacle. The second example in Figure 4 shows the water floating down the stairs in air fluid. Following tables show initial parameters and sizes of the scenes.

Bubble in a fluid [# of cells]		
	Start	End
total	512	512
air fluid (bubble)	91(27)	91(3)
water fluid	389	389
obstacles	32	32
# of time steps	50	
time of computation	8 [sec]	
Fluid falling down the stairs [# of cells]		
	Start	End
total	512	512
air fluid	48	48
water fluid	374	374
obstacles	90	90
# of time steps	70	
time of computation	10 [sec]	

Number of cells occupied by air and water fluid stays the same at the start and the end, that shows conservation of volume in this case. For both scenes fluids with properties shown in following table were used.

Fluids			
Fluid	Density	Viscosity	Tension
air	$0.1 [kg/m^3]$	$1 [Pa \cdot s]$	$0 [N/m]$
water	$10 [kg/m^3]$	$0.1 [Pa \cdot s]$	$35 [N/m]$

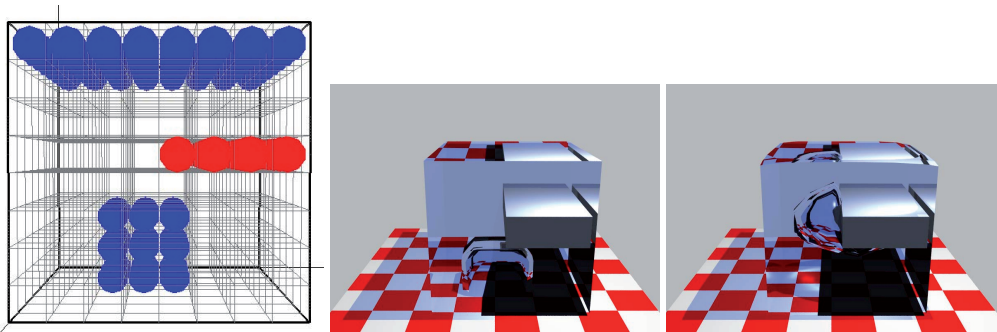


Fig. 3. Bubble. Left: the grid cells occupied by obstacle and fluids, the rest images are the key-frames from animation. There are two fluids used in the simulation air and the water.

Figure 5 shows interaction of two fluids air and water with a flowing cylinder. Cylinder movement is fully influenced by the velocity of two fluids.

## 8 CONCLUSION

In this paper we presented simulation of multiple fluid on adaptive grid particularly the octree structure. We have shown how to rewrite the update equation for the velocity, density, pressure and VOF values during the cell subdivision or cells gluing.

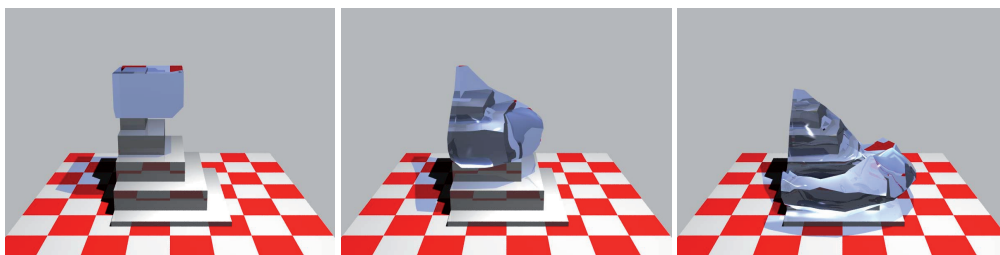


Fig. 4. Fluid falling down the stairs. There are two fluids used in the simulation air (was not rendered) and the water.

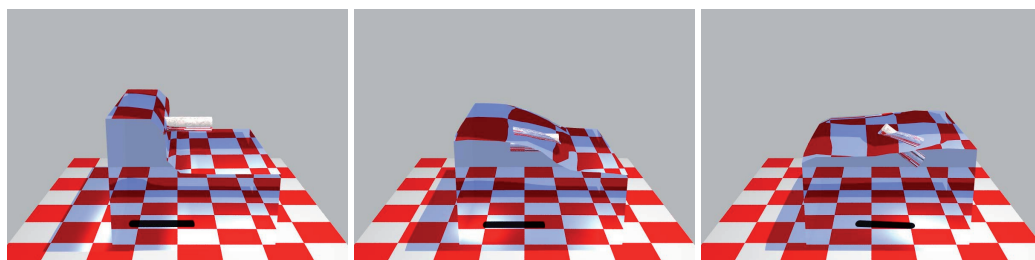


Fig. 5. Floating object in two fluids mixture. There are two fluids used in the simulation air (was not rendered) and the water.

Our results show that the volume of fluid is preserved in each simulation step, i.e. volume is not lost.

## References

- [1] J. U. Brackbill, D. B. Kothe, and C. Zemach. A continuum method for modeling surface tension. *J. Comput. Phys.*, 100(2):335–354, 1992.
- [2] Roman Durikovic and Katsuhiro Numata. Preserving the volume of fluid using multi-phase flow approach. In *Proceedings of the International Conference on Information Visualisation*, pages 757–760, Los Alamitos, CA, USA, 2006. IEEE Computer Society.
- [3] Nick Foster and Ron Fedkiw. Practical animation of liquids. In *Proceedings of SIGGRAPH 2001, Computer Graphics, Annual Conference Series*, pages 23–30, ACM SIGGRAPH, August 2001.
- [4] Nick Foster and Dimitris Metaxas. Realistic animation of liquids. *Graphical Models and Image Processing*, 58(5):471–483, 1996.
- [5] Nick Foster and Dimitris Metaxas. Modeling the motion of a hot, turbulent gas. In *SIGGRAPH '97: Proceedings of the 24th annual conference on Computer graphics and interactive techniques*, pages 181–188, New York, NY, USA, 1997. ACM Press/Addison-Wesley Publishing Co.
- [6] Jeong-Mo Hong and Chang-Hun Kim. Animation of bubbles in liquid. *Computer Graphics Forum*, 22(3):253–253, 2003.
- [7] Jos Stam. Stable fluids. In Alyn Rockwood, editor, *Siggraph 1999, Computer Graphics Proceedings*, pages 121–128, Los Angeles, 1999. Addison Wesley Longman.
- [8] Tsunemi Takahashi, Hiroko Fujii, Atsushi Kunimatsu, Kazuhiro Hiwada, Takahiro Saito, Ken Tanaka, and Heihachi Ueki. Realistic animation of fluid with splash and foam. *Computer Graphics Forum*, 22(3):391–400, 2003.
- [9] Tsunemi Takahashi, Heihachi Ueki, Atsushi Kunimatsu, and Hiroko Fujii. The simulation of fluid-rigid body interaction. In *SIGGRAPH '02: ACM SIGGRAPH 2002 conference abstracts and applications*, pages 266–266, New York, NY, USA, 2002. ACM.



- [10] Ken Tanaka, Heihachi Ueki, and Atsushi Kunitatsu. The cubic interpolated level set method for realistic fluid animation. In *SIGGRAPH '03: Proceedings of the SIGGRAPH 2003 conference on Sketches & applications*, pages 1–1, New York, NY, USA, 2003. ACM Press.
- [11] G.D. Yngve, J.F. O'Brien, and J.K. Hodgins. Animating explosions. In *Proceedings of SIGGRAPH 2000, Computer Graphics, Annual Conference Series*, pages 29–36, ACM SIGGRAPH, July 2000.

**Prof. RNDr. Roman Ďurikovič, PhD.**

Dept. of Applied Informatics,  
Faculty of Mathematics, Physics and Informatics,  
Comenius University,  
842 48 Bratislava, Slovak Republic;  
<http://www.sccg.sk/~durikovic>  
e-mail: [roman.durikovic@fmph.uniba.sk](mailto:roman.durikovic@fmph.uniba.sk)



# VALIDATION OF THE VIRTUAL GONIO-SPECTROPHOTOMETER BASED ON THE REAL MEASUREMENTS

*Andrej Mihálik, Roman Ďurikovič*

*Comenius University*

## Abstrakt

Navrhli sme virtuálny gonio-spektrofotometer schopný merať spektrum odrazeného svetla od povrchu materiálu, ktorý je reprezentovaný dvojsmernou distribučnou funkciou (BRDF). Náš virtuálny gonio-spektrofotometer je možné prispôbiť na merania spĺňajúce normy ako sú ISO 2813 alebo ASTM D523. Ukážeme aplikáciu navrhovaného virtuálneho gonio-spektrofotometra na ohodnotenie počítačovej reprezentácie vzhľadu materiálu použitím výsledkov meraní v laboratóriu. Virtuálny gonio-spektrofotometer je overený vzhľadom na merania získané reálnym gonio-spektrofotometrom, kde boli použité reálne vzorky materiálu. Prezentované overovanie je dosiahnuté porovnávaním celkového žiarivého toku odrazeného od reálnej vzorky a výpočtu prevedeného použitím matematickej reprezentácie vzorky ako je BRDF.

**Kľúčové slová:** meranie vzhľadu, lesk, BRDF

## Abstrakt

A virtual gonio-spectrophotometer is proposed to perform measurements of the reflectance spectrum of material surfaces mathematically represented by the bidirectional reflectance functions (BRDF). Our virtual gonio-spectrophotometer can be customized to allow measurements obeying industrial standards such as ISO 2813 or ASTM D523. We demonstrate the application of proposed virtual Gonio-spectrophotometer for the evaluation of digital representation of the material appearance utilizing laboratory measurements. Virtual gonio-spectrophotometer is validated according to measurements obtained with real gonio-spectrophotometer, where real material samples have been used. Presented validation is performed by measuring the total radiant flux reflected from real sample and comparing it to the mathematical representation of sample by BRDF.

**Keywords:** appearance measurements, gloss, BRDF

**Classification:** Rendering, Reflectance modeling

## 1 Introduction

The object appearance is determined by its surface geometry and the light scattering from it. To measure the surface properties, the gonio-spectrophotometers was developed [2]. A gonio-spectrophotometer is an instrument measuring the spectral distribution of reflected radiant power as a function of angles

of illumination and observation. The device consists of a light source aperture and a receptor enabling to orient them in variety of directions to perform comprehensive measurements.

Variety of the empirical models, that describe the reflection off the surface exist. An example is the empirical Wards's model [10], that uses the combination of functions capturing the reflection attributes such as the diffuse reflectance in all directions or the concentration of light scattering in a direction near the specular direction for glossy materials. Besides the empirical models, another sort of BRDF models exist applying the basic principles of physics to the surface microscopic structure, for example the Cook-Torrance's reflection model [3].

Manufacturers in industry often need to characterize the appearance of their products (eg. paint finish). Because of the complexity of full BRDF acquisition, it is more reasonable to relay on simple measurements often used in industry; those are for example, industrial spot measurement devices, such as colorimeters or glossmeters has been developed [4]. Glossmeters are build according to industrial standards such as ISO 2813 [8] or ASTM D523 [1], that define the geometry of specular gloss measurement including the incidence angles of light, and optics [7]. Gloss is the appearance attribute of surfaces that causes them to have appearance from shiny to mat. We can measure it by focusing on the light reflected off the surface and neglecting the material structure. Industrial standards prescribe black glass as a standard for the calibration of the gloss measuring devices. Perception of the gloss is influenced by physiological and psychological aspects of the human vision. Some psychophysically-based models of surface gloss have been found by multi-dimensional scaling algorithms based on the subjective evaluation of the images [12] [6].

Our goal is to design and implement the methodology devoted to the measurement, analysis and simulation of gloss and spectral reflectance from samples represented by BRDF. In practice, these measurements are generated by industrial devices using real material samples. Our task is to define the properties of a virtual surface generally represented by a BRDF and perform the measurements with the virtual device, simulating the real measurement device. Thus the obtained virtual measurements can be compared with actual measurements on real samples and afterwards we can evaluate the precision of virtual representation (model) of a surface scattering.

With the aim to find correspondence between the parameters of designed reflectance model and industrial measurement scales for albedo and gloss used by glossmeters and colorimeters, a concept of virtual gonio-spectrophotometer can be used. Virtual samples in such concept are represented by an analytical reflectance model and their parameters and complexity can be easily varied. Simulations can be further utilized for study of surface reflectance properties in many standardized scenarios.

Analytical model defines the scattering profile at a single point. Unfortunately, the measurement devices are unable to process a single ray or do the measurement at single point of the sample, therefore the virtual device should also do the measurements on a very small area corresponding to the real devices [11].

The remaining of this paper is organized as follows. In Section 2 we introduce definitions needed in our concept, in Section 3 we define the real measurement device measuring the optical characteristics of the material surface. Section 4 introduces the optical properties of a sample and properties of the light source required in our measurement concept. Proposed virtual device is described in Section 5. In Sections 6 and 7 we demonstrate some measurements on real samples and measurements on their respective virtual representations. In Section 8 we conclude our work by discussing the comparison of the virtual and real measurements.

## 2 Theoretical Background

To make physically-based numerical definitions, we need to define various expressions for how incident light energy is distributed by a material with respect to the position, direction, and wavelength.

The power radiated is referred to as the radiant flux  $\Phi$ . To find the flux  $\Phi(t)$  at a particular instant,

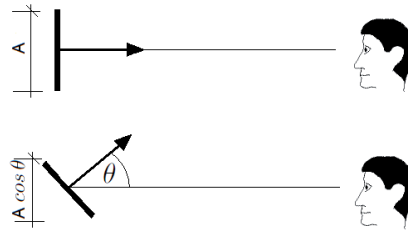


Fig. 1. The apparent size of a surface  $A$  is larger when it is projected in the direction of its surface normal, than when it is projected in a direction at an angle  $\theta$  to the normal.

we consider differential period of time  $dt$ . The differential amount of energy  $dQ$  transferred in  $dt$  is:

$$\Phi(t) = \frac{dQ}{dt}. \quad (1)$$

The average flux leaving per unit area, or radiant exitance  $M$ , is the total flux leaving divided by surface area  $A$ , or

$$M = \frac{\Phi}{A}. \quad (2)$$

To express the radiant exitance from a particular point  $(x, y)$  of the area, consider area around this particular point. By considering the infinitesimally small area  $dA$ , we can define the radiant exitance  $M(x, y)$  at a particular position:

$$M(x, y) = \frac{d\Phi(x, y)}{dA}. \quad (3)$$

This denotes the energy of light emitted from the point at coordinates  $(x, y)$  per second per unit area.

The radiant energy per unit time and area arriving at a surface is called the *irradiance*  $E$ . It is defined in the same manner as  $M$ , with the only difference being whether the radiant energy is approaching or leaving the surface.

To include directional effects, we should consider how the point of view affects perception of an area. When viewing direction is perpendicular to a patch then perceived area of this patch is greater than perceived area of a patch viewed at a more glancing angle, see Figure 1. Since we are dealing with infinitesimally small patches then, we can omit perspective deformation. Therefore the value of reduced area can be computed using orthogonal projection. Such projection is achieved by multiplication of the area by  $\cos \theta$ .

The key quantity radiance in a particular direction  $\Theta$  is defined as the radiant flux per unit solid angle and unit area projected in the direction  $\theta$  (angle between surface normal and direction  $\Theta$ ). The radiance  $L$  is defined as:

$$L(x, y, \Theta) = \frac{d\Phi(x, y, \Theta)}{\cos \theta dA d\omega}, \quad (4)$$

where  $d\omega$  is the solid angle. Solid angle is equal to the area of the segment of unit sphere.

The flux  $d\Phi(x, y, \Theta)$  is a fragment of flux  $d\Phi(x, y)$  emitted from infinitesimally small patch at  $(x, y)$ , which exits unit sphere through the solid angle  $d\omega$  in the direction  $\Theta$ , see Figure 2. Although rays emitted from a patch to an area of the solid angle may have not particular direction, when patch and solid angle become infinitesimally small, only rays from patch with the specific direction reach the area of the solid angle.

The other variable that we want to account for in addition to time, position, and direction, is a wavelength. To express flux, irradiance, radiant exitance, intensity, or radiance as a function of



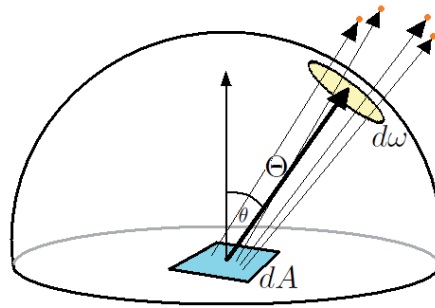


Fig. 2. Flux of the light emitted from the area  $dA$  exiting unit sphere through the solid angle.

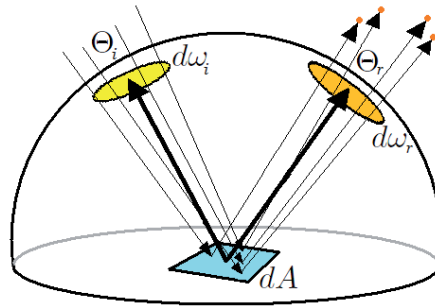


Fig. 3. Flux of the light entered unit sphere through  $d\omega_i$  and reflected from the area  $dA$  through solid angle  $d\omega_r$ .

wavelength, we consider the quantity at a value of  $\lambda$  within a small band of wavelengths between  $\lambda$  and  $\lambda + d\lambda$ . By associating a  $d\lambda$  with each value, we can integrate spectral values over the whole spectrum.

To describe how a surface redirects light, we consider light incident on the surface at  $\mathbf{x} = (x, y)$  with radiance  $L(\lambda, \mathbf{x} \leftarrow \Theta_i)$  (arrows mean that the light is emitted into particular direction from the surface point or is incident at the surface point, respectively) within a differential solid angle  $d\omega_i$ . The irradiance  $dE_i$  on the surface that will be either absorbed or redirected is:

$$dE_i(\lambda, \mathbf{x} \leftarrow \Theta_i) = L(\lambda, \mathbf{x} \leftarrow \Theta_i) \cos \theta_i d\omega_i. \quad (5)$$

The  $\cos \theta_i$  term appears because the radiance  $L$  means energy per unit area  $dA$  in the direction of travel  $\Theta_i$ , and that direction projected into the orientation of the surface we are considering is  $\cos \theta_i dA$ . The  $d\omega_i$  term enters in because we want to know the effect of energy coming from a single direction representing a differential section of all the possible directions above the surface. The light reflected by the surface in each direction can be described by the radiance in each direction. The effect of a material redirecting light is then given by a function that is the ratio of the radiance reflected in a particular direction  $\Theta_r$  as a result of the total incident flux per unit area from another direction  $\Theta_i$  as shown in Figure 3. This ratio is referred to as the BRDF defined by

$$f_r(\lambda, \mathbf{x}, \Theta_i \rightarrow \Theta_r) = \frac{dL_r(\lambda, \mathbf{x} \rightarrow \Theta_r)}{dE_i(\lambda, \mathbf{x} \leftarrow \Theta_i)}. \quad (6)$$

The BRDF is a distribution function, not a reflectance. It describes how the radiance is distributed in different directions, rather than expressing the fraction of energy reflected.

For physically correct BRDF, the fraction of the energy reflected to all directions from light incident in one direction must be between 0 and 1 if the surface is not emitting light

$$0 \leq \int_{\omega_r} f_r(\lambda, \mathbf{x}, \Theta_i \rightarrow \Theta_r) \cos \theta_r d\omega_r \leq 1. \quad (7)$$

## 2.1 Fresnel Reflectance

The Fresnel equations describe the amount of light is reflected and refracted at a perfectly smooth surface between two media.

The equations from the wave optics and polarization of light has to be considered. Key components of the Fresnel equations are the reflection coefficient (usually denoted  $F_r$ ), that gives the fraction of incident light that is reflected and the transmission coefficient  $F_t$ , that gives the fraction that is refracted. For parallel polarized light (p-polarized, the electric field oscillates in the plane of incidence) reflection coefficient is defined as:

$$r_{\parallel} = \frac{n_2 \cos \theta_i - n_1 \cos \theta_t}{n_2 \cos \theta_i + n_1 \cos \theta_t}. \quad (8)$$

For perpendicular polarized light (s-polarized, electric field oscillates perpendicular to plane of incident) it is:

$$r_{\perp} = \frac{n_1 \cos \theta_i - n_2 \cos \theta_t}{n_1 \cos \theta_i + n_2 \cos \theta_t}. \quad (9)$$

Here  $\theta_i$  and  $\theta_t$  are the angles between the surface normal and the directions of the incident and transmitted beams, and  $n_1$  and  $n_2$  are the indices of refraction of the media on the incident and transmitted side of the surface.

Note that  $r_{\parallel}$  and  $r_{\perp}$  describe the relationship between the amplitudes of the involved electric fields. For unpolarized light the reflection coefficient is

$$F_r = \frac{r_{\parallel}^2 + r_{\perp}^2}{2}. \quad (10)$$

The transmission coefficient is then

$$F_t = 1 - F_r. \quad (11)$$

Real materials are not perfect insulators. Therefore their index of refraction incorporates extinction coefficient  $k$ , that indicates the amount of absorption loss when the electromagnetic wave propagates through the material. Thus index of refraction can be written in complex form:

$$\hat{n} = n + ik, \quad (12)$$

where  $n$  is the refractive index indicating the phase velocity.

## 2.2 Cook-Torrance Reflectance Model

The Cook-Torrance model is a physically-based microfacet model that is focussed on (glossy) specular reflection [3]. It uses the surface roughness model developed by Torrance & Sparrow in [9]. This model treats surface as a collection of microscopic facets. The macroscopic optical properties of a surface are then analytically derived from properties of individual facets and statistical distributions of such properties.

Although, the surface has a normal  $\mathbf{N}$ , at a microscopic level the surface has height variations that result in many different surface orientations at a detailed level. At the perfectly flat surface a viewer is

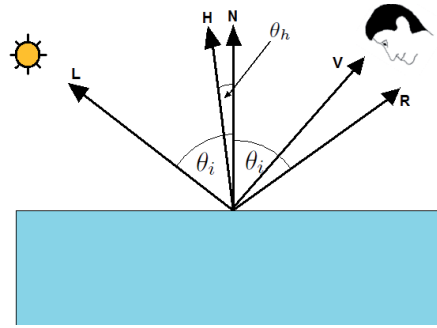


Fig. 4. The geometry of reflection showing the angle  $\theta_i$  between the surface normal  $\mathbf{N}$  and the direction of illumination  $\Theta_i \equiv \mathbf{L}$ .

able to see light source at the point where halfway vector  $\mathbf{H}$  is in the direction of an average surface normal  $\mathbf{N}$ . Halfway vector  $\mathbf{H}$  is a bisector of the angle between the direction of illumination  $\Theta_i \equiv \mathbf{L}$  and the viewer direction  $\Theta_r \equiv \mathbf{V}$ , see Figure 4.

Rather than explicitly model the small geometric features, general reflectance functions use statistical models. Statistical models are used because the variation in surface height is assumed to be irregular and random. A statistical model for surfaces in reflectance models generally takes the form of giving the distribution of facets that have a particular slope. The facet slope distribution function  $D$  represents the facets that are oriented in the direction  $\mathbf{H}$ . Let us consider parameter  $m$ , which is the root mean square slope of microfacets parameterizing the surface's roughness. Smaller values of  $m$  produces more specular appearance.

The commonly used distribution is the Beckmann distribution function. It is based on physical theory on scattering of electromagnetic waves and does not require the introduction of arbitrary constants. The formula is:

$$D = \frac{e^{-\frac{\tan^2 \alpha}{m^2}}}{m^2 \cos^4 \alpha}, \quad (13)$$

where alpha is the angle between the normal vector  $\mathbf{N}$  and the half vector  $\mathbf{H}$ .

If we assume V-grooved surface (Figure 5), then we need to count with self-shadowing and masking. The geometric attenuation factor  $G$  models the geometric effects shadowing and masking between microfacets that occur at larger angles of incidence or reflection. It is defined by the formula:

$$G = \min\left(1, \frac{2(\mathbf{H} \cdot \mathbf{N})(\mathbf{V} \cdot \mathbf{N})}{\mathbf{H} \cdot \mathbf{V}}, \frac{2(\mathbf{H} \cdot \mathbf{N})(\mathbf{L} \cdot \mathbf{N})}{\mathbf{H} \cdot \mathbf{V}}\right). \quad (14)$$

The Cook-Torrance model provides a good reproduction of the appearance of many real materials. Especially, metallic surfaces profit from the increased realism of the specular factor. Effects like the characteristic color shift towards the color of the incident light near grazing angles and the off-specular peak for very rough surfaces greatly improve the perceived realism of renderings. The off-specular peaks are the consequence of shadowing and masking causing asymmetries.

Combination of diffuse and specular component of Cook-Torrance's model can be written as:

$$f_r(\Theta_i \rightarrow \Theta_r) = \frac{k_d}{\pi} + k_s \frac{F_r D G}{\pi \cos \theta_i \cos \theta_r}, \quad (15)$$

where  $k_d + k_s \leq 1$ ,  $\theta_r$  is the angle between  $\mathbf{N}$  and  $\mathbf{V}$ , and  $F_r$  is Fresnel term given by the Equation 10. We assume mirrorlike microfacets which are reflecting the light from a source to the viewers direction just in constellation where  $\mathbf{H}$  is microfacet's normal.

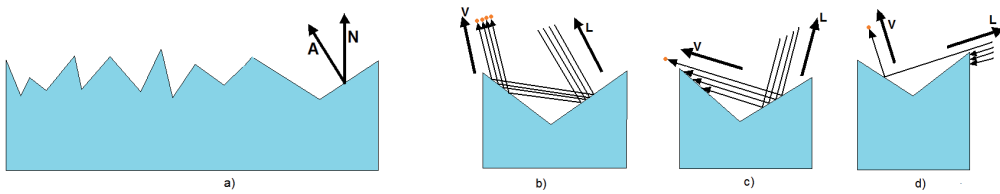


Fig. 5. Microfacet geometry. (a) Surface composed of microfacets with average normal  $N$ . Interaction between microfacets: (b) interreflection, (c) masking, (d) shadowing.

### 3 Definition of the Gonio-spectrophotometer

The measurement of the BRDF requires a system that consists of a light source, positioning system to hold a sample of the material, and a sensor that records the quantity of light scattered from the material. The measurement is performed usually by the measuring device such as gonio-spectrophotometer. A gonio-spectrophotometer is defined as an instrument that measures spectral power as a function of illumination and observation directions. The light flux that is incident on the material sample comes from an emitter. After being reflected by the surface, it is captured by a detector (spectrophotometer). For BRDF measurements the detector is placed on hemisphere above the sample. The device requires to move the receptor aperture and the light source. Both, the direction of illumination  $\Theta_i$  and viewing direction  $\Theta_r$  (see Figure 3) can be varied independently within the hemisphere above the material sample. The reflected flux is recorded for each position of the source and detector aperture. Number of positions depend on the angular accuracy of recorded BRDF. Since BRDF is reciprocal, that means we get the same results when we exchange the source and receptor aperture, the number of positions should be reduced to the half.

### 4 Required inputs

Proposed virtual gonio-spectrophotometer requires two inputs, a description of the spectrum of the illuminant and a description of the reflectance of the virtual surface described by the BRDF.

Illuminant is defined by its *spectral power distribution* (SPD). SPD is a representation of the radiant power emitted by a light source as a function of wavelength.

Although our implementation allows arbitrary SPD of the light source, in our experiments we use standard illuminant  $D_{65}$  sampled at 5nm intervals. Illuminant  $D_{65}$  defined by the International Commission on Illumination (CIE) represents the noon daylight with a correlated color temperature of approximately 6500 K.

To measure radiant flux reflected off the surface we need a description of how surface reflects the light in dependence of the angle of the illumination. Such distribution could be ensured by BRDF such as Cook-Torrance's BRDF.

In our experiments we have used complex refractive index of real materials as a function of the wavelength. This has been used to compute Fresnel term in analytical BRDF used in virtual measurements.

### 5 Virtual Gonio-spectrophotometer

In the simulation of gonio-spectrophotometer, the hemisphere over the sample is subdivided into small patches. Proposed virtual-goniospectrophotometer consists of light source and detector aperture. A patch belongs to the source or detector aperture (see Figure 6) if its position is close (within adjustable



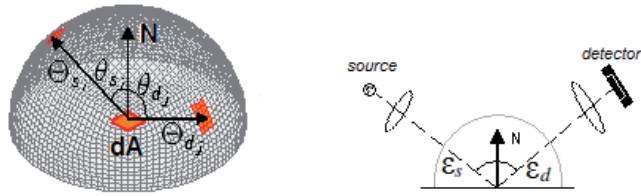


Fig. 6. Subdivided hemisphere and the geometry of the measurement. Angles  $\epsilon_s$  and  $\epsilon_d$  are angles between the surface normal and the direction to the center of source aperture and detector aperture, respectively.

tolerance which represents size of apertures) to direction of the illumination  $\Theta_i$  or observation  $\Theta_r$ , respectively.

Total flux reflected from the sample surface is computed by the sum of incident flux from the source aperture patches (from each source aperture patch in direction  $\Theta_{i_k}$ ) reflected toward the detector aperture patches (to each detector aperture patch in direction  $\Theta_{r_l}$ ). Thus total flux captured by the receptor aperture is computed by the numerical integration over the source and detector patches (adding the energy reflected from each patch  $i_k$  toward each patch  $r_l$ ).

To perform the integration over these apertures, we project them onto unit hemisphere. Then we subdivide hemisphere into the small patches (see Figure 6). Each patch area of the hemisphere serves us as the solid angle fraction. Particular radiant flux is coming through all source patches, that are incident with the surface. For each receptor patch, the contribution of reflected flux to this patch is computed. This leads to double summation, over the source and over the receptor aperture. The amount of energy reflected from the source to the receptor is determined by the BRDF. Total flux at a particular wavelength  $\lambda$ , reflected from patch at the surface area  $dA$  reaching detector aperture is computed by following formula:

$$\Phi = dA \sum_k L(\mathbf{x} \leftarrow \Theta_{i_k}) \cos(\theta_{i_k}) \Delta\omega_{i_k} \times \sum_j f_r(\lambda, \mathbf{x}, \Theta_{i_k} \leftarrow \Theta_{r_l}) \cos(\theta_{r_l}) \Delta\omega_{r_l}, \quad (16)$$

where  $dA$  is area of a patch at the surface,  $\Delta\omega$  (index  $i$  refers to the source patches, index  $r$  refers to the detector patches) is area of particular patch on the hemisphere,  $\Theta$  is the direction from surface patch to the particular patch on the hemisphere,  $\theta$  is the angle between the surface normal and that direction, see Figure 6. Function  $f_r$  is BRDF and  $L$  is incident radiance, where fragment of the radiant flux  $\Phi$  is determined by the spectral energy of the light source.

The real measurement devices such as glossmeters can not measure the light reflection at a single point of the sample, but rather they measure reflection in a small region. Inhomogeneous surfaces such as metallic or pearlescent varnishes have varying  $f_r$  at each surface point. This can happen often when there is a drawing on the surface, for example. It is therefore necessary to divide the sample into smaller parts and make a calculation in each of its parts.

## 6 Real Measurements

To validate our virtual gonio-spectrophotometer, firstly, we calibrate our virtual gonio-spectrophotometer using real measured black glass. With calibrated virtual gonio-spectrophotometer we will simulate measurements of the material reflectance and we compare it with results of real reflectance measurements. For that purpose we set up reflectance measurement device, that measure spectral reflectance of the real material samples. This device consists of the light source and the spectrometer, see

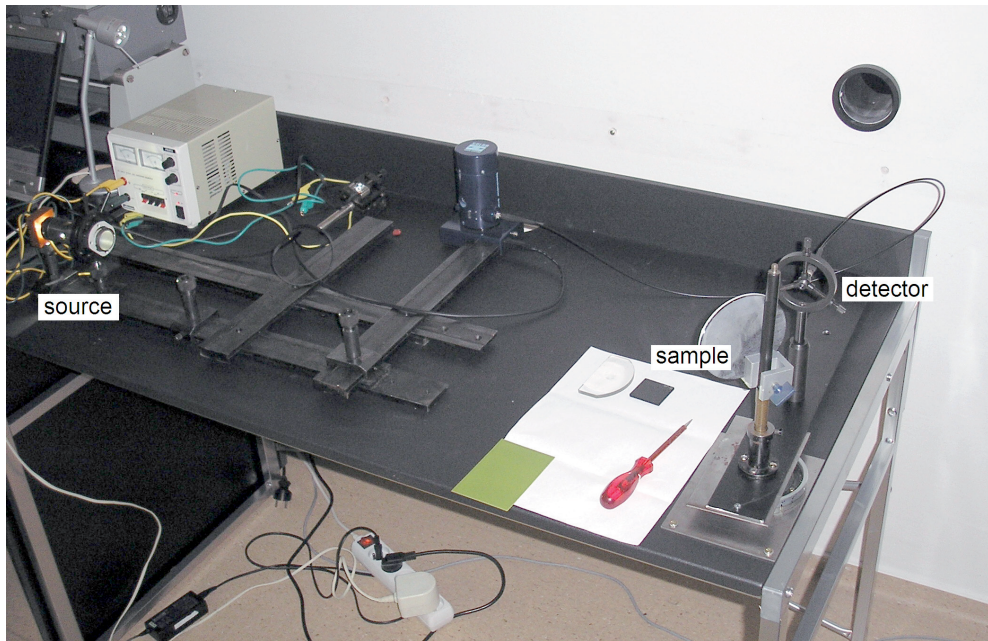


Fig. 7. We set up the measuring device containing light source and spectrometer. Device is able to measure spectral reflectance under multiple angles.

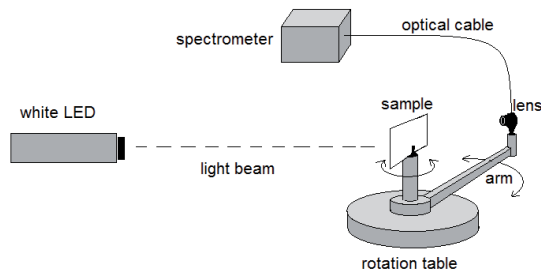


Fig. 8. Scheme of the device for the validation of the virtual gonio-spectrophotometer.

Figure 7. Light source is in the fixed position. It is LED STAR 2,5 WHITE 120LM/120° LAMBERTIAN with power input 2.5W, luminous flux 100-120 lm, radiation angle 120° and color temperature 6500-8000K. The receptor is able to move around the sample. It is connected by the optical cable to the spectrometer Solar S100 (grating 300l/mm, TCD linear image sensor, spectral range 190-1100nm, spectral resolution 1nm, dynamic range 900:1). The distance between the source and the sample is 90cm. The sample itself can be rotated in arbitrary angles.

In the Figure 8 is depicted scheme of the measuring device with two degrees of freedom. On the arm is in the distance of 20cm from the sample mounted lens with optic cable connected to the spectrometer.

We performed measurements of real material samples like polished copper and black glass. To compute relative reflectance, we performed measurements of the perfect mirror. Then we measured car paint samples. We obtained the absolute spectral power function from spectrometer. Then we divide absolute results with those obtained from perfect mirror which represent spectral power of the light source. Example of such result is depicted in the Figure 9.

For the purpose of the calibration we choose black glass with refractive index of 1.567. This

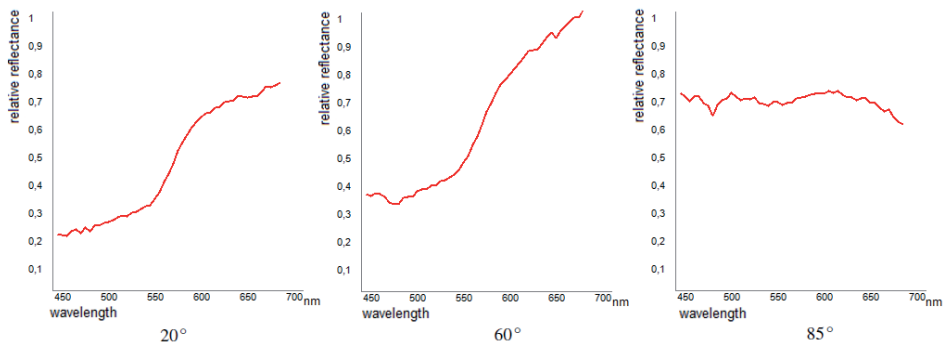


Fig. 9. Relative reflectance of the copper surface sample measured under angles  $20^\circ$ ,  $60^\circ$  and  $85^\circ$ .

material is referred as the standard for device calibration in industrial measurements according to ISO 2813. Also as we will see in the next chapter, we have mathematical expression of the black glass standard. Taking into account this fact, we can perform calibration of our virtual gonio-spectrophotometer following result given by real black glass.

## 7 Virtual Measurements

Industrial gloss measurements satisfy the standards such as ISO 2813 or ASTM D523. Those standards usually prescribe the measurement to be taken at angles  $20^\circ$ ,  $60^\circ$  and  $85^\circ$  to the surface normal (both directions, to the light source and detector are in the same plane with the surface normal;  $\epsilon_s = \epsilon_d = \{20^\circ, 60^\circ, 85^\circ\}$  in the Figure 6), because these degrees of specular gloss measurements offer numerical values which are roughly linearly correlated over a range of values to perceived gloss of high-gloss, medium-gloss and low-gloss surfaces, respectively [5].

### 7.1 Calibration of virtual measurements

The flux reflected off the black glass standard is computed by the following summation:

$$\Phi_{glass} = dA \sum_k L(\mathbf{x} \leftarrow \Theta_{i_k}) \cos(\theta_{i_k}) \Delta\omega_{i_k} F_r(\cos \theta_{i_k}), \quad (17)$$

where  $F_r$  is Fresnel term (see Equation 10). We use complex refractive index  $\hat{n}$  as a function of the wavelength. Equation 17 is derived from Equation 16 by incorporating  $f_r$  of the black glass standard.

Our virtual measurement of black glass standard was used to find the correspondence with real measurement of black glass. We calibrate virtual gonio-spectrophotometer by setting the parameters that minimize the the root mean square error (RMSE) according to the real black glass measurements. We set the parameters and then we utilized our virtual gonio-spectrophotometer to perform computations of other samples.

Adjustable parameters of our virtual gonio-spectrophotometer are: angles to the detector and source aperture, size of the apertures and the refinement of the subdivided hemisphere. We simulated reflectance of the black glass standard using Equation 17. We performed simulations with variety of parameters setups. We set angles according to the mentioned standards to achieve correspondence with our real measurements of the black glass. Other parameters like aperture sizes and the degree of subdivision were varied. From the variety of setups we got one setup which produces minimal difference to the results acquired from real measurements of the black glass. We evaluated this difference in the terms of RMSE. By the minimization of this error we got virtual gonio-spectrophotometer parameters that we will use to calibrate our virtual gonio-spectrophotometer for the purpose of virtual

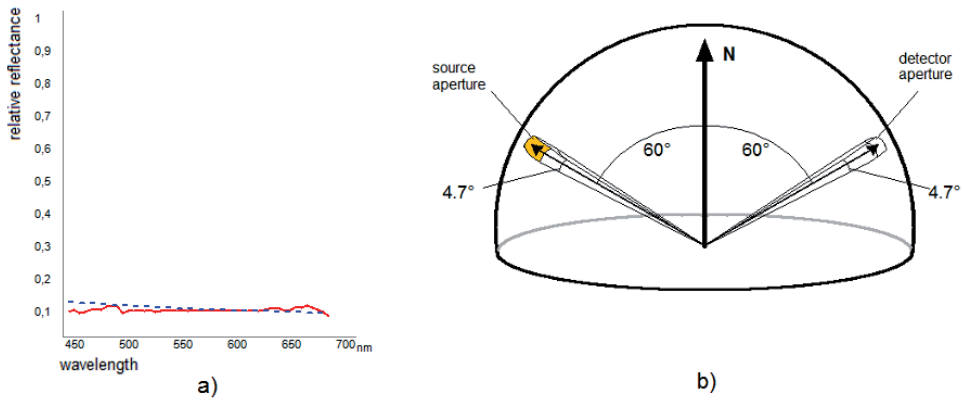


Fig. 10. a) Results of black glass real measurement (solid line) and virtual measurement (dotted line) measured under  $60^\circ$ . b) Geometry of the measurement.

measurements. RMSE describes difference between results of real measured black glass and the simulation. In our experiment, we found RMSE to be 0.0058 using 196608 patches per hemisphere. Further subdivision does not produce smaller error. We found that size of receptor aperture should be at least of the source aperture size. To find this minimal RMSE, we used angular source aperture size of  $4.7^\circ$  (see Figure 10 (b)) and we set detector aperture to the same size. Measurements were taken under  $60^\circ$  and the result of virtual and real measurements is depicted in Figure 10 (a).

## 8 Validation Results

We adjusted parameters of our virtual gonio-spectrophotometer according to the black glass measurements. To validate our virtual gonio-spectrophotometer we evaluate error of measurements based on the Cook-Torrance model. We choose copper as a sample because Cook-Torrance reflectance model proved as suitable approximation of metallic surfaces [3]. For the sake of comprehensiveness we also performed measurements of black glass based on this model.

Our virtual measurements were used to find the correspondence between real samples and analytical Cook-Torrance's  $f_r$  in the terms of RMSE. We empirically found the root mean square slope  $m$  (see Table 1) parameter of the Cook-Torrance model corresponding to the real samples. To evaluate Fresnel term in the Cook-Torrance formula, we used the real measured complex index of refraction, which is the function of the wavelength. Then we evaluated virtual measurements by comparing them with real measurements.

To compute spectral power we first perform computation of radiant flux  $\Phi$  using Equation 16 with  $f_r$  of the measured material, which is represented by the Cook-Torrance formula (see Equation 15). We set the parameters of the virtual gonio-spectrophotometer as we discussed earlier (see Section 7.1).

We performed real measurements of copper and black glass under three proposed angles ( $20^\circ$ ,  $60^\circ$  and  $85^\circ$ ). As a result we got relative spectral reflectance. We have computed reflectance of the virtual materials by our virtual gonio-spectrophotometer. We have compared results for each sample and angle of measurement and computed relative RMSE. In Table 1 we can see parameter  $m$  of Cook-Torrance model and relative RMSE for each sample. In Figure 11 we can see the resulting relative reflectance from virtual and real measurements of the polished copper. Results of the black glass virtual measurements based on the Cook-Torrance's  $f_r$  are depicted in Figure 12. Virtual gonio-spectrophotometer based on the Cook-Torrance model, proves its robustness with error less than 5% in the case of the polished copper. In the case of the glass, results are affected by error, due to the nature of the Cook-Torrance model which is devoted mainly to the metallic materials.

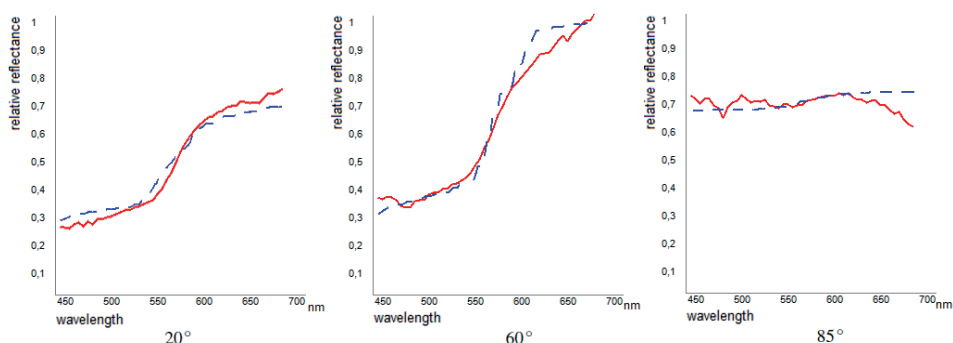


Fig. 11. Relative reflectance of the polished copper under  $20^\circ$ ,  $60^\circ$  and  $85^\circ$ . Dotted line represents virtual measurements, solid line represents real measurements.

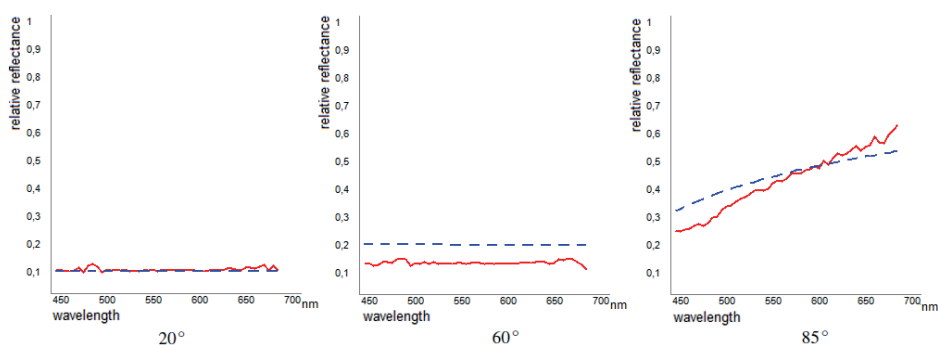


Fig. 12. Relative reflectance of the black glass standard under  $20^\circ$ ,  $60^\circ$  and  $85^\circ$ . Dotted line represents virtual measurements, solid line represents real measurements.



## 9 Conclusion

We have developed Virtual Gonio-spectrophotometer, it consists of the simulator of the standard light source and the virtual receptor aperture, that performs measurements on the virtual material samples represented by the BRDF. The Virtual Gonio-spectrophotometer consists of the standard light source and the receptor aperture. Parameters of apertures (eg. position, size) are highly customizable to allow simulations of devices like colorimeter or glossmeter.

We have set up the real measuring device to evaluate our virtual gonio-spectrophotometer and to BRDF acquisition of the real materials. We have experimentally studied simple materials and compared the obtained results to simulations based on the analytical BRDF.

In the future we would like to focus on more complex materials such as metallic car paints. These materials exhibits sparkling effects, therefore their computer representation is more extensive (eg. bidirectional texture function).

## Acknowledgments

We would like to thank Dušan Chorvát from International Laser Center for his help with the assembling of measurement device in their lab.

## References

- [1] ASTM D 523-89. *Standard Test Method for Specular Gloss*. ASTM, 1999.
- [2] Shruthi Achutha. BRDF acquisition with basis illumination. Master's thesis, Department of Computer Science, University of British Columbia, Vancouver, Canada, 2006.
- [3] R. L. Cook and K. E. Torrance. A reflectance model for computer graphics. *ACM Trans. Graph.*, 1(1):7–24, 1982.
- [4] Julie Dorsey, Holly Rushmeier, and Francois Sillion. *Digital Modeling of Material Appearance*. Morgan Kaufmann, San Francisco, USA, 2008.
- [5] R. Đuriković and I. Šed'o. Real-time friendly representation of arbitrary BRDF with appearance industry measurements. *Journal of the Applied Mathematics, Statistics and Informatics*, 3(1):17–26, 2007.
- [6] J.A. Ferwerda, F. Pellacini, and D.P. Greenberg. A psychophysically-based model of surface gloss perception. In *Proceedings SPIE Human Vision and Electronic Imaging '01*, pages 291–301, 2001.
- [7] Richard S. Hunter and Richard W. Harold. *The Measurement of Appearance*. John Wiley & Sons, Inc., New York, NY, USA, 1987.
- [8] ISO2813. *Paints and varnishes -Determination of specular gloss of non-metallic paint films at 20 degrees, 60 degrees and 85 degrees*. Internation Organization for Standardization, 1994.
- [9] K. E. Torrance and E. M. Sparrow. Theory for off-specular reflection from roughened surfaces. *JOSA*, 57(9):1105–1114, 1967.
- [10] Gregory J. Ward. Measuring and modeling anisotropic reflection. *SIGGRAPH Comput. Graph.*, 26(2):265–272, 1992.



	relative RMSE (%)			$m$
	20°	60°	85°	
polished copper 	2.12	3.53	4.57	0.065
black glass 	0.94	6.44	21.65	0.013

Table 1. The root mean square error of the measurement under specific angle and the root mean square slope  $m$  of microfacets parameterizing the surface's roughness in Cook-Torrance model.

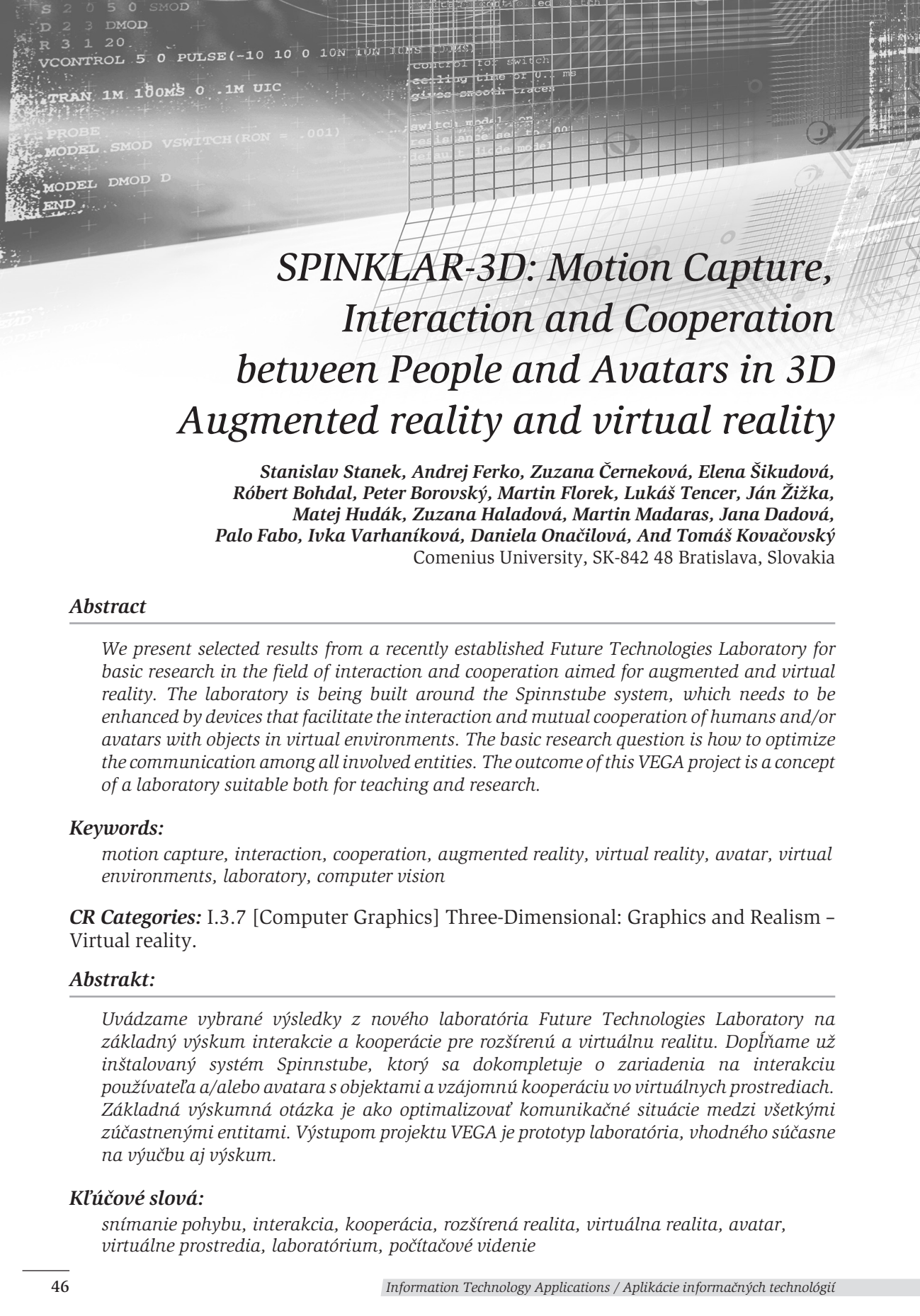
- [11] Harold B. Westlund and Gary W. Meyer. Applying appearance standards to light reflection models. In *SIG-GRAPH '01: Proceedings of the 28th annual conference on Computer graphics and interactive techniques*, pages 501–511, New York, NY, USA, 2001. ACM.
- [12] Josh Wills, Sameer Agarwal, David J. Kriegman, and Serge J. Belongie. Toward a perceptual space for gloss. *ACM Trans. Graph.*, 28(4), 2009.

**Mgr. Andrej Mihálik, PhD.**

Dept. of Applied Informatics,  
Faculty of Mathematics, Physics and Informatics,  
Comenius University,  
842 48 Bratislava, Slovak Republic;  
e-mail:mihalik@sccg.sk

**Prof. RNDr. Roman Ďurikovič, PhD.**

Dept. of Applied Informatics,  
Faculty of Mathematics, Physics and Informatics,  
Comenius University,  
842 48 Bratislava, Slovak Republic;  
<http://www.sccg.sk/~durikovic>  
e-mail:roman.durikovic@fmph.uniba.sk



# SPINKLAR-3D: Motion Capture, Interaction and Cooperation between People and Avatars in 3D Augmented reality and virtual reality

Stanislav Stanek, Andrej Ferko, Zuzana Černeková, Elena Šikudová,  
Róbert Bohdal, Peter Borovský, Martin Florek, Lukáš Tencer, Ján Žižka,  
Matej Hudák, Zuzana Haladová, Martin Madaras, Jana Dadová,  
Palo Fabo, Ivka Varhaníková, Daniela Onačilová, And Tomáš Kovačovský  
Comenius University, SK-842 48 Bratislava, Slovakia

## Abstract

We present selected results from a recently established Future Technologies Laboratory for basic research in the field of interaction and cooperation aimed for augmented and virtual reality. The laboratory is being built around the Spinnstube system, which needs to be enhanced by devices that facilitate the interaction and mutual cooperation of humans and/or avatars with objects in virtual environments. The basic research question is how to optimize the communication among all involved entities. The outcome of this VEGA project is a concept of a laboratory suitable both for teaching and research.

## Keywords:

motion capture, interaction, cooperation, augmented reality, virtual reality, avatar, virtual environments, laboratory, computer vision

**CR Categories:** I.3.7 [Computer Graphics] Three-Dimensional: Graphics and Realism – Virtual reality.

## Abstrakt:

Uvádzame vybrané výsledky z nového laboratória Future Technologies Laboratory na základný výskum interakcie a kooperácie pre rozšírenú a virtuálnu realitu. Dopĺňame už inštalovaný systém Spinnstube, ktorý sa dokompletuje o zariadenia na interakciu používateľa a/alebo avatara s objektami a vzájomnú kooperáciu vo virtuálnych prostrediach. Základná výskumná otázka je ako optimalizovať komunikačné situácie medzi všetkými zúčastnenými entitami. Výstupom projektu VEGA je prototyp laboratória, vhodného súčasne na výučbu aj výskum.

## Kľúčové slová:

snímanie pohybu, interakcia, kooperácia, rozšírená realita, virtuálna realita, avatar, virtuálne prostredia, laboratórium, počítačové videnie

## 1. INTRODUCTION

This project research contributes, in general, in optimizing of data flows in augmented and virtual reality in the terms of speed and precision (as stated in the original preceding ARISE project – Spinnstube development, from this European project we obtained the virtual reality setup) [1]. A free-hand environment allows for the interaction and cooperation of adequate as well as unconventional objects. Following up the project ARISE mission and standard methodology [2], [6]. [11-14], we focus to more specific communication situations, more accurate motion capture, colors, and using more accurate methods for computer vision. We combine teaching with usage of the devices and research in progress. This way we get synergistic effect. We upgrade of autonomous agent, avatars and their communication possibilities with user, to examine for new ones. Partial results of our measurements and research are innovative by themselves for color processing, object reconstruction, communication scenarios and methodology for education in specific environment. We subdivided the research into the following research lines.

## 2. SPINKLAR-3D RESEARCH OUTLINE

**2.1** We investigate optimal color representation for semantic information extraction from images/videos in three steps. Methods for perceptually equivalent gamut mapping and extraction/analysis of semantic information are synthesized within experiments with qualities/defects classification based on color information. We employed object color measurements and object/face recognition for image classification.

**2.2** We aim to visualize an interactive city model using specialized VR environment and dedicated Spinnstube setup. For virtual reality education we developed tools and modules enabling students to program their own tasks. The ARISE targeted Spinnstube for elementary schools but our retargeting to university students and public exhibitions was welcome in both groups. We assumed ongoing system development for virtual cities and other complex objects for radical acceleration, scaling and more comfort usability, even for cellular automata based models development.

**2.3** We study the possibilities of 3D display devices for the fields of Information Visualization and Scientific Visualization to achieve real-time rendering. We involved undergraduate students with bachelor and master theses for implementations and comparisons of selected visualization techniques.

**2.4** A comparison of the 3D surface interpolations based on the radial basis functions on a scattered data and an implementation of Clough-Tocher method with normals computed using local interpolants was done.

**2.5** Miniprojectors as new human-computer interaction tool (computer vision and new interactive methods) offer benefits over traditional methods. We consider real-life deployment scenarios now.

**2.5** We work on integration of methods for construction, presentation, and evaluation of communication situations in VR, namely new prototypes of motion capture, extending the functionality of avatars and/or autonomous agents and analyze the transfer of animation standards for interaction and cooperation. This requires both the development of theory, e.g. reference models by Bimber-Raskar and Ignatiev, error and stability issues and practical incremental building of lab research, database of measurements.

However, the research of all above outlined questions is limited by funding shortage.

### 3. SELECTED RESULTS

In the following, we survey five selected particular achievements.

#### 3.1 *Crowd simulation in an exhibition environment*

We introduce a novel grid based method of presenting participants in a crowd [3]. We propose a psychological approach in the special case scenario in the exhibition environment. For this environment we use 3D approach for emotions, that is widely used in psychology. We map context-specific axes to achieve better emotional control for our specific environment. Moreover, we discuss also possibilities of low level behavioral control, collision detection. We extend the pedestrians movement methods with our novel behavior model for the setup.

#### 3.2 *Automated usability measurement of arbitrary desktop application with eyetracking*

Nowadays, in software development process more attention is paid to the final usability of the product. To achieve such usability we use various methods from user centered design up to the usability evaluation methods, requiring much attention from usability experts. The presense of these experts are needed both during capturing and analysing usability data, which eventually costs too much. We propose a tool for automated data capturing during user tests as well as a captured data analysis in order to evaluate the recorded interaction and guide the attention of software developers. Furthermore, we provide a simple statistics of user tests as well as a means to browse recorded data with the interaction context extended with eye tracking data [4].

#### 3.3 *Skeleton Texture Mapping*

A novel way of mapping of textures onto a surface of 3D model is introduced [9]. Our technique is based on two interlocking mappings. The first one maps surface vertices onto a computed skeleton and the second one maps the surrounding area of each skeleton segment into a rectangle with size based on the surface properties around the segment. Furthermore, these rectangles are packed into a squared texture – skeleton texture map (STM) by approximately solving a palette loading problem. Our technique enables the mapping of a texture onto the surface without necessity to store texture coordinates with the model data and it is also suitable for surfaces with a topology non-homotopic to a sphere with higher order genus and unlimited structure branching.

#### 3.4 *Computer graphics education from high school to university*

We analyze the introductory courses of computer graphics [10], having two goals in mind. First, we studied how computer graphics ideas in another context are taught before entering university, at high school level. Second, what is the content of introductory courses and how connected it with previous knowledge. Our findings are summarized into three stages of knowledge, and five levels of education. We described the educational process by analogy with selected models and theories – the reference model for computer graphics, mathematic language ruptures by Kvasz, Piaget's development theory, and a cognitive process of mathematic by M. Hejny.

#### 3.5 *Terrain Models for Mass Movement Erosion*

We present a particle-based method for large scale long time progressive simulation of terrain erosion containing wet granular particles [7]. The wetting process and the propagation through granular material is based on defining the wetness value for each particle representing the amount of water absorbed by granular particles and stored between them, as was originally proposed by Rungjiratananon. We extend this model by adding a non homogeneous material to



simulate differences between different types of soil-like granular material, based on physical constants like stability, plasticity and wetness. With this approach we can create a physical animation of erosion process like mass movement or mass wasting.

### 3.6 Scalable Multifunctional Indoor Scanning System

The main goal of this work was to extend the system SMISS functionality. It is a scanning system for automatic 3D reconstruction in metric space. It works on a triangulation principle, using structured light from digital projector to spatially code the space. For the data acquisition, the system uses a digital camera. We address the problem of low dynamic range of similar systems and propose a novel approach, first of its kind, to solve the problem using simple additional hardware and designed algorithms. Our solution, in form of extension HDR SMISS is also a powerful and flexible tool for future improvements. We also introduce a deeper study of methods, which use structured light for coding the scanning space. We contemplate the possible usage of 3D reconstruction in different fields of human life. Moreover, we offer a way to visualize the captured data in form of a view dependent stereo vision. While solving the problems, we care about choosing physically correct approaches and we solve the problems using combination of hardware and software. Therefore we introduce descriptions of prototypes built for specific purposes and for international propagation.



**Fig. 1 – Results of 3D reconstructions**

Project SPINKLAR has supported the Master Thesis “Scalable Multifunctional Indoor Scanning System”, which received Rector’s Award and 2nd place in best IT Master thesis competition ACM-SPY in Czech-Slovak region. SPINKLAR project allowed the student to use advance technology to present his work to professionals and general public [8].

### 3.7 Interactive Bivariate Mode Trees for Visual Structure Analysis

The number of modes in a kernel density estimation of a certain data distribution strongly depends on the chosen scale parameter. We present an interactive mode tree visualization that allows to visually analyze the modality structure of a data distribution. Due to the branched structure of the bivariate mode tree, composed of many curved arcs in 3D, we need to utilize advanced techniques, including clutter removal through transparency, on demand outlier suppression or preservation, and best views, to improve the visualization mapping [5].

## 4. OTHER ACTIVITIES

### 4.1 CESC 2012

The student conference CESC 2012 took place in Smolenice Castle in Slovak Republic. The paper HDR SMISS was presented with the hardware support of the SPINKLAR project. The work received best presentation and second best paper award.



Fig. 2 – Results of 3D reconstructions and installation setup at CESC 2012

## 4.2 Noc Výskumníkov 2012



Fig. 3 – 3D reconstruction at the exhibition “Noc Výskumníkov”

The exhibition “Noc Vyskumníkov” is European Union project on popularisation of Science. One of the the exhibited scientific project was face scanning using structured light. This system, called SMISS is developed at the Comenius University and is capable of geometrical face reconstruction. These data are then visualised. We use our developed solution to track user eyes and register the real and space, so that, we are able to project the face scan on a 3D display (supplied by SPINKLAR project). This projection creates illusion than the object is registered in volume and looks realistic. This technique is called view dependent stereoscopic vision.

## 4.3 Virtuálny Svet 2012

The exhibition “Virtuálny Svet 2012” took place in AVION Shopping Center, which is located in Bratislava. The event was organized by Faculty of mathematics, physics and informatics of the Comenius University. The main idea of the exhibition was to present new ideas and the study at the University.

### 4.3.1 3D Scanner

The project SPINKLAR-3D supported the part of the exhibition by supplying the hardware for visualization. The 3D scanning solution was available to general public for one month. Every visitor of the shopping center was allowed to scan his face by simply sitting in the chair. The system in realtime and automatically recognized human face and started voice communication. After instruction has been said by the system, the system executed the scanning process and reconstructed the visitor’s face. The result was then projected to supply 3D TV screen.



Fig. 4 – 3D reconstructions setup at the exhibition “Virtuálny svet 2012”

#### 4.3.2 Information Kiosks

The project SPINKLAR-3D supported renovation of the hardware and software setup for the kiosk. The kiosk was created as a part of a project “Považské múzeum 3D online” to motivate people to visit the museum „Považské múzeum“ personally.



Fig. 5 – Kiosk and its instalations (exhibition “Virtuálny svet 2012”, FMPH UK)

But now the kiosks are used as information center for many other projects created by working group on Faculty of Mathematics, Physics and Informatics and anybody touching the screen can access these projects and play with them partly when the kiosk is offline and fully when the kiosk is online.

#### 4.4 Spektrum Vedy – Virtuálne Svety 2012

A part of television documentary about science in Slovak Republic. This part, named Virtual Worlds, was dedicated to 4 different research projects from FMFI of Comenius University. The already mentioned project SMISS was presented in this documentary and it was broadcasted by Slovak National Television.





Fig. 6 – A part of television documentary about 3D reconstruction

## 5. CONCLUSION

By support of the project SPINKLAR-3D and as one of the main goals of this project was to create also a Besides the support of the VEGA project SPINKLAR-3D, the laboratory is also supported by Faculty of Mathematics, Physics and Informatics, Comenius University, Bratislava. By public voting we named this laboratory “Future Technologies Laboratory”. The mission of this laboratory is dealing further with the fertile research fields of computer vision, computer graphics, augmented reality and virtual reality. For more about FTlab, visit, please, its webpage at [www.ftlab.sk](http://www.ftlab.sk). The complete results and outcomes can be found at [15], resp. [16].



Fig. 7 – Logo of the laboratory

## ACKNOWLEDGEMENTS

All projects, publications and activities mentioned in this paper are supported by Project SPINKLAR-3D -Project VEGA No. 1/1106/11. We thank to CVUT Prague team for noble-minded donation of the Spinnstube prototype.

## References:

- [1] ARISE portal. Augmented Reality in School Environments. <http://www.arise-project.org/>
- [2] Bimber, O. and Raskar, R. *Spatial Augmented Reality*. AK Peters 2005.
- [3] Dadová, J., Ferko, A., Běhal, D. Crowd simulation in an exhibition environment. *IADIS 2012*. Lisbon: IADIS Press 2012. pp. 127-131.
- [4] FABO, P., and Ďurikovič, R. Automated usability measurement of arbitrary desktop application with eyetracking. *InfoVis*. Los Alamitos: IEEE CS, 2012. pp. 625-629.
- [5] Florek, M. and Hauser, H. Interactive bivariate mode tree. *WSCG 2011 - Poster Papers Proceedings*. Pilsen: Vaclav Skala - Union Agency, 2011. pp. 41-45
- [6] Gutiérrez, M. et al. *Stepping into Virtual Reality*. Springer 2008.

- [7] Hudák, M., and Ďurikovič, R. Terrain models for mass movement erosion. *Theory and Practice of Comp. Graphics 2011*. Goslar: Eurographics Association, 2011. pp. 9-16
- [8] Kovačovský, T. and Žižka, J. HDR SMISS – Fast high dynamic range 3D scanner. *CESCG 2012*. Vienna: University of Technology 2012. pp. 125-132
- [9] Madaras, M. and Ďurikovič, R. Skeleton texture mapping. *SCCG 2012*. Bratislava: Comenius University 2012. pp. 133-139
- [10] Onáčilová, D. Computer graphics education from high school to university. *19th Conference of Geometry Graphics Computer, CGGC 2012. Ustron, Poland*. pp. 76-79.
- [11] QVORTRUP, L. ed. *Virtual Interaction*. Springer 2001.
- [12] QVORTRUP, L. ed. *Virtual Space*. Springer 2002.
- [13] Raskar, R. et al. *Computational Photography. STAR*. Vienna: EG 2006.
- [14] Šonka, M., Hlaváč, V., Boyle, R. *Image Processing: Analysis and Machine Vision*. CENGAGE-Engineering 1998.
- [15] FTLab Results. [online] [www.ftlab.sk/projects\\_spinklar\\_results.html](http://www.ftlab.sk/projects_spinklar_results.html)
- [16] FTLab Vystupy. [online] [www.ftlab.sk/vystupy](http://www.ftlab.sk/vystupy)

---

**Stanislav Stanek**, stanek@sccg.sk, **Andrej Ferko**, ferko@sccg.sk,  
**Zuzana Černeková**, cernekova@sccg.sk, **Elena Šikudová**, sikudova@sccg.sk,  
**Róbert Bohdal**, bohdal@fmph.uniba.sk, **Peter Borovský**, borovsky@sccg.sk,  
**Martin Florek**, florek@sccg.sk, **Lukáš Tencer**, lukas.tencer@gmail.com,  
**Ján Žižka**, jizka@gmail.com, **Matej Hudák**, subseth.mato@gmail.com,  
**Zuzana Haladová**, zhaladova@gmail.com, **Martin Madaras**, martin.madaras@gmail.com,  
**Jana Dadová**, dadova.jana@gmail.com, **Palo Fabo**, fabo@sccg.sk,  
**Ivka Varhaníková**, varhanikova@sccg.sk,  
**Daniela Onáčilová**, daniela.onacilova@fmph.uniba.sk,  
**Tomáš Kovačovský**, tomas.kovacovsky@gmail.com



# TOWARDS THE TABLETOP INTERACTION WITH FINGERS AND HAND

*Pavol Fabo, Roman Ďurikovič*

*Comenius University*

## Abstrakt

Článok prezentuje vývoj dotykovej, viacdotykovej a stolovej interakcie. Predstavená je základná idea dotykovej interakcie vzhľadom na paradigmu priamej manipulácie a popísané sú dva spôsoby akým je možné dosiahnuť rozšírenie pôvodnej paradigmy priamej manipulácie. Neskôr je dôraz kladený na stolové dotykové zariadenia, kde je vysvetlená dôležitosť a výhodnosť použitia infračerveného svetelného spektra pre rozšírenie interakčných možností na týchto zariadeniach. V závere sú prezentované idey pre budúcu prácu v oblasti dotykovej interakcie.

**Kľúčové slová:** interakcia človek počítač, interakcia na dotykových stoloch, multidotyková interakcia

## Abstract

We present an evolution timeline of touch, multi-touch and tabletop interaction. We show the basic idea of touch-based interaction in respect to a direct manipulation paradigm as well as different approaches to enhance this direct manipulation paradigm. Furthermore we focus on tabletop devices and show the main advantage of usage of near infrared light spectrum in order to augment the interaction of tabletop devices. Finally, we present ideas for our future research aims in the field of touch interaction.

**Keywords:** human computer interaction, tabletop interaction, multi-touch interaction

**Classification:** HCI design and evaluation methods, Interaction devices: Touch screens

## 1 Introduction

Multi-touch interaction is the most promising and today one of the most researched areas in the field of Human Computer Interaction. Multi-touch user interface paradigm spread across numerous hardware devices ranging from the small mobile devices up to large conference displays or presentation tabletop displays.

The entire multi-touch interaction and its main idea is based on the direct manipulation paradigm as defined by Shneiderman[11], which is the most common user interface paradigm used by millions of people every day. In the former standalone systems users have been using an input device, like a mouse or a keyboard in one space and the feedback was given in an entirely different space as shown in Figure 1.

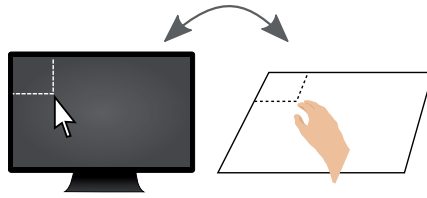


Fig. 1. Former system's users have been using an input device in a physically different space than the output device.

## 2 Review of our Contribution

There are two approaches to integrate input and output spaces into a single one. In the first approach, the output space is moved into the same space where the input of the user has taken place. Such systems usually employ a haptic feedback devices, where either a tactile [3] or kinesthetic feedback is used [6] as shown in Figure 2.

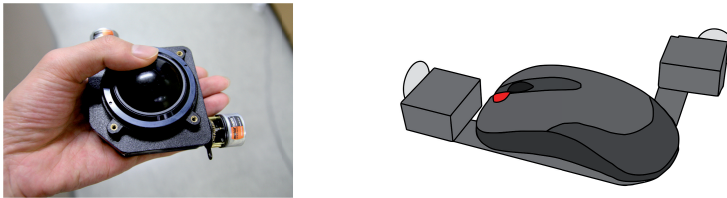


Fig. 2. Haptic feedback devices. Left a Touchball tactile feedback device from [3], right a kinesthetic feedback mouse, where two servo motors controls the movement of the mouse [6].

The second approach is to integrate the input interaction space into the output interactions, which is the basic principle of touch devices. The touch paradigm has been perfected by enabling the usage of multiple touch points or even gestures defined by the movement of these touch points.

The proposed multi-touch device used for tabletop interaction provides even more interaction possibilities by simply scaling the interaction space to larger dimensions. Because of the larger dimensions, it is profitable to use an optical implementation of proposed touch detection, which brings a lower costs of implementations and, what is more, some extra interaction possibilities.

The majority of optical implementations, as described in [2], use a near infrared light spectrum<sup>1</sup>, which is not visible to a human beings, but clearly visible for most standalone computer cameras placed usually beneath the touch surface. By using only the near infra red part of the spectrum there is a significant increase in a signal to noise ratio, thus making the detection of touch points very straightforward, as shown in Figure 3.

The large scale of tabletop touch sensitive displays, usage of the near infrared light spectrum and the straightforward detection algorithms lead to the enhancement of the interaction with physical objects. For example The reacTable [8] make use of such physical objects that are used as a passive haptic devices called "props". The individual props are recognized by special markers known as fiducials as shown in Figure 4.

The usage of fiducial markers on physical objects together with the multi-touch input might be viewed from two different perspectives. Firstly, from the perspective of the interaction paradigms, where a touch interaction paradigm is coupled with the tactile user interface paradigm or eventually an integration of two different direct manipulation paradigms. Secondly, a 2D touch interaction (like touching a button) is combined with a 2.5D physical object interaction (manipulating with an actual physical object) resulting in higher dimensionality (4.5D) user interaction.

<sup>1</sup>Light with wavelengths from 800 nm up to 1400 nm.

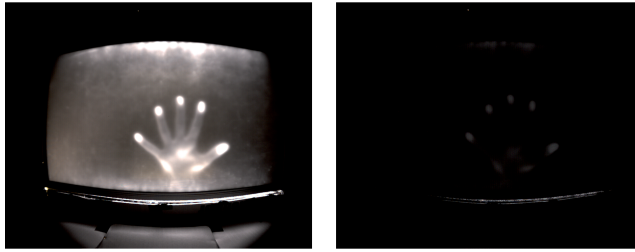


Fig. 3. Touched display with five fingers and the hand above the display giving 3 dimensions in total. A comparison of camera image in visible and infrared spectrum (left image), and image of only infrared spectrum (right image), from [7].

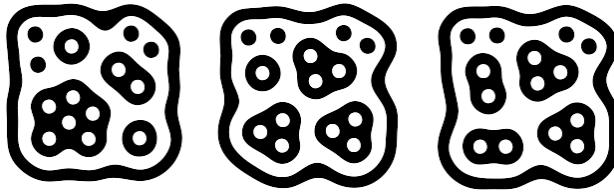


Fig. 4. An example of fiducial markers used in the implementation of The reacTable [8].

Going even further, a trivial extension is a combination of touch input interaction with a 3D user interaction above the actual touch interaction space as proposed by [5]. Here a 3D gesture interaction was proposed to be used for three-dimensional spatial object manipulation, whereas two-dimensional touch input defined the temporal characteristics of the resulting animation. The actual implementation by [4] enhanced the proposed solution by adding a shutter glasses and stereoscopic display technology to render three-dimensional output above the tabletop display.

### 3 The Future of the Tabletop Interaction

Although it might seem that there is no further research to be done in tabletop human computer interaction, we believe there is still a room for some enhancements.

Firstly, the integration of physical objects with touch interaction seems to be very promising unfortunately, the number of possible fiducial markers is limited. An extension to fiducial markers is the use of QR codes, that are trackable in real-time [12] but also the amount of coded information is substantially increased. Specifically, the large QR code is able to store about 4000 alphanumeric characters. Moreover, there is another essential property of QR code, which is its error correction, where up to 30% data lost can be restored [12].

Secondly, there is still a lack of interaction semantics. The entire touch interaction is based on either the static touch inputs or dynamic gesture inputs, where the semantic of the input is determined by either the touch target or the type of the gesture executed. This semantics determination is done after the actual user's input. Our improvement in this phase is the identification of the semantics after as well as before the specific user input. Trivial example of before touch input semantics is usage of special keyboard switches changing the type of the interaction that is about to take place. On the other hand, since the tabletop device is using hands and finger, it is very convenient to use either hands<sup>2</sup> or finger identification or even the combination of both.

There are several approaches to solve the finger identification problem on tabletop devices. Firstly,

<sup>2</sup>Hand identification as defined in bimanual interaction introduced by [9].

an identification by computing the sum angles to the adjacent finger has been published by [1], where a standalone capacitance touch device has been used, thus before the actual interaction user has to touch with all the five fingers to register the hand model. On the other hand, in [10] a Kinect depth map has been used for detection of user's fingertips and the kinematic human hand model was matched to the detected fingertips.



Fig. 5. In the left picture a camera's view of optical tabletop implementation and sufficient brightness difference between the fingertips, hand shadow and background scene. In the center picture a processed image is shown. In the right image contours of hand and detected finger touches are depicted.

Our proposed solution uses optical tabletop implementation based on frustrated total internal reflection [2], where an ambient infra red light provide sufficient brightness difference between the fingertips, hand shadow and background scene from the camera's point of view as shown in Figure 5 along with an entire image processing process. Using a frame division, morphology, threshold and contour finding algorithms the actual contour of the user's hand is found along with the contour of individual touch points. We propose to count the angle difference of fingertips adjacent to the actual touch point, that is enough to identify the actual touch finger. Such algorithm will be successful only in case of the hand with all five fingers visible. It is unnatural for the user to always work using hand with all five fingers spread, we propose further user testing and analysis in order to sufficiently define the touch interaction techniques using different fingers. This analysis will help to create much successful algorithm for finger identification without the need for spreading the fingers.

## 4 Conclusion and future work

We have shown that there is a bright future for the tabletop and multi-touch interaction. To go little bit further we see a responsive tabletop interaction, where the tabletop system is aware of its presence in respect to the user performing the interaction. Giving a multimodal feedback might be useful to navigate the user in the tabletop interface and coupling the 3D user interface with actuators to rotate the entire tabletop. By this way we create 360 degree 3D input around the entire tabletop. Since, the optical tabletop implementation usually uses near infrared spectrum a various infrared pointers or even an infrared data communication is possible far away from the touch sensitive device.

## References

- [1] AU, O. K.-C., AND TAI, C.-L. Multitouch finger registration and its applications. In *Proceedings of the 22nd Conference of the Computer-Human Interaction Special Interest Group of Australia on Computer-Human Interaction* (New York, NY, USA, 2010), OZCHI '10, ACM, pp. 41–48.
- [2] AUTHORS, N. G. *Multi-Touch Technologies*. NUI group, 2009.
- [3] CHOI, M., AND KIM, G. J. Touchball: a design and evaluation of a hand-held trackball based touch-haptic interface. In *Proceedings of the SIGCHI Conference on Human Factors in Computing Systems* (New York, NY, USA, 2009), CHI '09, ACM, pp. 1535–1538.

- [4] DE ARAÚJO, B. R., CASIEZ, G., AND JORGE, J. A. Mockup builder: direct 3d modeling on and above the surface in a continuous interaction space. In *Proceedings of the 2012 Graphics Interface Conference* (Toronto, Ont., Canada, Canada, 2012), GI '12, Canadian Information Processing Society, pp. 173–180.
- [5] FABO, P. Human computer interaction on touch-based animation, 2011.
- [6] FABO, P., AND DZIUBAN, V. Concept of haptic device for user interface navigation and guidance. In *Študentská vedecká konferencia FMFI UK* (2010), p. 330.
- [7] FABO, P., ĎURIKOVIČ, R., AND NISHITA, T. Multi-touch display using combination of ftir and hd lcd. In *Proceedings of the 13th International Conference on Humans and Computers* (Fukushima-ken, Japan, Japan, 2010), HC '10, University of Aizu Press, pp. 11–14.
- [8] JORDÀ, S. The reactable: tangible and tabletop music performance. In *Proceedings of the 28th of the international conference extended abstracts on Human factors in computing systems* (New York, NY, USA, 2010), CHI EA '10, ACM, pp. 2989–2994.
- [9] KRUEGER, M. W. *Artificial reality II*. Addison-Wesley, 1991.
- [10] KUNG, P., KÜSER, D., SCHROEDER, C., DEROSE, T., GREENBERG, D., AND KIN, K. An augmented multi-touch system using hand and finger identification. In *CHI '12 Extended Abstracts on Human Factors in Computing Systems* (New York, NY, USA, 2012), CHI EA '12, ACM, pp. 1431–1432.
- [11] SHNEIDERMAN, B. Direct manipulation: A step beyond programming languages. *Computer* 16, 8 (aug. 1983), 57–69.
- [12] SZENTANDRÁSI, I., HEROUT, A., AND DUBSKÁ, M. Fast detection and recognition of qr codes in high-resolution images. In *Proceedings of 28th Spring conference on Computer Graphics* (2012), Comenius University in Bratislava, p. 8.

**Mgr. Palo Fabo, PhD.**

Dept. of Applied Informatics,  
Faculty of Mathematics, Physics and Informatics,  
Comenius University,  
842 48 Bratislava, Slovak Republic;

**Prof. RNDr. Roman Ďurikovič, PhD.**

Dept. of Applied Informatics,  
Faculty of Mathematics, Physics and Informatics,  
Comenius University,  
842 48 Bratislava, Slovak Republic;  
<http://www.sccg.sk/~durikovic>  
e-mail:roman.durikovic@fmph.uniba.sk





# Why and How to Search for Best Views

## Ako a prečo hľadať najlepšie pohľady

Ivana Varhaníková

### Abstrakt

Výber najlepších pohľadov sa v poslednej dobe stáva kľúčovým prvkom vo viacerých oblastiach počítačovej grafiky. V tomto článku analyzujeme výhody najlepších pohľadov vo virtuálnych múzeách, načrtujeme niekoľko metód na ich hľadanie a diskutujeme aj možnosti rozšírenia využitia najlepších pohľadov.

### Kľúčové slová:

najlepší pohľad, najhorší pohľad, klasifikácia, kvalita pohľadu, percepcia, tvarová (gestalt) psychológia, virtuálne prostredie, virtuálne múzeum, virtuálna riadená prechádzka

### Abstract

Selection of good views is rapidly becoming a key issue in multiple computer graphics applications. In this paper we discuss the importance of finding the best views in virtual environment. We present several selected approaches for finding the best view and some possibilities of enhancement of the best view.

### Keywords:

best view, worst view, classification, view quality, visual perception, Gestalt psychology, virtual environment, virtual museum, virtual guided tour

**CR Categories:** I.3.7 [Computer Graphics] Three-Dimensional: Graphics and Realism -Virtual reality; I.2.10 [Computing Methodologies] Vision and Scene:Understanding - Perceptual reasoning.

## 1. INTRODUCTION

“Virtual Museum is a multimedial collection of telematic available digital data and cognitive space with infinite capacity to enlarging, combination, composition and recomposition [1].” As long as we would like to make the exploration in virtual museum the most interesting we should show the museum showpieces from the best view.

What is “the best view” on a virtual object? Although the phrase “best view” is very common, it is very hard to define. We can define best view as the one that minimizes visible redundant information such as symmetry or we can maximize the visibility of interesting contents using metrics (saliency, shape distinction or viewpoint entropy) [2]. The result we get is that the term “best view” is far from having a unique definition.

Is it then possible to optimize creation of virtual museum fly-over through best views? Generally, if we know how to count up best view for each object in the scene, could we navigate visitor of the virtual museum so that he explores the most interesting objects of museum? Because for every visitor means best view something else, we can only approximate view on showpieces in virtual museum and consider that this view will satisfy most of visitors.

## 2. Methods for searching for the best view

Finding the best view on virtual object became serious problem not only in computer graphics. There exist many methods for trying to find the view, which could be considered for the most similar to the observer's selection. The same holds for classification of these methods. We can split them into low level methods and high level methods, or we can choose another division: into geometrical or semantic methods. And as long as virtual museum is specific kind of virtual space (it is mostly an indoor environment with many showpieces, their textures and specific lighting) we have to carefully choose the method we use because we can obtain a great geometrical view with the biggest number of edges, but when the object is completely in the shadow from this viewpoint or it has a texture on other side of this view, it become a little bit senseless. For this short introduction we chose five of the most used methods.

### *Degenerated edges and faces*

First publication in this area based on geometrical information is from 1988 by Kamada and Kawai [3]. They propose a method, which minimizes the number of degenerated object surfaces in orthogonal projection, i.e. surfaces which are projected as edges and edges which are projected as points (Fig 1). This method is not suitable for realistic scenes, because it does not account for visibility of individual scenes parts. Barral et al. [4] modified Kamada's coefficient in order to cope with perspective projections. Then they propose a heuristic with parameters that weight both the number of faces seen from each point and the projected area. Moreover they add an exploration parameter which accounts for the faces already visited. Plemenos and Benayada [5] brought in a method based on the number of visible surfaces and size of the projected area. Simple extension of this method based on position of light sources in the scene was presented in [6].

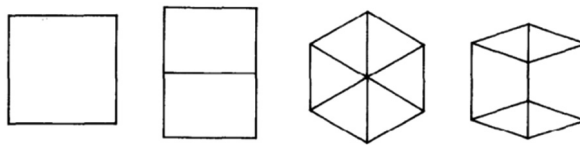


**Figure 1: Four of the computed views on cube according to Kamada and Kawai**

### *Viewpoint complexity*

The term “complexity of a scene” is very intuitive [7]. Given two different scenes, people are able to say which scene is more complex than the other. The viewpoint complexity of a scene depends on the point of view. Viewpoint complexity of a scene from a given point of view is a quantity which depends on:

- The number of surfaces visible from the point of view.
- The area of visible part of each surface of the scene from the point of view.
- The orientation of each (partially) visible surface according to the point of view.
- The distance of each (partially) visible surface from the point of view.

### Viewpoint entropy

Viewpoint entropy [8] is a low level method based on Shannon entropy. To define viewpoint entropy, the relative area of the projected faces over the sphere of directions centered in the viewpoint is used as probability distribution. Thus, the viewpoint entropy for scene  $S$  and viewpoint  $p$  is defined as

$$I(S, p) = - \sum_{i=0}^{N_f} \frac{A_i}{A_t} \log \frac{A_i}{A_t},$$

where  $N_f$  is the number of faces of the scene,  $A_i$  is the projected area of face  $i$  over the sphere,  $A_0$  represents the projected area of background in open scenes, and  $A_t$  is the total area of the sphere. In a closed scene, or if the point does not see the background, the whole sphere is covered by the projected faces and consequently  $A_0 = 0$ . Hence,  $A_i/A_t$  represents the visibility of face  $i$  with respect to point  $p$ .

### Silhouette length

A simple version of this descriptor measures the total length of all silhouette edges in the image plane. Since this cannot be done reliably in the image space, the visible silhouette edges are computed in object space analytically and the length of their projected versions is calculated [9].

### Silhouette entropy

A more sophisticated descriptor uses silhouette entropy instead of total length. The entropy of a curve is defined as the entropy of its curvature distribution, as proposed by Page [9]. In the discrete version, the entropy of all turning angles between adjacent silhouette edges is computed. But in some cases, spurious silhouette edge crossings can make the result quite unstable.

Hence the number of existing methods for finding the best view is enormous we decided to take a brief look only on methods we study in our research. Extended list of methods can one find in [16] and [17].

## 3. Possibilities of enhancement

### 3.1 Animation

The automatic generation of in-betweens (intermediate frames) is one of the techniques used in computer animation. This technique is based on a set of key frames entered by the user. This principle is also used in computer assisted 3D animation (camera and object positions are defined only at key points) and the calculation of intermediate positions is left to the computer. When we use found sequence of views on given objects (sorted from the best to the worst one) as key frames for animation we can generate a tour around any object in virtual museum.

The objective characteristic of this approach is the lack of smoothness in the motion. Because of the sudden changes in the direction of animation can be the key frames pretty visible. But there can be also visible the discontinuities in the speed of camera motion (when we requests a different number of frames between key frames). A third common problem is the possibility deformation of the path when the movement has a rotational component. To avoid respect of these serious drawbacks of linear interpolation we assume that adequate solution for automatic path through the virtual environment is based on the Kochanek-Bartels splines [10].

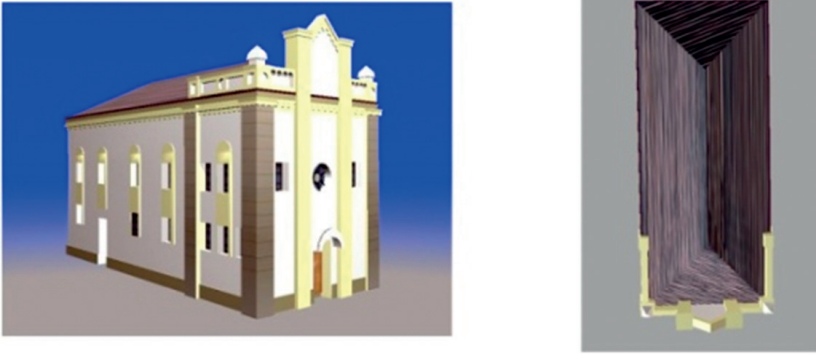


**Figure 2:** *The best (a) and the worst view (b) computed for the church with Viewpoint entropy method*

### 3.2 The worst view

As an ancillary commodity of finding the best view we get the worst view. Most of computer graphics users spill it or they use it just to compare the result of their recent best view finding method [11]. But what if we use these views to upgrade the visit in virtual environment? We can use them as a starting position instead of the best view to make visitors think of what they see. For finding worst views we can use any of methods mentioned above (for instance in Fig 2 we present the best and the worst view found using Viewpoint entropy method).

When we obtain the final values for the views we can line up the values uplink from the lowest to the highest one. On the top is now the worst view, which we can use as a starting for automatic path around objects. This path is made by joining views from the worst to the best by using adequate curves. We think that using worst views we can upkeep attention of visitors longer and so he may spend more time in virtual museum without feeling bored.

### 3.3 Classifications of objects

Is for every kind of museum showpiece adequate only one method for searching the best view? Or such as for everyone is the best view something else has every kind of objects his own special best view?

To find out, we prepared the questionnaire with dataset (25 renders of virtual objects x 13 views (Fig 3)) [12], which was available online to general public. In the questionnaire participated 145 people, aged from 11 to 56 years.

The dataset contained various types of 3D models, including colored and monochromatic, models with faces, symmetric models, models of real and fantastic objects. The respondents were supposed to select best view (according to their opinion) for each object from given 13 views of each object. Firstly, we gave the observer the view on the frontal side of object and as the last we gave them the view from the top of the object. Every object was considered separately to the others.

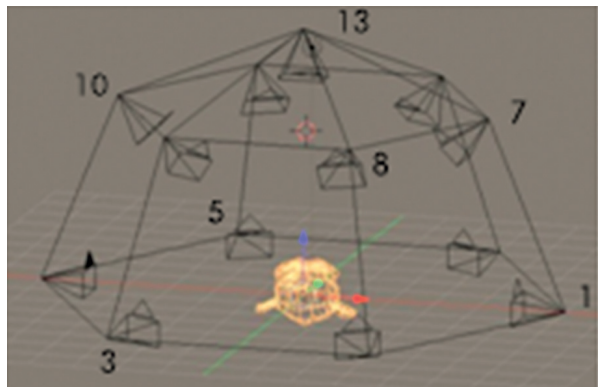


**Figure 3:** *Camera layout in the process of computing views on object in the scene.*

After evaluation of questionnaire we found out some interesting facts. If the model contained face, the people have tendency to choose the view, where the face is visible. As well as, in case of symmetric views they choose the first in row. We computed then results from three tested methods for finding best views (Fig 4): Visual attention method: Itti's approach, Geometrical method and Image based method.

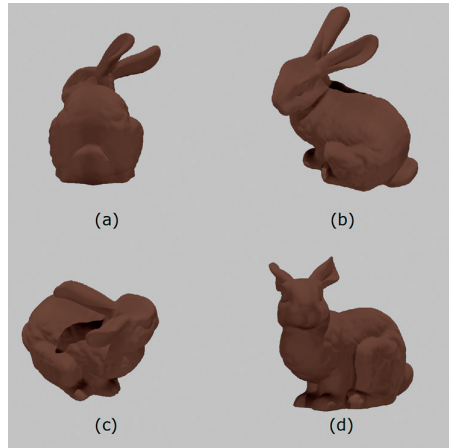


**Figure 4: Examples of the selected best views for every method:**  
**(a) Geometry based method, (b) Visual attention based method,**  
**(c) Entropy based method, (d) Questionnaire.**

Then we confronted these methods with the questionnaire results. Obtained results are shown in the Fig 5, where the sbest views are depicted for every method and next to it the percentage of votes from questionnaire is presented. For our surprise only in two cases all three methods selected the same or the symmetric view. The relevant objects were symmetric and colored. In 9 cases visual attention method and geometry based method performed the best and gave the same view. Visual attention based method performed better on objects with large amount of differences in color, intensity and edge orientations. The geometry based method gave the best results from all the methods on other 6 objects. The entropy based method gave good results mostly on colored objects.

	Best view		Best view		Best view		Best view	
	Visual Attention	Questionnaire %	Geometry	Questionnaire %	Entropy	Questionnaire %	Questionnaire	Questionnaire %
happy buddha	1	14,08	1	14,08	7	14,08	2	45,07
Stanford dragon	2	36,88	10	0,71	2	36,88	8	53,19
hippo	8	30,99	12	15,49	2	19,01	8	30,99
gazebo	5	10,56	4	3,52	1	21,83	2	28,87
pillow	1	61,97	1	61,97	6	10,56	1	61,97
mouse	12	19,72	2	2,11	6	12,68	7	50,00
T-rex	6	47,89	6	47,89	1	3,52	6	47,89
armadillo	9	0,71	1	53,90	6	6,38	1	53,90
standford bunny	11	20,42	4	0,70	8	1,41	6	57,04
statue	3	2,13	7	38,13	11	0,72	7	38,13
bug	12	14,08	7	22,54	7	22,54	8	35,21
car	8	7,75	8	7,75	1	0,70	2	52,82



	Best view		Best view		Best view		Best view	
dragon	6	27,00	6	27,00	7	0,00	2	40,15
chessboard	12	6,34	12	6,34	6	3,52	8	28,87
knight	4	13,48	5	14,18	6	7,09	1	22,70
plane	1	0,71	7	9,22	4	0,71	8	38,30
snowman	10	0,00	1	22,70	6	32,62	6	32,62
suzie	7	7,09	1	43,79	3	1,42	1	43,79
bee	11	2,14	12	8,57	6	24,29	2	33,57
church	6	57,86	6	57,86	12	3,57	6	57,86
cube	9	8,96	9	8,96	13	0,00	7	54,48
glass	6	0,00	10	0,71	7	54,29	7	54,29
church2	10	0,00	2	45,00	6	34,29	2	45,00
crocodile	13	3,70	7	11,11	1	8,15	2	31,11
yellow submarine	8	24,29	8	24,29	6	22,14	2	42,14

**Figure 5:** *Performance of the methods and results from the questionnaire. For every method, there is selected best view and next to it the percentage of votes, which obtained the selected view in the questionnaire.*

In all cases at least one of our methods correctly chose the view ranked among the three “best views” chosen by people. At the end, we can conclude that proper combining of these three methods could lead us to the results satisfying human perception.

We can then say that through experimental results we observed that each of the tested method is suitable for different type of models. It means, that it could be better to start with classification of objects according to saliency parts first and then use some of known methods for finding the best view similar to the preference of observer.

### 3.4 Visual perception

The main reason why are we trying to find best views for virtual objects is to give the visitor of virtual environment most information. In the [13] they assume that the observer gets most information about object from that view where from each side of object is 19 % background. So the object should be centered as much as it is possible and there should be at least some free space around it.

Moreover according to visual perception [14] it is necessary to give to observer information in such order, that he firstly gets known information and then new ones. The meaning is that he gets worse view before he gets better one. Otherwise is he trying to apply the information from the best view on another view and he sees what isn't there.

Let us consider we found best view (Fig 2a) on the church. Using Gestalt psychology rules [15], we can find the most attractive part of our object. Gestalt psychology rules attempt to describe how people tend to organize visual elements into groups or unified wholes when certain principles are applied. According this rules (Fig 6) we can assume that something different from the rest on the object can catch eye first. So we target on that detail. For this example we choose the detail of the window in the front part of the church. Now we use the premises to find a good view for whole object to his part and we get eventual worst view (Fig 7). When we have now the worst view, we can continuously get to best view (computed by some of

the methods mentioned in the chapter 2) only by ascending and again we could let visitor guess what is on the screen.



Figure 6: Dissimilarity rule in Gestalt psychology [15].

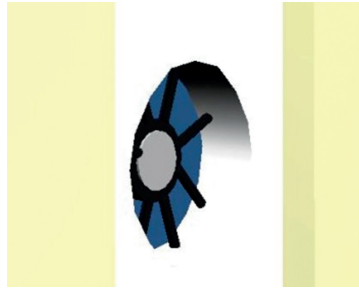


Figure 7: The worst view on church according to dissimilarity method.

## 4. CONCLUSION

In this paper we chalked out some methods useful for finding best views, possibilities of usability enhancement adequate mainly for virtual museum creators such as exploitation of found best views in animation presentation of the virtual museum. Our recent research is focused on classification of objects according to the best view. And in the end we briefly outlined the ways of improve searching for the best view using the perception and Gestalt psychology rules.

In the future work we would like to create automatic tool for classification the objects in virtual museum and follow-up usage of the right method for searching the best view.

## ACKNOWLEDGEMENTS

We would like to thank to “COMENIANA – metódy a prostriedky digitalizácie a prezentácie 3D objektov kultúrneho dedičstva”, ITMS: 26240220077, which partly supported this paper.

## References:

- [1] QVORTRUP, L., et al. 2002, *Virtual Space: spatiality in virtual inhabited 3D worlds*. Springer, 2002, Great Britain, 2002. ISBN 1852335165.
- [2] LAGA, H. 2010, *Semantics-driven approach for automatic selection of best views of 3d shapes*. Eurographics Workshop on 3D Object Retrieval, ISBN 978-3-905674-22-4.
- [3] KAMADA, T., KAWAI, S., 1988. *A simple method for computing general position in displaying three-dimensional objects*. Computer Vision, Graphics, and Image Processing 41, 1, 43–56.
- [4] BARRAL, P. et al., 1999, *Visual understanding of a scene by automatic movement of a camera*. GraphiCon, Moscow (Russia).
- [5] PLEMENOS, D., BENAYADA, M., 1996. *Intelligent display in scene modeling. new techniques to automatically compute good views*. In Proceedings of International Conference on Computer Graphics and Vision, GraphiCon'96, St Petersburg (Russia).

- [6] PLEMENOS, D., SOKOLOV, D., 2006. *Intelligent scene display and exploration*. In Proceedings of International Conference on Computer Graphics and Vision, GraphiCon'2006, Novosibirsk (Russia).
- [7] PLEMENOS, D., et al. 2004. *On viewpoint complexity of 3d scenes*. International Conference GraphiCon 2004, Moscow, Russia.
- [8] VÁZQUEZ, P.-P., et al, 2001. *Viewpoint selection using viewpoint entropy*. In Proceedings of the Vision Modeling and Visualization Conference 2001, Aka GmbH, ACM, 273-280.
- [9] PAGE, D. L., et al, 2003. *Shape analysis algorithm based on information theory*. Proceedings of the IEEE, International Conference on Image Processing, Barcelona, Spain, 1, 229-232.
- [10] KOCHANÉK, D., BARTELS R., 1984. *Interpolating splines with local tension, continuity, and bias control*. Computer Graphics, 33-41.
- [11] VARHANÍKOVÁ, I and FERKO, A. 2011: *The worst view for virtual museum presentation*, Eurographics 2011: The Eurographics Association, 2011, 21-22
- [12] VARHANÍKOVÁ, I., KUČEROVÁ, J., ČERNEKOVÁ, Z., 2012: *Best view methods suitability for different types of objects*. Spring Conference on Computer Graphics SCCG 2012: Conference Proceedings, Bratislava: Comenius University, 2012, 61-67
- [13] BERTÓK, I., JANOUŠEK, I., 1988: *Computers and art*. SPN, 1988. ISBN 80-08-00037-6.
- [14] GOLDSTEIN, B.: *Encyclopedia of Perception*. SAGE Publications, Inc., 2010. ISBN: 978-1-4129-4081-8.
- [15] WERNER K., DIEKMAYER U., 1997: *Creativity training*. Prague, 1997. ISBN: 80-7178-227-0.
- [16] VARHANÍKOVÁ, I. 2011. *Scene Geometry and Animation Curves Optimizing for Virtual Environments*. UK Bratislava, 2011.
- [17] SECORD, A., et al 2011. *Perceptual Models of Viewpoint Preference*. ACM Transactions on Graphics, Vol. 30, No 5, Article 109, 2011

---

Ivana Varhaníková,  
FMFI UK Bratislava

# Selected Methods of Semantics Extraction

## Vybrané metódy extrakcie sémantiky

Zuzana Černeková, Zuzana Haladová, Júlia Kučerová, Elena Šikudová

FMFI UK Bratislava

### Abstrakt:

*V tomto článku predstavujeme extrakciu sémantickej informácie z rôznych domén. Prinášame prehľad metód pre detekciu a popis zaujímavých bodov v obraze, modelovanie vizuálnej pozornosti a významných oblastí a podávame prehľad problémov riešených na TRECVID 2011, ktoré používajú sémantickú informáciu. Detektor a deskriptor pre kľúčové body sme otestovali v aplikáciách, ktoré v galériách rozpoznávajú maliarske diela a detekcia významných oblastí bola použitá v oblasti kompresie videa.*

### Kľúčové slová:

*sémantika, detekcia objektov, významné oblasti*

**ACM classification:** CCS → Information systems → Information retrieval → Retrieval tasks and goals → Information extraction, CCS → Information systems → Information retrieval → Specialized information retrieval → Multimedia and multimodal retrieval

### Abstract:

*The paper introduces extraction of semantic information in various domains. We bring an overview of the methods for detecting and describing interesting point in an image, modelling visual attention and saliency and review the tasks of the TRECVID 2011 that deal with using semantic information. We have tested the keypoint detectors and descriptor in an application that recognizes paintings in galleries. Detection of salient regions was used in compression of video sequences of sign language.*

### Keywords:

*semantics, object detection, saliency*

## 1. INTRODUCTION

An image is worth a thousand words. This is very true in the digital era, when people are browsing vast image databases on the internet. However, the problem of the image description remains unsolved. The semantic gap between the information that can be computationally extracted from the visual data and the interpretation that the user derives from the same data is crucial. When browsing, the users most of the time seek semantic similarity, but the databases provide similar images based only on low-level features as colour, texture, shape, etc.

In our paper, we will describe methods that identify important regions in images, extract features from these regions and assign basic semantic meaning to them. Important regions can



be found using low-level or higher-level properties. Low-level importance lies in local contrast, colour or texture difference, shape or orientation change, etc. The higher level takes into account the properties of human visual system and the concept of visual attention.

The first main part of our paper describes the method for detecting and describing interesting points in an image. The second part covers the area of visual attention and saliency. In the third part a brief overview of the TRECVID 2011 tasks using semantic information together with the best approaches is given.

## 2. Object detection

Object detection (finding if the object is presented on the image) and recognition (determining the object's category) is the key aspect of the semantics extraction process. The recognition can be seen from two different points of view:

1. Recognition of a concrete object instance (for example the mountain shelter Zamkovského chata).
2. Recognition of a class of objects (for example bugs).

Different input images for these two tasks can be seen in Figure 1.



**Figure 1:** Examples of different object recognition tasks. Top line: Recognition of a generic class: bugs. Bottom line: Recognition of concrete object instance: Zamkovského chata.

In general, we can say that in both tasks the ultimate goal is to recognize the object in all possible circumstances: different scale, rotation, background, composition with other objects, partial occlusion, varying illumination etc. This goal is very challenging, so nowadays some partial problems with imposed constraints (lighting, selected object category, etc.) are under investigation.



## 2.1 Feature extraction

The first step in the recognition process is usually the extraction of features, which describe the object to be recognized by the classifier. The features should be invariant to affine transformations, illumination and occlusions in order to recognize all instances of the object. Different types of features have emerged since the start of computer vision research, which can be generally divided in to three groups: colour, texture, and shape. We can also divide the features based on the area they describe into local and global ones.

Global features extract the information from the whole image. If we want to extract a feature, e. g the energy of the co-occurrence matrix, we first create the co-occurrence matrix for all pixels in the image and then compute the energy of this matrix.

Local features on the other hand extract information only from the parts of the image, which are „interesting“. Interesting part is the part of the image with strong variation of intensity in the local neighbourhood. Most local feature detection methods use only intensity of the images. If we examine an image of a flat white wall, we will not detect any local features. Local features are extracted in two steps. Firstly, the interesting points are detected, then the features are computed for all detected points and finally feature vectors (descriptors) are created. The classical and most cited method for detection and description of the local features is the SIFT [1]. Nowadays the methods generating local features are very popular and many new ones are published every year.

There are many different methods in the area of the interesting points detection (called interest points detectors), however three of them are used the most:

The oldest method is the Harris' corner detector [2], which computes the eigenvalues of the second moment matrix of an image at some point. Harris' method was boosted in [3] where the authors propose taking the minimum of the eigenvalues and compare it to a given threshold. If it is bigger, the point is considered a corner. SUSAN (Smallest Univalve Segment Assimilating Nucleus) [4] is another description method, which utilizes second moment matrix. SUSAN utilizes a circular mask and compares the intensity of the pixels in the map with that of its nucleus.

The second method uses the approximation of Laplacian of Gaussian with the difference of Gaussians (DoG) and looks for the local extremes in the scale-space pyramid. Scale space pyramid consists of different image scales, so called octaves (scales of the image are 1, 1/4, 1/16 etc.), with each octave containing progressively smoothed image with a Gaussian kernel. This methods is used in the well-known SIFT's and SURF's detectors [1, 5].

The third method is based on the accelerated segment test (AST). This approach examines the neighbourhood of every point of the size of the Bressenham's circle with diameter  $d=7$ . The points are concerned as interesting if there are more than  $n$  (usually 8) points in the neighbourhood that fulfil the following criteria. The intensity difference between the examined pixel and the neighbourhood pixel must be larger than a given threshold. We can find this method in the FAST detector [6].

## 2.2 Feature description

Feature descriptors can be divided into two groups: integer and binary. The main advantage of binary descriptors is that two binary strings can be compared using the Hamming distance instead of the Euclidean distance. Hamming distance can be computed very fast and it saves the matching time. Integer description methods typically use the computation of the histogram of gradients (HoG) in the patch placed around the interesting point (for example the SIFT, SURF or DAISY descriptors [7]). On the other hand, binary methods use the binary intensity tests

which compare the line endings in the mikado like patch (for example BRIEF [8] or ORB [9] descriptors).

### 2.3 Feature description matching

Another important aspect of the object recognition using local features is the matching of the feature vectors. In the matching phase, the feature vectors extracted from the unknown object are matched with the database of the feature vectors extracted from the labelled objects. An example of matched correspondences between the labelled and the unlabelled image can be seen in Figure 2. The unknown object is labelled with the same label as the object with the most matches. This phase can be time consuming when performing all-to-all brute-force matching. Different methods for organizing of the database of features for faster search and match have been published. They are based on, to name few, kd-trees (in the later implementation of SIFT), random trees [10] or spectral hashing [11] .

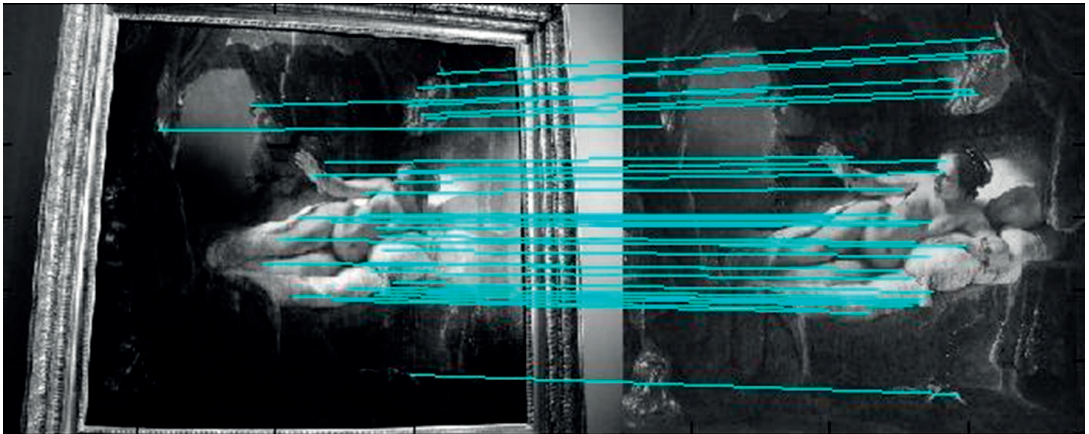


**Figure 2:** Correspondence of interest points between unlabeled image (on the left side) and labeled image (on the right side) matched with SIFT.

### 2.4 Detector/descriptor evaluation

Our tests of selected local feature approaches proved that the detectors based on AST in combination with descriptors based on binary intensity tests are much faster than DoG based detectors and HoG based descriptors. We have evaluated three methods: ORB SIFT and SURF. The results were partially published in [12]. Our database consists of 100 tourists photographs of paintings acquired in galleries and 15 training paintings. We have classified the images into 16 classes (15 paintings and 1 for paintings not presented in the database). We have achieved 90% accuracy with the SIFT and SURF methods and 80% accuracy with the ORB method. On the other hand, ORB proved to be 80 times faster than SIFT and 30 times faster than SURF. SURF is known as a faster modification of the SIFT method.

### 2.5 Test case

In our work [13] we used a combination of local and global features to speed up the process of descriptor matching. We have tested the organization of the database by sorting of the labelled images of objects. We have decided to choose global features, which are fast and efficient to compute. In the pre-processing phase, we extract one chosen global feature for all images in the database. In the run time, prior to the matching phase we extract the same global feature from the image to be labelled. Then we sort our database based on the similarity according to the

global feature. Then we match the unlabelled image with the sorted database. The first labelled images with more matches than a threshold  $t$  is considered a correct match.

In order to extract the correct value of the global feature, we need to segment the object from the unlabelled image (to avoid the background of the image affecting the feature). In our study fine art paintings are used. The segmentation consist of finding the frame of the painting.

We have tested 9 global features: average intensity, percentage of light pixels, normalized intensity histogram, entropy, normalized hue histogram, number of pixels that belong to the most frequent hue, most populated hue, hue contrast, and hue count. The colour features were computed from the image transformed to CIE Lab colour space and hue was calculated as the four-quadrant arctangent of  $b/a$ . We evaluated individual features as well as their combinations to see which feature (combination) is the best to sort the database.

The tests on the database showed that after sorting according to the best global feature the number of needed local feature descriptors comparisons dropped to the half of the number needed in the matching without sorting. During the tests for our database, the height of the highest peak in the normalized histogram of grey values proved to be the fastest (in computation time), and the second most precise in sorting of the database. It also preserves the accuracy of the recognition at 80 and 90% in ORB and SIFT/SURF respectively.

## 2.6 *Special object category – human face*

One important type of objects for detection and recognition is the human face. Face detection and recognition is important in many human-computer interaction systems. Face detection is a difficult problem because of the wide variety of faces to match, variations in colour and shadows, presence of facial hair, partial occlusion by glasses, scaling and rotation, etc.

There are many different approaches for detecting faces in the images: knowledge-based methods, feature invariant approaches, template matching, appearance-based methods. A well-known method is the Viola/Jones' face detector. This system is used for real-time face detection. Training in this face detection system is slow, but the detection is very fast. The key ideas of this face detector are integral images for fast feature evaluation, boosting for feature selection and attentional cascade for fast rejection of non-face windows. The features used by this method represent difference of sums of image intensities of specific rectangular areas. The sums are easily computed using the integral image. An integral image is a grid data structure of the size of the original image and in each point  $(x,y)$  it contains the sum of intensities in the upper-left corner starting at  $(x,y)$  of the original image. During training weak classifiers are combined into stronger ones. This is done by using the AdaBoost algorithm [14].

Face detection in coloured images involves the knowledge of skin colour distribution. The simplest method to mark the skin locus in the chosen colour space is to design a boundary using simple thresholds or more complex curves. Skin colour can be also easily modelled by a histogram generated from pixels with known labels (skin pixels). But the most popular method for skin detection is the Gaussian density function; either unimodal or so called mixture of Gaussians. Other non-parametric skin modelling methods involve neural networks, support vector machines or Bayesian decision rules [15].

Face recognition can be used as an identification or verification tool. In face identification, the query face image is compared against all the images in the database to determine the identity of the query face. During face verification, the query face image is compared solely against the face image whose identity is being proved. There are several types of face recognition algorithm including PCA, ICA, LDA, graph matching, kernel methods, active appearance model, and many more.

Principal Component Analysis (PCA) finds a subspace whose basis vectors correspond to the maximum variance direction in the original image space. In the training phase the mean face is found and subtracted from the training data. Then the  $k$  biggest eigenvectors (principal components) of the covariance matrix are computed and used to project each training image onto the subspace stated by the principal components. In the case of face recognition the eigenvectors are called eigenfaces. In the recognition phase, also the novel image is projected onto the subspace and the closest training face (within a threshold) is identified as a match.

### 3. VISUAL ATTENTION AND SALIENCY

Attention is the process of concentrating on specific features of the environment, or on certain thoughts or activities. It has a large effect on what we are aware of, on perception, on memory, on language, and on solving problems [16].

Humans cannot attend to all things at once. Their visual system has the ability to pay attention to some parts of the observed scene – salient objects. Visual attention models detect these salient objects in scene. There are two general visual processes for detecting salient objects:

- bottom-up
- top-down

The bottom-up process is task-independent. This process computes the saliency map by predicting which parts of the observed scene could attract more attention. It could be used in machine vision, automatic detection of objects in nature scenes, intelligent image compression, etc. Salient objects in scene are for example a burning candle in a dark room or the lips and eyes of a human face (because they are the most significant elements of the face). If there are many salient objects in the scene, they become obscure because of their big amount.

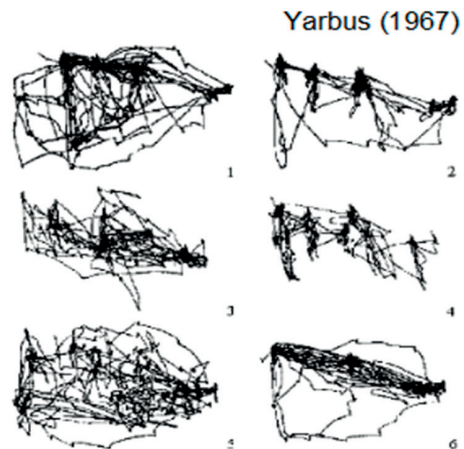


**Figure 3:** Repin's picture was examined by subjects with different instructions;  
 1. Free viewing, 2. Judge their ages, 3. Guess what they had been doing before the unexpected visitor's arrival, 4. Remember the clothes worn by the people, 5. Remember the position of the people and objects in the room, 6. Estimate how long the visitor had been away [22].

The top-down process is volition-controlled and task-dependent. The task and the volition drive the observer's attention to one or more objects that are relevant to the observers goal when studying the scene. For example, the task could be to find a red car on a car park, or to count

particular objects in a scene. When the observer is concentrated on finding some objects in the scene, he will fob off some salient objects. For that reason some objects that are salient in the bottom-up process could not be found with the top-down process. In 1967, the psychologist Yarbus recorded the eye movements of participants watching an image [16]. The subjects' task was to observe Repin's picture "An Unexpected Visitor" and to answer a number of different questions. Figure 3 show the painting and the observed eye movements for different questions.

### 3.1 *Visual attention models*

Visual attention has been studied for over a century. Early studies of visual attention were simple ocular observations. Since then the field has grown and nowadays it is involved in many scientific disciplines.

Detecting of the salient regions (which attract human vision) in the image using an eye tracking system is efficient but could be time and money consuming. Therefore, in past few years, many different visual attention models were proposed. These models are based on bottom-up, top-down visual processes and their combination.

Computational models based on the bottom-up visual process usually extract and combine low-level visual features such as colour, intensity, orientation, etc. One of the first models based on the bottom-up process was developed by Itti et al. [17]. In this model, the visual attention is based on the behaviour and the neural architecture of the early primate visual system.

Although models based on bottom-up approach [18, 19, 20, 21] are able to detect salient regions, they are just a basic description of the human vision. They are based on biological presuming of human visual attention, but in most of them, the importance of cognitive processing is missing. In visual observation of a scene there is a very important prior knowledge coming from our perceptual learning, our memory and our previous experience. The combination of low-level features and prior knowledge is a promising approach in visual attention detection.

One of the ideas of using more than low-level features is proposed in [22]. This research is based on the analysis of eye tracking data. The authors created a unique database of eye tracking data. By analysing these data they find out that observers focus their attention on faces, humans (as well as drawings and sculptures of humans) and text. They also used the data for creating a new visual attention model. In their study, they used low-level, mid-level and high-level features. This combination of features gave very good results compared to other visual attention models.

At the moment we are at the beginning of designing of a computational visual attention model that will use the prior knowledge. It is very difficult to detect all salient regions in observed scene and using prior knowledge will help to solve this challenge. Nowadays researchers focus on solving partial problems in this field.

### 3.2 *Visual attention in image and video compression*

Recently, image and video compression techniques have drawn much attention. A very popular approach for reducing the size of compressed image or video is selection of a small number of interesting regions (Regions of interest ROI) and to encode them in priority.

Regions of interest, such as humans, faces, text, etc., are very important in humans perceiving of a scene. Up to this day, many different approaches for ROI detection were proposed. Some of ROI detection approaches are very simple, other requires very difficult computations. In many approaches for image and video compression, the saliency map detection is used for ROIs determination.



The information about ROI is usually in binary form [23, 24, 25]. The compression based on this information gives very good results, but in some cases, binary information about ROI is deficient and more information is required. Therefore, in [26] different compression rate at different hierarchical salient locations is used. In this approach, original resolution is retained in the first salient region; the lowest resolution is applied in the unapparent salient regions and the middle resolution is decided by the saliency order from high to low. This method achieved variable resolution image compression by the model of visual attention.

### 3.3 Video quality assessment using visual attention approach

Visual information is very important for hearing-impaired people, because it allows them to communicate personally using the sign language. In our research [27] we focused on the fact that some parts of the person using the sign language are more important than others (e.g. hands, face). We presented a visual attention model based on detection of low-level features such colour, intensity and texture and combination with the prior knowledge – in our case information about skin in image (Figure 4). Information about the visually relevant parts allows us to design an objective metric for this specific case. We presented an example of an objective metric based on human visual attention and detection of salient object in the observed scene. The proposed metrics were compared to existing metrics and the results were very promising for the following research.



**Figure 4:** Image taken from the experiment [27]: a) original and b) product of the original image (only Y canal from YUV colour space) and the saliency map.

## 4. SEMANTIC EXTRACTION FROM VIDEOSEQUENCE

There is a huge use of semantic information in video search. The ability to detect features is an interesting challenge by itself, but it takes on added importance to the extent it can serve as a reusable, extensible basis for query formation and search. Nowadays, the researchers focus mainly on solving the problems of finding the semantic information in video sequences. To promote progress in content-based retrieval from digital video via open, metrics-based evaluation is a goal of the TRECVID conference. The organizers of TRECVID want not only to provide a common corpus of video data as a testbed for different algorithms, but also to standardize and oversee their evaluation and to provide a forum for the comparison of the results [28]. In the last years, most of the TRECVID tasks focused on extracting semantic information from the video sequences. The next sections briefly describe the TRECVID 2011 tasks [29] together with the best approaches.

## 4.1 Semantic indexing

A potentially important asset to help video search and navigation is the ability to automatically identify the occurrence of various semantic features such as “Indoor/Outdoor”, “People”, “Speech” etc., which occur frequently in video information.

Systems developed for this task focused on robustness, merging many different representations, use of spatial pyramids, improved bag of word approaches, improved kernel methods, sophisticated fusion strategies, and combination of low and intermediate/high features. The best performance in semantic indexing was obtained using Gaussian mixture model (GMM) supervectors and tree-structured GMMs [30, 31]. GMM supervectors corresponding to six types of audio and visual features are extracted from video shots by using tree-structured GMMs. The extracted features are SIFT features with Harris-Affine detector, SIFT features with Hessian-Affine detector, SIFT and hue histogram with dense sampling, histogram of oriented gradients (HOG) with dense sampling, HOG from temporal subtraction images and Mel-frequency cepstral coefficients (MFCCs). The computational cost of maximum a posteriori (MAP) adaptation for estimating GMM parameters are reduced by tree-structured GMMs by keeping accuracy at high levels [32].

## 4.2 Known-item search

Imagine a situation in which someone has seen a video before, and they want to find it in a provided collection, but does not know where to look. To begin the search process, the searcher formulates a text-only description, which captures what the searcher remembers about the target video. This task is very different from the TRECVID ad hoc search task in which the systems began with a textual description of the need together with several image and video examples of what was being looked for.

The best result among all automatic search runs was achieved using the automatic text-based search system consisting of several main components, including text pre-processing, keywords extracting and processing, text-based retrieval, results fusion and re-ranking [33]. Authors of this approach proposed also a bio-inspired method. In this approach, a query topic is first parsed by a text analyser to produce several search cues, and then the cue-based bottom-up saliency map and the top-down cue-guided concept/object detection are fused and refined by the aid of context cues. This approach did not obtain as good results as the text-based search but can be promising if the attention model and knowledge base are further improved.

## 4.3 Instance search

In many situations involving video we need to find more video segments of a certain person, object, or place, given one or more visual examples of the specific item. Given a collection of test videos, a master shot reference, and a collection of queries that delimit a person, object, or place entity in some example video, the task is to locate for each query 1000 shots most likely to contain a recognizable instance of the entity.

The best results in this task were obtained using large vocabulary quantization by hierarchical k-means and weighted histogram intersection based ranking metric [34]. In the offline indexing phase the algorithm searches for matching in a computationally cheaper high dimensional bag-of-words feature space. Three frames per second are chosen from every video clips, and then SIFT descriptors are sparsely extracted. Then all SIFT descriptors are projected into the vocabulary tree and they get only one bag-of-words histogram as its representation. In the online searching phase, the SIFT features are extracted from the probe image and they are projected to the vocabulary tree. Thus, one histogram is obtained as the representation for

current probe topic. Histogram intersection metric is then taken to rank the similarity between each probe topic with every candidate video clip.

#### 4.4 Multimedia event detection

A user searching for events in multimedia material may be interested in a wide variety of potential events. Since it is an intractable task to build special purpose detectors for each event a priori, a technology is needed that can take as input a human-centric definition of an event that developers (and eventually systems) can use to build a search query. The events for multimedia event detection were defined via an event kit, which consisted of:

- An event name which is a mnemonic title for the event.
- An event definition which is a textual definition of the event.
- An event explication which is an expression of some event domain-specific knowledge needed by humans to understand the event definition.
- An evidential description which is a textual listing of the attributes that is indicative of an event instance. The evidential description provides a notion of some potential types of visual and acoustic evidence indicating the event's existence but it is not an exhaustive list nor is it to be interpreted as required evidence.

The Raytheon BBN's VISER system [35] showed the best performance among all the submitted systems. The VISER system incorporates a large set of low-level features that capture appearance (SIFT, SURF, D-SIFT, CHoG), colour (RGB-SIFT, OpponentSIFT, and C-SIFT), motion (Space-Time Interest Points – STIP, D-STIP), audio, and audio-visual co-occurrence patterns in videos. The system also uses high-level (i.e. semantic) visual information obtained from detecting scene, object, and action concepts. Furthermore, the VISER system exploits multimodal information by analysing available spoken and videotext content. These streams are combined into a single, fixed-dimensional vector for each video. Two combination strategies are explored: early fusion and late fusion. Early fusion is implemented through a fast kernel-based fusion framework and late fusion is performed using both Bayesian model combination as well as a weighted-average framework.

## 5. CONCLUSION

Emerging new technologies demand tools for efficient indexing, browsing and retrieval of image and video data, which causes rapid expansion of areas of research where the semantic information is used. New methods that work with semantic information in image, video, and audio are developed frequently these days, which means that our list of methods is not final. Nevertheless, we picked the most used ones and tested them. We brought an overview of the methods for detecting and describing interesting points in an image, modelling visual attention and saliency and reviewed the tasks of the TRECVID 2011 that deal with semantic information. We have tested the keypoint detectors and descriptors in an application that recognizes paintings in galleries. We have evaluated the use of visual saliency for compression of video sequences containing sign language.

### Acknowledgements

This work was funded from projects KEGA 068UK-4/2011 and VEGA 1/0602/11.

### References:

- [1] Lowe, D. G. 2002. *Distinctive image features from scale-invariant keypoints*. International Journal of Computer Vision, 60(2):91-110, 2002.

- [2] Harris, C. – Stephens, M. 1988. *A combined corner and edge detector*. In Proc. of Fourth Alvey Vision Conference, pages 147§151, 1988.
- [3] Shi, J. – Tomasi, C. 1994 *Good features to track*, *Computer Vision and Pattern Recognition, 1994. Proceedings CVPR '94, 1994 IEEE Computer Society Conference on*, vol., no., pp.593-600, 1994.
- [4] Smith, S. M. – Brady, J. M. 1995. ***Susan – a new approach to low level image processing***. *International Journal of Computer Vision*, 23:45§78, 1995.
- [5] Bay, H. – Ess, A. – Tuytelaars, T. – Gool, L. V. 2008. ***Speeded-up robust features (surf)***. *Computer Vision and Image Understanding*, 110(3):346 § 359, 2008.
- [6] Rosten, E. – Drummind, T. ***Machine learning for high-speed corner detection***. In A. Leonardis, H. Bischof, and A. Pinz, editors, *Computer Vision – ECCV 2006*, volume 3951 of *Lecture Notes in Computer Science*, pages 430§443. Springer Berlin / Heidelberg, 2006.
- [7] Tola, E. – Lepetit, V. – Fua, P. 2008. *A fast local descriptor for dense matching*. In *Conference on Computer Vision and Pattern Recognition*, 2008.
- [8] Calonder, M. – Lepetit, V. – Strecha, C. – Fua, P. 2010. ***Brief: Binary robust independent elementary features***. In *Computer Vision – ECCV 2010*, volume 6314 of *Lecture Notes in Computer Science*, pages 778-792. Springer Berlin / Heidelberg, 2010.
- [9] Rublee, E. – Rabaud, V. – Konolige, K. – Bradski, G. 2011. *ORB: An efficient alternative to SIFT or SURF*, *Computer Vision (ICCV)*, 2011 IEEE International Conference on, vol., no., pp.2564-2571, 6-13 Nov. 2011
- [10] Lepetit, V. – Fua, P. 2006. ***Keypoint recognition using randomized trees***, *Pattern Analysis and Machine Intelligence, IEEE Transactions on*, vol.28, no.9, pp.1465-1479, Sept. 2006 doi: 10.1109/TPAMI.2006.188
- [11] Ventura, J. – Hollerer, T. 2011. *Fast and scalable keypoint recognition and image retrieval using binary codes*, *Applications of Computer Vision (WACV)*, 2011 IEEE Workshop on, vol., no., pp.697-702, 5-7 Jan. 2011 doi: 10.1109/WACV.2011.5711573
- [12] Haladova, Z. – Šikudova, E. 2011. ***Limitations of the SIFT/SURF based Methods in the Classifications of Fine Art Paintings***. In *Computer Graphics and Geometry*. Vol.12 No. 1, 2010 the summer issue, s. 40-50. ISSN 1811-8992.
- [13] Haladová, Z. – Šikudová, E. 2013. Combination of global and local features for efficient classification of paintings, in *Proc. Spring Conference on Computer Graphics SCCG 2013*, Bratislava, 2013, pp. 21-27
- [14] Freund, Y. – Schapire, R. E. 1999. A Short Introduction to Boosting. In *Journal of Japanese Society for Artificial Intelligence*, 14(5):771-780, September, 1999.
- [15] Šikudová, E. 2007. Comparison of color spaces for face detection in digitized paintings, In. *Proc. Spring Conference on Computer Graphics SCCG 2007*, pp. 135-140
- [16] Yarbus, A.L. 1967. Eye movements during perception of complex objects. In *Eye Movements and Vision*, Plenum Press, New York, Chapter VII, pp. 171-196.
- [17] Itti, L. et al., 1998. A model of saliency-based visual attention for rapid scene analysis. *IEEE Transactions on Pattern Analysis and Machine Intelligence* 20, 11, 1254-1259.
- [18] Bur, A. – Hugli, H. 2007. Optimal cue combination for saliency computation: A comparison with human vision. In *Proc. . 2nd int. work-conference on Nature Inspired Problem-Solving Methods in Knowledge Engineering, IWINAC '07*, pages 109-118.
- [19] Le Meur, O. – Le Caller, P. – Barda, D. 2007. Predicting visual fixations on video based on low-level visual features. *Vision Res*.
- [20] Oliva, A. – Torralba, A. – Castelhana, M. S. – Henderson, J. M. 2003. Top-down control of visual attention in object detection. In *Proc. of the IEEE Int'l Conference on Image Processing (ICIP '03)*.
- [21] Zhang, L. – Tong, M. – Marks, T. – Shan, H. – Cottrell G. 2008. Sun: A Bayesian framework for saliency using natural statistics. *J Vis*, 8(7):32.1§20.
- [22] Judd, T. – Ehinger, K. – Durand, F. – Torralba, A. 2009. Learning to predict where humans look. In *IEEE International Conference on Computer Vision (ICCV)*.

- [23] Fukuma, S. –Tanaka, T. – Nawate, M. Switching wavelet transform for ROI image coding. IEICE Trans. Fundam. Electron. Comm. Comput. Sci., E88-A(7):1995-2006, July 2005.
- [24] Ouerhani, N. – Bracamonte, J. – Hugli, H. – Ansorge, M. – Pellandini, F. Adaptive color image compression based on visual attention. In Proc. Image Analysis and Processing, pages 416-421, Sep 2001.
- [25] Harding, P. – Roberston, N. Task-based visual saliency for intelligent compression. In Signal and Image Processing Applications (ICSIPA), 2009 IEEE International Conference on, pages 480 – 485, Nov. 2009.
- [26] Wei, L. – Sang, N. – Wang, Y. – Wang, D. –Wang, F. Variable resolution image compression based on a model of visual attention. Pages 74950P, 2009.
- [27] Kučerová, J. – Polec, J. – Tarciová, D. 2012. Video quality assessment using visual attention approach for sign language. volume 65, pages 194§-199. World Academy of Science, Engineering and Technology.
- [28] Smeaton, A. F. – Over, P. – Kraaij, W. 2006. Evaluation campaigns and TRECVID, *MIR'06: Proceedings of the 8th ACM International Workshop on Multimedia Information Retrieval*, 2006, Santa Barbara, California, USA, ACM Press, pp 321–330,
- [29] Over, P. et al. 2011. TRECVID 2011 – An Overview of the Goals, Tasks, Data, Evaluation Mechanisms, and Metrics, *TRECVID 2011*
- [30] Inoue, N. – Shinoda, K. 2011. A Fast MAP Adaptation Technique for GMM-supervector-based Video Semantic Indexing Systems. In Proc. of *ACM Multimedia* (short paper), 2011
- [31] Inoue, N. et al. 2010. High-Level Feature Extraction using SIFT GMMs and Audio Models. In Proc. of *ICPR*, 2010.
- [32] Inoue, N. et al. 2011. TokyoTech+Canon, *TRECVID 2011*
- [33] Zhao, Z. et al. 2011. BUPT-MCPRL, *TRECVID 2011*
- [34] Le, D. – et al. 2011. National Institute of Informatics, Japan, *TRECVID 2011*
- [35] Natarajan, P., 2011. BBN VISER TRECVID 2011 Multimedia Event Detection System, *TRECVID 2011*

---

**Zuzana Černeková, Zuzana Haladová,  
Júlia Kučerová, Elena Šikudová**  
FMFI UK Bratislava



# Use of Cellular Automaton in Crowd Animation

Jana Běhal Dadová, Roman Franta, Petra Gottlieberová,  
Dominik Kapišinský, Ján Ruhalovský

## Abstract:

Our work is focused on crowd simulation with cellular automata. We used this automata for control of collisions, behavior even motion. To create believable motion we use motion retargeting and motion graphs, which create also large database of motions. Moreover we also present example with non photorealistic rendering that is well suitable for some crowd simulations.

## Keywords:

Crowd Simulation, Cellular Automata, Motion Graph, Motion retargeting, Labanotation

## ACM classification:

I.3.8 [Computer Graphics]: Applications; I.3.0 [Computer Graphics]: General;

## 1. Introduction

Crowd simulation could be used for various problems. This problems include emergency simulations, virtual museum evaluations or enrichment of virtual worlds. In emergency simulation bottlenecks of flow could be identified by simulated crowd. In virtual museum, or exhibition halls, placement of exhibits could be evaluated by crowd simulation. In both of these problems it is important to have simulation where participants behave according to patterns that are in real crowd in this environment. On the other hand, for simulation that are used to enrich virtual environments it is necessary to create also believable motion of individuals and rendering.

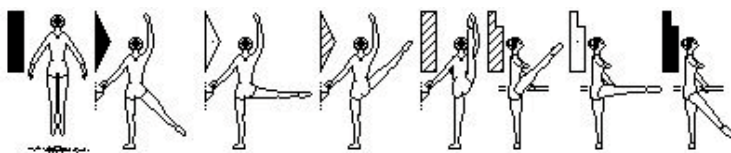
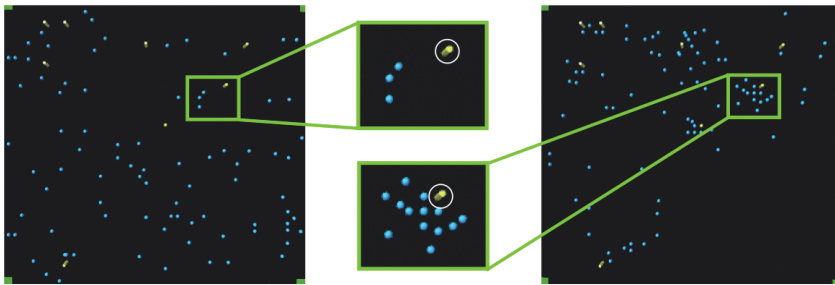


Fig. 1. Labanotation for leg movement [1].

## 2. Related Work

During process of creating crowd simulation there are these four groups of topics that need to be considered: initialization, movement of a crowd (planning, collision detection, behavior), movement of individuals, rendering. Initialization includes distribution of individuals and setting their initial values for simulation purposes [7]. Next step includes planning of movement where individuals behaves as one large group, which was originally presented by Reynolds [5]. For more interesting behavior, it is important to choose specific environment, in our case museum, and study behavior of visitors [6]. On the other hand each individual has also set of rules that defines personality and desire [7]. According these rules individuals plan their movement and behavior. This step is independent on actual shape and movement of individual participants.

In next step, which is movement of individuals, it is important to have believable motion. This can be achieved by using motion capture data, that are specially retarget to used shapes [2]. Moreover, more motion can be created by motion graphs, where in nodes are motions, or keyposes, that are obtained from motion capture and on edges are transitions [4]. With simple graph walk we can created new, longer motions. It is also possible to store motions in special language, Labanotation, which is similar to staff scheme [1]. Disadvantage is that this language is highly empiric and therefore some modifications are needed to be easily used by algorithms. Examples are shown in fig. 1.



**Fig. 2.** Various stages of the simulation. (left) initial step, (right) step during movement. Blue spheres are participants that are interested in objects (yellow cylinders) and are grouped around these interesting objects.

For the rendering problem, also in crowd simulation it is important to emphasize some features of the crowd and therefore non-photorealistic rendering could be used for simulation purposes, for example cartoon style [3]. On the other hand, crowd animations for entertainment purposes are usually rendered in highly realistic detail, but these type of crowd animations are not scope of our work.

## 3. Cellular Automata Behavior Control

Cellular automata are used for easy collision detection, because neighborhood is well defined and therefore neighbors are easily found. Moreover behavior control is also easier, because close environment is also well defined. We use cellular automata for crowd simulation in virtual exhibition hall. Interesting objects and whole crowd are placed in this environment during simulation process, individuals are moving according to their behavior rules and are grouped near interesting objects, see fig. 2.

Special behavior model is needed, because this environment is different from standard pedestrian simulations. We use dimensional approach from psychology, where behavioral

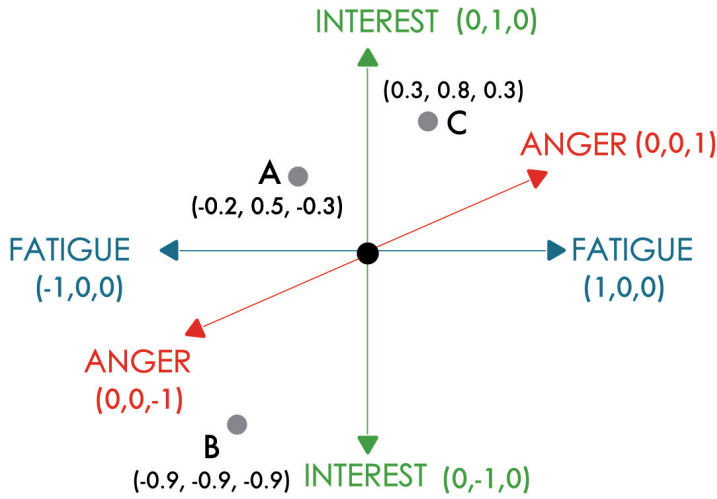


**Fig. 3.** Three dimensional behavior model. A, B, C are actual moods with their coordinates in space.

patterns are mapped on three axes (interestingness, fatigue, anger) according to [6] and actual mood is vector from this space. Example is shown in fig. 3.

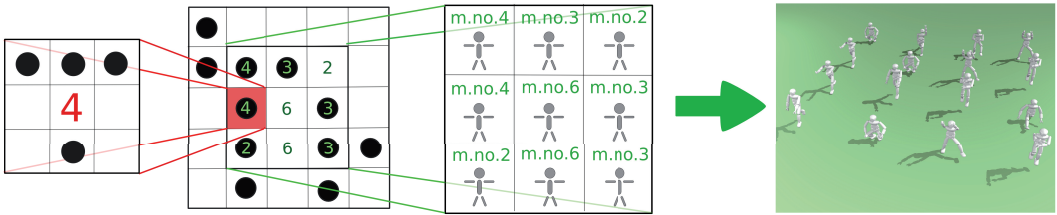


**Fig. 4.** Our approach in a nutshell: (a) Moore neighborhood (8-neighborhood) of a cell with neighbors in black (b) One step of an automaton (3x3 grid) (c) mapping to movements of a group (d) final render.

## 4. Cellular Automata Motion Control

Cellular automata could be used not only for behavior control and motion in the environment, as is used in other similar works [7], but also for movement of participants itself. If automaton is changed according to powerful rules, such as Game of Life, then values from cells can be associated with participants in crowd. This connection is shown in fig. 4. These values define index to database of motions and specified motion for individuals in each timestep is chosen from database of motions and retarget to individuals.

Values in cells of automaton are changed in each timestep according to pre-defined rules and neighborhood of cells. In case of Game of Life neighborhood is defined by standard Moore's (8-neighborhood). Poses in keyframes and during each timestep are shown in fig. 5.

To create larger and robust database of motion, motion graph is used. We define key-poses in each node, then edges are created by transitions, which are automatically calculated between similar poses. Also price is given to edges according to the similarity between nodes. By specifying two nodes and automatic calculation of graph walk with minimal price we can

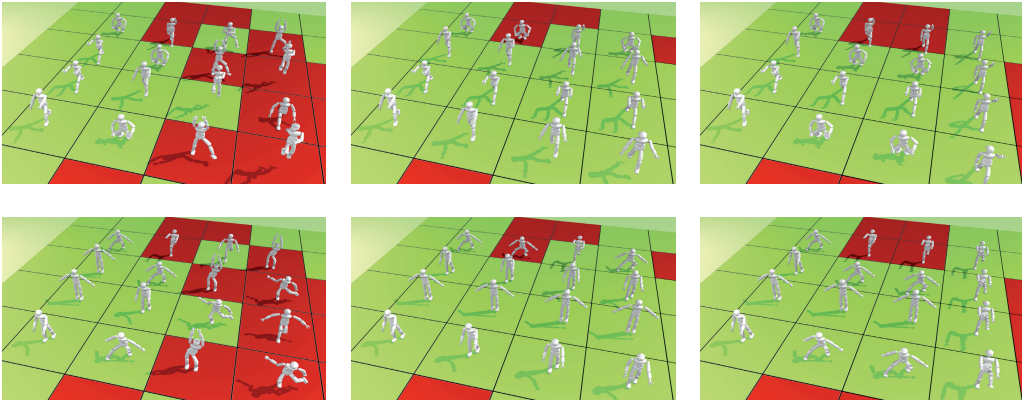


**Fig. 5.** Results from our approach in a three following steps. Top row - beginning of the movement, Bottom row - middle stage of the movement. Red cells are occupied, green cells are free.

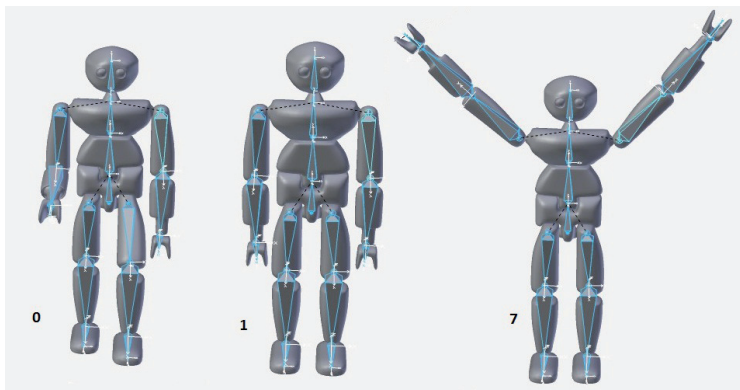


**Fig. 6.** Starting pose (0), ending pose (7), pose generated by graph walk (1)

created motions for each timestep. Example of inbetween pose is shown in fig. 6.

## 5. Rendering

In this section we would like to present use of cartoon style for crowd simulation. There are situations where realistic rendering is not preferred. When we use crowd simulation to emphasize shape that crowd creates, or target where crowd is heading it is better to use non-photorealistic rendering and highlight this features. Example of crowd rendering with target is shown in fig. 7 where members of a crowd that are nearer to the target are more saturated and with sharper edges.

## 6. Future work and Conclusion

In conclusion, we presented various subproblems in crowd simulation and examples of the solutions. For this experimental solution we used Python API in Blender Modeling Software. These solutions are not complete and evaluated, there is still space to improve behavioral model with visual system and memory, transitions between movements and more sophisticated rendering. In the future work we would like to created simulations that we could evaluated

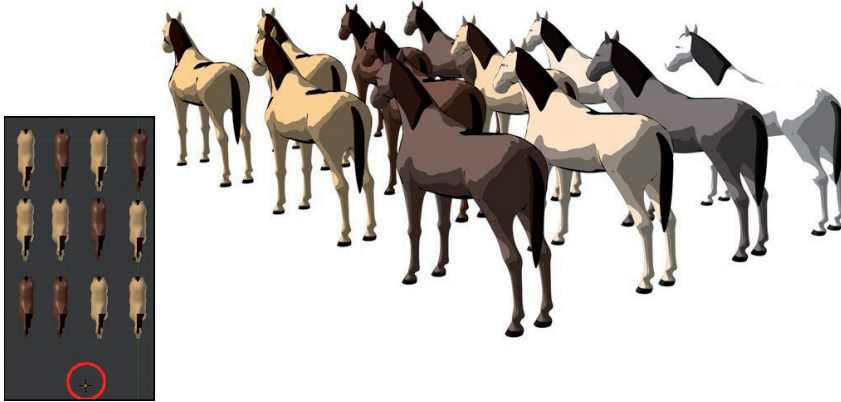


Fig. 7. Crowd rendering with cartoon style and target settings.

with behavior from real world situations. More about our work can be found in <http://www.sccg.sk/~dadova/publications.html>.

## References

- [1] Introduction to labanotation [online][cit. 5.1.2012]. <http://user.uni-frankfurt.de/~griesbec/LABANE.HTML>.
- [2] Michael Gleicher. Retargetting motion to new characters. In *Proceedings of the 25th annual conference on Computer graphics and interactive techniques*, SIGGRAPH '98, pages 33–42, New York, NY, USA, 1998. ACM.
- [3] Amy Gooch, Bruce Gooch, Peter Shirley, and Elaine Cohen. A non-photorealistic lighting model for automatic technical illustration. In *Proceedings of the 25th annual conference on Computer graphics and interactive techniques*, SIGGRAPH '98, pages 447–452, New York, NY, USA, 1998. ACM.
- [4] Lucas Kovar, Michael Gleicher, and Frédéric Pighin. Motion graphs. *ACM Trans. Graph.*, 21:473–482, July 2002.
- [5] Craig W. Reynolds. Flocks, herds and schools: A distributed behavioral model. *SIGGRAPH Comput. Graph.*, 21(4):25–34, July 1987.
- [6] Edward S. Robinson, Irene C. Sherman, Lois E.C. Strayer, Horace H.F. Jayne, and Philadelphia Museum of Art. *The behavior of the museum visitor*. Publications of the American Association of Museums. American Association of Museums, 1928.
- [7] Daniel Thalmann and Soraia R. Musse. *Crowd Simulation*. Springer, 1 edition, October 2007.



.....

**Jana Běhal Dadová**

Department of Algebra, Geometry and Didactics of Mathematics,  
Faculty of Mathematics, Physics and Informatics, Comenius University,  
Mlynská dolina, 842 48 Bratislava, Slovakia.  
jana.daodva@fmph.uniba.sk

**Roman Franta**

Department of Applied Informatics,  
Faculty of Mathematics, Physics and Informatics, Comenius University,  
Mlynská dolina, 842 48 Bratislava, Slovakia.  
roman.franta@fmph.uniba.sk

**Petra Gottlieberová**

Department of Applied Informatics,  
Faculty of Mathematics, Physics and Informatics, Comenius University,  
Mlynská dolina, 842 48 Bratislava, Slovakia.  
petra.gottlieberova@fmph.uniba.sk

**Dominik Kapišinský**

Department of Informatics,  
Faculty of Mathematics, Physics and Informatics, Comenius University,  
Mlynská dolina, 842 48 Bratislava, Slovakia.  
dominik.kapisinsky@fmph.uniba.sk

**Ján Ruhalovský**

Department of Informatics,  
Faculty of Mathematics, Physics and Informatics, Comenius University,  
Mlynská dolina, 842 48 Bratislava, Slovakia.  
jan.ruhalovsky@fmph.uniba.sk



# MUVIS: a PUBLIC participatory urban planning and multidimensional visualization ONLINE SYSTEM

Matej Novotný, David Behal, Peter Borovský, Zuzana Černeková, Andrej Ferko, Martin Florek, Ján Lacko, Martin Samuelčík, Stanislav Stanek, and Elena Šikudová  
Comenius University, SK-842 48 Bratislava, Slovakia

## Abstract:

MUVIS (Multidimensional Urban Visions) is an applied research project aimed to create an extensible platform for online participatory urban planning and multidimensional visualization. In the Virtual Petržalka case study we facilitate model creation and visualization as well as support discussion of urban planning and its visions from any creative author. We describe selected problems in Bratislava urban planning in the past and we discuss our approach, its usability, acceptance, and estimation of its future impact.

## Keywords:

Virtual worlds software, Geographic visualization, Visualization toolkits

## Abstrakt:

MUVIS (Multidimensional Urban Visions) je rozširovateľná platforma na internetovú podporu tvorby mesta pomocou verejnej diskusie. Pre ľudí, miestne samosprávy a investorov umožní dialóg všetkých zúčastnených a na príklade virtuálnej Petržalky poskytne nástroj na tvorbu, vizualizáciu a diskusiu o víziách a plánoch na podporu čo najlepších rozhodnutí o budúcnosti našich miest. Opíšeme vybrané problémy urbánneho rozvoja Bratislavy z minulosti a vyhodnotíme náš prístup, jeho použiteľnosť a prijateľnosť aj možný budúci význam.

## Kľúčové slová:

Softvér pre virtuálne svety, Geografická vizualizácia, Vizualizačné nástroje

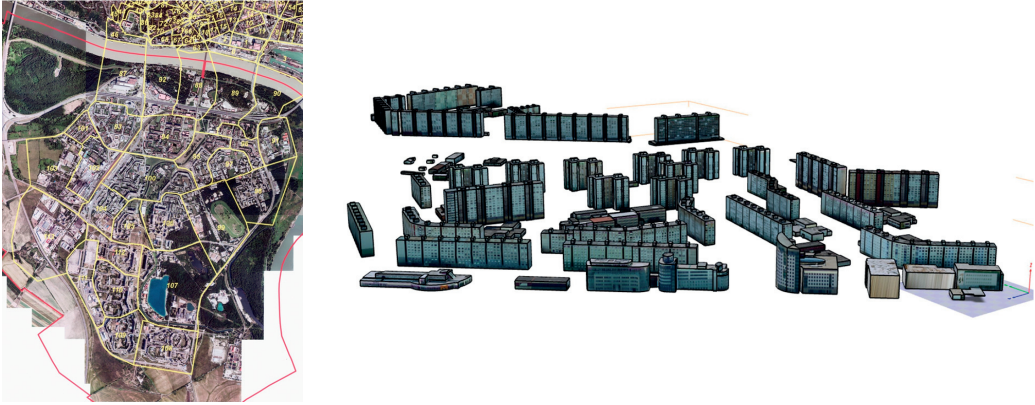


**Figure 1:** (a) Left: Bratislava historic center is separated from Petržalka (encircled by the red border) by the Danube river. The whole area was subdivided into smaller parts (yellow borders) for the purpose of model creation. Aerial photo courtesy of Eurosense Slovakia. (b) Right: Petržalka is a controversial urban area with miserable architecture, infrastructure, and many unsolved problems. Building MUVIS database starts with aerial images, rooflines, and building footprints from Cadaster Portal of Slovakia. Initial Petržalka dataset without terrain and vegetation rendered by Martin Samuelčík illustrates the urban problem, where the people have to live in.

## INTRODUCTION

MUVIS offers a recent technology solution, transfers the ideas from academy to practice and attempts to affect – in the best possible way – the future of our cities. MUVIS, finishing in March 2013 will offer the people, local authorities, and investors a dialogue of all participants. In this paper we overview the methodology, technology, and both digital content creation and presentation. In the rest of the paper we introduce Bratislava and Petržalka motivation, the previous work, methodology and technology. In more detail, we present our project decisions and achievements. Finally, we conclude and discuss the future work.



**Figure 2:** Historic discontinuity visualization: (a) Left, a painted veduta from 18<sup>th</sup> century serves as a symbol for the old city, (b) Right, a screenshot from Virtual 3D Bratislava Navigation Tool by Stanislav Stanek. Aerial photo courtesy of Eurosense Slovakia, terrestrial photo by Matej Zeman. The popular statue symbolically wonders the highway damaging old city beauty.

## BRATISLAVA AND PETRŽALKÁ MOTIVATION

Bratislava (Pressburg, Posonium, Istropolis) urban development and phenomenon of genius loci [Norb00] suffered a lot from many historical and ideological discontinuities. One of the victims of such deformations was the Bratislava Castle vicinity, visible in Fig. 2(a) left in its original organic urban context and today, Fig. 2(b). In the year 2009, the archaeological research discovered an old Celtic castle underneath the current Bratislava Castle. Probably, it is – according to Austrian professor Werner Jobst [Mus10] – the lost Carnuntum the capital of the Noricum province, mentioned by in written history – in the year 6. The castle was destroyed by fire in 1811, however, being considered as a symbol of feudalism, this ruined memorial without a roof and surrounding prominent urban area was not renovated until about 150 years later the fire. Next to the castle we can find probably the top anti-cultural damage of a historic old town – a highway between the Castle and the Coronation Church Fig. 2(b). The valuable historic urban area, an original place of history and local atmosphere, was cut by modernistic and noisy transport route built as a prolongation of a postmodern bridge.

Despite these and others urban atrocities, the biggest urban area under permanent public discussion is Petržalka, illustrated in Figure 1. Petržalka is a giant habitat built from the cheapest housing alternative – panel buildings. The biggest and longest blocks of them are nicknamed the Chinese Wall. Its 150 000 population makes Petržalka, so to say, the third biggest city in Slovakia (the second one Kosice (eastern Slovakia) is the European Cultural Capital 2013) with the highest divorce rate, remarkable crime problems and other poor indicators of the quality of life. One of the general solutions for the future urban development seems to be the public participation in decision making. As the current urban disaster cannot simply be replaced, we have opened a new communication channel for public participation in its current and future urban development and improvement. The abovementioned context motivated our decision to choose Petržalka as the first case study for the MUVIS project. Virtual model of Petržalka extends the existing virtual model of historic Bratislava southwards and MUVIS was verified, tested, and evaluated using this urban database.

## PREVIOUS WORK

Many authors identified the alienation of modern architecture and urbanism. A public participation GIS (PP GIS) is often proposed as a promising alternative [Kyem09]. MUVIS is an extensible platform for online participatory urban planning and multidimensional visualization. Exploiting a layered multidimensional content structure, aware of time and space in the virtual city, MUVIS users will share and co-author “The City as a Process in Time and Space” [Fers02], at least virtually. Urban planners search for shapes and functions on multiple scales, forming a new version of “urban text”, but there is no complex vocabulary of scales, shapes and functions, they are discovered and created ad hoc. The valuable old cities – among others Graz, Prague, Vienna, Bardejov (eastern Slovakia) – were included into the UNESCO’s World Cultural and Natural Heritage List. The unlucky ones, like Petržalka, heavily influenced by the unqualified past decisions, especially inorganic changes, suffer from alienation, anonymity, missing infrastructure and another miserable phenomena.

The organicity of change and proportionality of shapes can be approximately measured using fractal geometry [Sali03]. We guess the famous Waterfall by Wright induces a largely different measure compared to the Bratislava highway cut through the heart of the old town – placing the Coronation Church facade right next to everyday pressure of trucks, cars, and buses. The collective imagination in this case is not formed, but deformed. The first experiments with Bratislava fractal measurements arose in a PhD thesis [Mesz10] at the Slovak University of Technology. The PP GIS approach studied Viera Joklova [Jokl07]. She identifies urban area as being influenced by an intersection of a professional and a public approach, sharing multiple



modalities of maps, models, and metadata, Fig. 3.

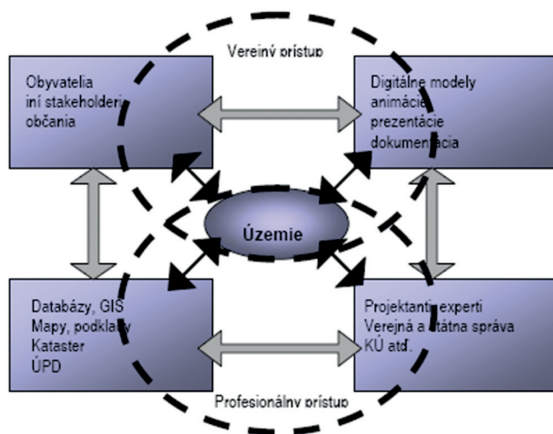
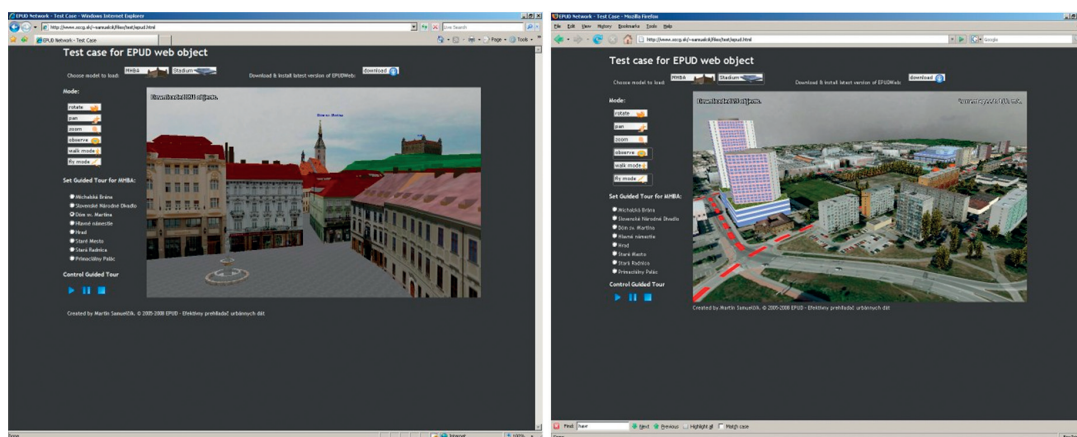


**Figure 3:** Multiple intersections of interests and needs in urban area. Image courtesy by Viera Joklova.

Schéma 8 : Participácia v území

### 1.1 A Few Urban Planning Notions

The city has, among other places (squares, riversides, streets, quarters), the *city verticals*, given by towers, memorials, silhouettes, rivers and wells (old water sources). The oldest known ancient algorithm for founding a new city has been preserved in Latin books. The founders of Rome were the Etruscans – “engineers” invited by the rural Romans who had no knowledge in the field that time. The Etruscans computed the city location, ploughed the city border around, erected the city tower to transcend the city to the sky and – nearby – they dug a *mundus*. The *mundus* was not necessarily a well, but it meant the symbolic root of the city, transcending the city downwards, into the earth and into the depth. (One can see in erecting and rooting the male and female principles.) The Etruscan language, being isolated from Indo-European ones, did not survive up to now. Despite the fact we use two fundamental Etruscan words. This cultural heritage preserved Latin for us – *urbs* (the city) and *mundus* (the world, the meaning was



changed by the Latin users in ancient Roman Empire).

**Figure 4:** (a) Left, one of the first experiments to fly over virtual Bratislava using Microsoft Internet Explorer. The screenshot displays Bratislava Castle Hill without vegetation and the Coronation Church tower as seen from the Old City Hall. EPUD software tool was



*used as web object here. (b) A model of a part of Petržalka in Mozilla Firefox using our EPUDWeb object.*

There are several well-known urban thinking milestones, for city creation the famous Ten Books on Architecture by Vitruv [Vitr09], for city perception Lynch's Image of the City [Lync60]. His perceptual notions - especially **imageability** - express the **readability, areas, squares, borders...** Individual perception of a particular place, **genius loci**, has phenomenological explanation in [Norb81]. **The place** is, after Forte, the author of virtual museum definition [Qvor01], the opposite of an alienated **space** (e.g. hypermarket). The architectural alienation is discussed e.g. in [Bang07], the alienation of architecture and urbanism was studied e.g. by Rem Koolhaas, and socio-psychological problems of urbanism in [Mits69]. Bangs judges that the architecture missed classic craft in mastering proportions and preserving archetypes like cave, glade... The habitat (flat, house) should balance the needs for privacy and public space, which is not possible in noisy panel houses. Nowadays, nobody has a legal way to coordinate investor's egoisms, which would lead [Mits69] to unthinkable limitation of private property rights. Therefore, long-term **public participation (PP)** is one of the experiments to overcome the alienation. **The Aarhus Convention** [Aarh98] is a new sort of an environmental deal, trying to harmonize both human and environmental rights [Jokl07, p. 73]. PP can be characterized as a forum for exchange of opinions, experiences, knowledge, organized to support communication of all segments, solving the specific problems in given area [Renn95]. PP can support social inclusion, better concurrency, social cohesion, environmental balance and public feedback for decision making [Gave98]. PP classification and its computerized support is offered in [Jokl07, p. 73n] and PP is mandatory in Germany by law [Jokl07, p. 79]. The risky aspect of PP is that the public is not prepared for it. Therefore, MUVIS mission includes the technology enlightenment/evangelization part, as well. We distinguish **GIS** as a professional planning tool used for decision-making [Jokl07] from **PPGIS (Public Participation Geographical System)**, combining methods and technologies, conveying interactive presentation of various alternatives of geospatial data, based on problem-oriented selection. A relatively recent survey of PPGIS projects and dilemmas offers [Kyem09]. Another alternatives represent **geobrowsers** (Google Earth [GooE09], MS Virtual Earth [MSVE09]), compared e.g. in [Lebe07], and **VEPS (Virtual Environment Planning Systems)** [Jokl07]. The functionality of each of the above alternatives necessarily covers file and database management, search and navigation in space, time, or semantics, calibrating, filtering and storage, versioning, urban database editing, multimedia presentation of ideas, feedback, comments, forum and voting subsystems. Since all of them are VR systems, their architecture can be broadly subdivided into four categories: scene graph, semantic database, generic system, or distributed system [Guti07].

## 1.2 Cyber Cities

The vision of future internet outlines the Semantic Web [Bern01], requiring autonomous agents and globally built ontologies like CIDOC CRM [Crof05] for cultural heritage and INSPIRE [Jan09] for geodata. The cyber cities [VirC09] methodology started with a few chapters in [Leon00]. Work-flow issues for automation are analyzed by F. Leberl et al. [Lebe00] into three parts: 1. Aerial photogrammetry, 2. Digital canopy elevation model, and 3. Building geometry extraction. The Model building pipeline is characterized by G. Roth [Roth00] as: 1. Calibration, 2. Acquisition, 3. Registration, 4. Point Creation, 5. Model Creation, 6. Model (Mesh) Compression, and 7. Texture creation. Multiple modifications were elaborated in [Ferk04], [Lebe07], [Klei09], where even "ontological scales" appear and from where the evaluation [Mose08] for virtual Berlin [VirB09] is inspired. MS Virtual Earth (renamed to Bing Maps later) workflow was described in [Lebe07] as: 1. Surface Point Cloud, 2. Orthorectified Image, 3. Classification Map, 4. Bare Earth Topography, 5. 2.5D Textured Buildings. There are also experiments with procedural cyber city creation which can be used for less important city parts

or in computer games where the exact model is not necessary. The goal of virtualization can be formulated as converting space into places, where place is defined by Christian Norberg-Schulz as “dynamic unity of architecture, population, and interactions among them”. There are three levels of quality for virtual places [Came07, s. 337]: 1. Visualization virtual places, 2. Activity-based virtual places, and 3. Hermeneutic virtual places – culturally coded places where one can hide himself, identify with, own or collect cultural objects (in our case visions, presentations, opinions). The fundamental double-book on semiotics for virtual reality is Virtual Space [Qvor01] and Virtual Interaction [Qvor02], whereas the VR technology seems to be best taught in [Guti08]. The alternatives for W3C Semantic Web initiative are represented by digital libraries, e.g. Europeana [Euro09]. The quality measure for virtual museums visits formalizing the interestingness by time spent can be found in [Came07], but a specialized cyber city reference and a generally accepted measure of the quality of virtual museums is still missing. Obviously, the (low-level) geometric and radiometric errors in subspaces of a standard 8D  $(x, y, z, t, r, g, b, \alpha)$  state space can be evaluated using standard measurement or estimation methods. The complexity in the field is discussed e.g. in [Zara02]. The cyber city initiative resulted into a fast growing international network around the CityGML portal [City12] and one of the first CityGML modeling tools was Toposcopy [Gron08]. “*CityGML is a common information model and XML-based encoding for the representation, storage, and exchange of virtual 3D city and landscape models. CityGML provides a standard model and mechanism for describing 3D objects with respect to their geometry, topology, semantics and appearance, and defines five different levels of detail. Included are also generalization hierarchies between thematic classes, aggregations, relations between objects, and spatial properties. CityGML is highly scalable and datasets can include different urban entities supporting the general trend toward modeling not only individual buildings but also whole sites, districts, cities, regions, and countries*” [City12]. This seems to be complete enough, but a city has a heritage layer, consisting of tangible and intangible parts, for their complete interoperability vocabulary refer to ISO standard [Crof05]. Recently, the heritage layer of Adelaide was released in May 2012, including: 1. heritage listed properties (State and local listings) and 2. 77 properties proposed for heritage listing as part of the City Heritage Development Plan Amendment. We discuss this layer later for the case of Bratislava and metadata semantics in MUVIS project.

### 1.3 Virtual Bratislava

Chronologically, the development of Virtual Bratislava model and related methods can be traced back in time through multiple academic projects over a time span of more than 10 years: MUVIS, Multidimensional urban visions (OPVaV-2008/4.2/01-SORO; 26240220009), Geometry Processing for Virtual Reality (VEGA 1/0763/09), Complexity of Geometric Algorithms for Realtime Rendering in VR (VEGA 1/3083/06), PM3Donline (AV 4/0023/05), EPUD (APVT-20-P05105), Natural Phenomena Visualization using Unstructured Grid (ASO SK-04-BA-010), STRAPAMO 18: MetropoVis, Virtual Heart of Central Europe (www.vhce.info, Culture 2000 n. 2003 – 1467/001/001 CLT CA12), Virtual Environments for WWW (VEGA 1/0174/03), Navigation and Cooperation in Virtual Environments – Virtual Bratislava (APVT 20-025502), Advanced Methods for Virtual Habitat (Aktion AT-SK No. 323-6/2003), Computer Graphics and Image Processing Applications (VEGA 1/7666/20), and Multimedia Historic Bratislava DVD (MDPT 456/131/2005). These group projects were solved in accordance with tens of dissertations, master and bachelor theses [Beha08], [Dušk09], [Feki07], [Majo09], [Varh09]. The complete list of all coauthors includes up to 200 names.

In this paragraph we recall selected experience and/or results from the above projects, described more in [AMVH03], [Ftac07], [PMZA08], [Ferk09]. The first online 3D Bratislava models were cultural heritage highlights at [VHCE09], optimized for IE (2004) [Ferk04], namely the Bratislava Castle, a National Cultural Monument and the well-known landmark or St.

Martin's Cathedral (also known as Coronation Church), a three-ships gothic church where 11 kings and 8 queens (including Mary Therese) were crowned between 1563-1830. Both memorials can be seen in Figure 2. The first Slovak virtual museum is specified in [Mrva07], [Ferk09] and published online [PMZA09]. As the real museum is in an old castle surrounded by a historic park, we also developed a method of park reconstruction using, to a certain extent, dendrologic data [SmHe08], [Ferk09]. Laser measurements were needed for the Bratislava castle well reconstruction. Combining real data and hypothetic lighting scenario, we reconstructed the interior of Chatam Sofer Memorial, presented at [VHCE09]. For Multimedia Historic Bratislava DVD [Ftac07], [Boro08] we experimented with sound gallery for presenting the emotional history highlights and with a matrix-like organization of digital assets – in one direction the memorials, city sights or themes and in the second direction, orthogonally to the first one, the output multimedia – photographs, videos, interactive 3D models. The navigation thus becomes intuitive and idiomatic in sense of [Coop95] and even elderly people just learning how to operate our novel multimedia kiosks can navigate quickly. The ideas from applied research project were combined with basic research findings – geometry processing using data-dependency [Toth06], mesh refinement [Noci07], specialized triangulations, false fundamental matrices for speeding-up epipolar reconstruction, extracting semantics from pictorial data [Šiku03], [Šiku06a], [Šiku06b], information visualization [Novo07], encrypting multimedia data, video segmentation [Čern06], image-based and real-time rendering methods, reconstruction quality [Samu08], [Lack09], streaming, guided tours planning, and empathic avatars [Stan09]. For presenting the past, we experimented with digital storytelling, which resulted into the discovery of LOD-stories [Pato10]. However, some problems remain open and the vision of a 3D Xerox, i.e. an automatic conversion of input data into a cyber-city or museum, requires much more efforts, ideas, and future work. For cyber-city internet presentation the real-time rendering in an online environment seems to be the crucial one.

## OUR APPROACH

We define our approach as **a cooperative creation and evaluation of possibilities in geometric-semantic domain**. It might seem natural to just adopt one of the existing PP GIS solutions, but the financial and legal situation in transforming countries differs heavily from established market economies. For short, there is neither legislative nor market prepared for cyber cities, virtual cultural heritage, digital libraries, or digitization of museum collections. The complete initiative in this segment comes from academy and EU funding. This is the reason behind the obvious gap between functional virtual Berlin, Graz, or Vienna, already possible as everyday professional tool of respective divisions at city municipalities, and the striving virtual Prague, Bratislava, Budapest, Warsaw, Petersburg or Moscow, depending on academic projects and their (usually underfed) budget.

We identify three major target groups in the MUVIS project – authors, specialists, and public. Each of these groups comes with a different motivation, different skills and different information technology available. For example the latter are not well prepared for using modern information technology tools (e.g. we had to develop special urban reconstruction tutorials in Slovak for our own students [Ona07]). Wide public audience will share the MUVIS visualization and in given cases it will participate on urban planning forum. No special education is assumed and we can't count on a powerful hardware being used on their side either. These factors limit the amount of their active participation on creating or modifying the virtual space. The authors, on the other side, have the full access (passive and active) to the digital content and provide both the virtual working ground for the other two target groups and the administration of the project itself. They also maintain the database and develop future MUVIS version. The last group – the specialists – represent a force in the urban planning, coming either from the municipal administration domain or from the professional domain, such as e.g. architects, real estate developers etc. This

group has a presumably higher level of experience than the general public yet still has not a limited access to the underlying digital content.

MUVIS cross-platform functionality necessarily covers file and database management, search and navigation in space, time, or semantics, calibrating, filtering and storage, versioning, urban database editing, multimedia presentation of ideas, feedback, comments, forum and voting subsystems for given localities. We combine two architectures – scene graph and semantic database to certain extent. Scene graph architecture supports the geometric criterion for visualization part. On the other hand, the urban database has to be constructed with respect to semantics. For possibly distributed memory system for preservation and storage of enormous datasets we take into account Bigtable [Chan06], proven in multiple similar projects, e.g. web indexing or Google Earth [GooE09].

The project development is subdivided into the design and development of three conceptually separate fields of functionality – a server-side application handling the storage, index and retrieval of digital content, an active-access providing client application (editor), and a passive-access client application (viewer).

The digital content used in our project is rooted in a 4D domain and extended by semantic relations between objects, by multidimensional object attributes and by multimedia content documenting the modeled places from an empathic point of view. The created database offers creating arbitrary and abstract relations through semantic triplets, thus supporting a higher-level knowledge built above the raw city model. The client-server protocol is open and platform-independent which creates opportunities for future extensions and involvement of other domain experts, such as statisticians, sociologists, ecologists and many others.

The editor is partly built upon our previous works on effective presentation of urban data and is being extended to facilitate both technological improvement, e.g. in the form of forming relations and higher-level semantics, and technical improvement, e.g. by introducing vegetation or variable lighting conditions.

The viewer development forks into producing a high-quality viewer oriented on the specialists and technically experienced public and a medium-quality viewer offering less options in both interaction and visualization but being more accessible to the wide audience. Thus, in the end, each of the user groups will be provided with tools to satisfy their needs without being bothered with excessive or overwhelming options or requirements. Each of them uses its own conveying technology; the high-quality viewer is based around our Effective Presenter for Urban Data [Samu08] and uses a GPU-accelerated client-side web object, while the medium-quality viewer uses Adobe FLASH technology which is available to the wider audience for the price of simpler and less detailed visualization.

As the specification of these modules is not open for public yet, we hope to present them in detail in one of our future publications.

We cooperate with EUROSENSE Slovakia, contributing with preprocessed aerial photos in the urban area shown in Figure 2. The detailed project requirements and functional specification take into account recent findings and they will be tested both with the full urban model and respective target groups within the case study Petržalka.

## **RESULTS**

Since the project start in September 2009, we built the geometric model first. Data, tools, and methods from previous projects [Ferk04], [Boro07], [Boro08] were either adopted or under development to meet new requirements. Thinking about MUVIS in terms of cooperative creation and evaluation of possibilities in geometric-semantic domain, neither geometric nor semantic aspect was not significantly reduced in given application area. This is why we required

multidimensional attributes or metadata beyond the 3D/4D spatial domain. Previous version of Virtual Bratislava model represented a cyber-city heavy model, available on DVD only. Microsoft® Virtual Earth™ is a geospatial mapping platform for layered data for given location [MSVE08], [WIVE08]. Google Maps is both service and technology [WiGM08], related to the virtual globe of Google Earth [GooE08], [WiGE08] and even extending to the outer space. Both global projects have limited use and precision and they simulate mainly flyover options and exploit satellite and aerial photos of Earth. Our previous project [Ftac07] can be considered as an analogy to Google Earth. The challenging task of online browsing or even editing higher precision urban models is done in Virtual Old Prague [VirP09] or Virtual Berlin [VirB09] by downloading data and/or viewer. MUVIS aims to offer an acceptable online solution like Virtual Adelaide [Adel12]. The model already includes the virtual vegetation and an inserted urban vision – visualization of one of multiple not really built alternatives of the ice hockey stadium for the World Hockey Championship in Bratislava 2011.

## 1.4 MUVIS DATABASE SERVER

MUVIS Database Server is the database backend for all MUVIS clients. We have developed client-server network protocol independent of internal client graphics and data file formats. At the moment of writing, MUVIS clients use COLLADA format as a 3D models carrier together with appropriate file formats for multimedia (e.g. JPEGs for pictures). Administrator of the database is able to manage these file formats. Data are then obtained accordingly to their purpose: any entity that can be time- and geo-referenced (3D building models, panoramas, photographs taken by tourists, etc.) is handled via its reference (point in time and space) and a set of attributes. Attribute list is maintained by administrator, who assigns privileges for reading/writing the attribute values (e.g. users can name owners of house models they built). Database entities are organized in four ways:

- 1) entity can be georeferenced, thus accessible by its space/time reference,
- 2) entities can be organized into separate layers (e.g. layer for terrain, buildings, vegetation, traffic or other infrastructure),
- 3) two or more entities can be assigned into “relation” (e.g. all buildings in student campus can form one relation),
- 4) there is a semantic hierarchy of entities available. Entities are organized into semantic tree, which usually represents administrative division of the underlying city (city is divided into districts, districts are divided into streets, streets are divided into lots, etc.), however the exact semantics is precisely defined by the administrator.

MUVIS Server is able to retrieve information based on search criteria combined from geo-referencing intervals (axis-aligned bounding boxes), layers, relations, semantics and attribute values. Only users authorized by administrator are allowed to write new or edit existing entities.

## 1.5 MUVIS DATA

We divide data into three main categories: 3D data (ortho and terrestrial textured buildings), multimedia (text, videos, images, panoramas) and attributes. In the layer of 3D data we have obtained original data from Eurosense company. These data need to be refined and retextured due to consistency. After these steps 3D data from center of model and some of the most important objects were retextured by terrestrial textures. We need to photograph about 2500 photographs for selected 105 objects, and we prepared about 460 textures. We also prepared semitransparent images for vegetation objects and 4 3D models of buildings, which user can add into the system.



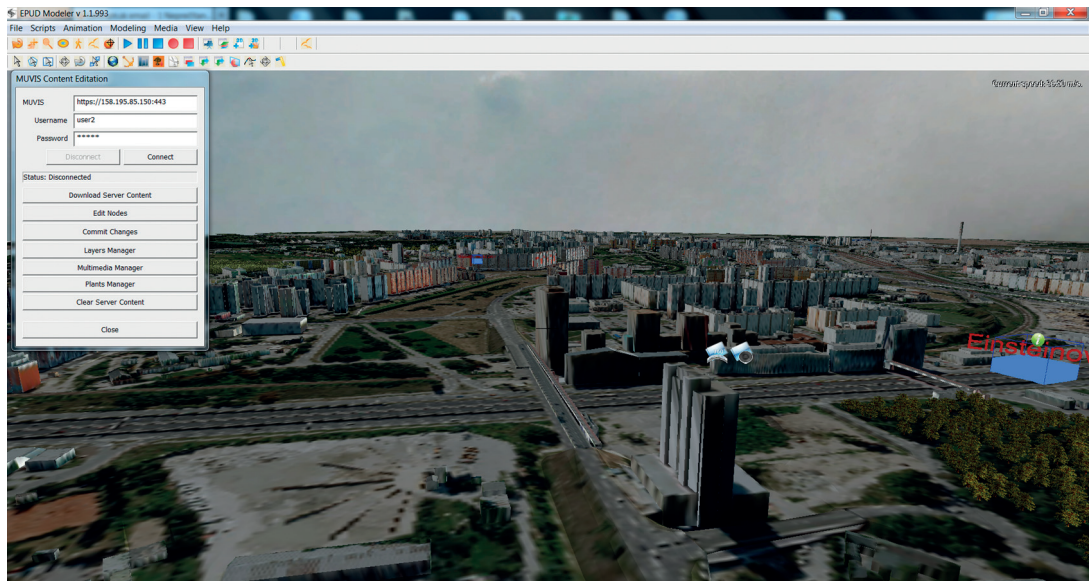
We also prepared the multimedia files consist of about 10 text files, 200 photographs, 4 audio files, 20 panoramas and 9 videos.

We present attributes in the 3D model via text information based on INSPIRE attributes model, which consist from different categories assigned to 3D objects in the scene. We present them as the information in the table.

## 1.6 MUVIS EDITOR

We were working on the complex application (Figure 5) for viewing and editing content of the MUVIS project. Therefore our work consists of two major parts, modeling system and viewing application.

These parts have some common parts, like communication system with server and rendering system. In the modeling part of project, we created standalone application that is capable of preparing data, storing data and rendering data. In the preparation phase, user can use external object model and import it inside system, the do some minor transformation with object. Special tools are dedicated to work with objects representing vegetation, buildings and terrain, and also for preparation of all data for easy and fast rendering. As additional information inside virtual world, modeler application can insert several types of multimedia like texts, picture, panoramas or sounds into scene attached to several objects. Prepared data are then uploaded in efficient way to MUVIS server. Viewer application is mainly used for efficient obtaining data from MUVIS server and for its displaying. We prepared caching system for optimization of download process. Objects are displayed on the screen immediately after download and processing of the object is finished. We implemented fast rendering system for displaying large virtual scenes with many objects. We also include several image enhancing effects. As additional form of rendering, this application can show multimedia data.



Viewer application can be used as standalone application as well as plugin inside web browser, where plugin can cooperate with browser layer.

**Figure 3:** MUVIS editor with 3D model of Petržalka and Multimedia assets.

We have developed an easy to use graphical user interface (GUI) to insert (and interact with) 3D models in a virtual urban environment. It has capability to add a high resolution 3D model and also its low resolution alternative, which is used in the Flash version of EPUD viewer. This GUI also allows to edit multiple objects at once.

Another GUI we developed for EPUD modeler is for quickly planting a big number of trees, plants, etc.. Even any 3D model can be used instead of vegetation. User have to just draw an arbitrary polygon to mark the area where he wants the vegetation (even non-convex one) then set a vegetation type (e.g. a type of tree, or plant) and finally set a height and density (how dense these trees should be placed to each other) and then the EPUD modeler places 3D models of the vegetation on the marked area.

Framework used for GUI is wxWidgets, which is multiplatform, so all the user interfaces can be easily ported to other platforms like Linux.

## 1.7 MUVIS VIEWER

Both web based solutions, the EPUD viewer and Flash based player, are embedded in a operating web page to use our solution on Internet. The user can choose which version of player he wants. The page is responsible for common parts as for user login, registration, working with layers etc., which are independent of the player. Therefore it provides one interface for the client no matter which player is presented. However it uses two different protocols to communicate with the EPUD viewer and the Flash player. On one hand the operating web page have to control the player and transfer the requests from the user to the player. And on the other hand he page is also responsible for responses on player requests. If the player requests to show multimedia in external environment, the operating page will process the request and present the external media as part of the HTML.

The purpose of the implemented Flash-based viewer is to bridge the technological gap between general public and usual GIS systems. Our goal was to introduce a solution that establishes a reasonable trade-off between ease of use and functionality. The choice of Adobe Flash technology as the platform for the viewer stems from the combination of the high percentage of Flash player installations across personal computers and the availability of hardware-accelerated 3D graphics. Introduced in Flash Player 11, the Stage3D API largely erased the former abysmal difference between 3D performance of desktop applications and rich internet applications. The older competing technologies (VRML, X3D) are now obsolete and the upcoming web-standard WebGL was not mature enough yet for a reliable implementation of the functionality required by MUVIS.

The final implementation takes advantage of the Away3D library that supports Stage3D and provides sufficient support for data import in form of Collada files. We considered other available solutions (e.g. Alternativa3D) for Stage3D implementations but no other provided the necessary functionality and support.

Despite the high performance of Flash's Stage3D, extensive optimization still has to be made. Mostly on the memory part, where a combination of local storage, CPU RAM and GPU RAM was devised that balances the RAM limitations against the user-unfriendly object download. The displayed objects are also chosen from a limited surrounding of the camera position to further decrease the memory demands (Our full test case model counts for as much as 4GB of Flash data.) A portion of the unused data is locally cached to prevent repetitive HTTP requests and to shorten the download time during the operation of the Flash viewer.

## CONCLUSION AND FUTURE WORK

MUVIS (Multidimensional Urban Visions) is a three-year applied research project for creating an extensible platform that will support online participatory urban planning and related

multidimensional visualization. MUVIS will support and initiate public discussion and dialogue between the people, the local authorities, and the real estate investors. We use Virtual Petržalka as a place to demonstrate our efforts in a real-world case study, a place to support creation and visualization of the current state and the future visions. MUVIS offers a state-of-the-art technology solution, transfers the ideas from academy to practice and attempts to influence the future development of our cities in the best way possible.

We plan to experiment using MUVIS with MARS [Mars12], a multi-touch augmented reality system that uses two displays – one with multi-touch capability and second with augmented reality display. We especially devised the combination of these two visual spaces in a way that is seamless for the user when shifting the attention between them. Joint presentation of 2D and 3D data is a frequent situation in architecture, urban development or real estate business. Our experience shows that building a mental model which merges two-dimensional floor plans and three-dimensional visualizations is not an easy task for the average user. The interactivity and the feel of direct manipulation improve this situation. We propose a usage scenario where the table holds the neighborhood map, floor plans or geometry plans from the land register. The focused 3D model of the building is added to the augmented view. Basic user interaction such as panning and zooming can easily be performed in the table space.

This scenario can also be adapted for similar needs where the ground plans are combined with a 3D object geo-located within the 2D environment. These include: archaeology, geology or crime investigation.

All of them can also benefit from the secondary context where a different view of the ground plane can be displayed: satellite map, weather map, etc...

From the point of view of the widest target group, our intention is to enable people not only in poor Petržalka to be consciously and interactively participating with their contribution to the future of their own environment. We hope that our model of cooperation, our workflow, and project results might be inspiring within the arising information society.

The public and experts were involved into the process of application design through the usability testing and in the future, they will use the application as the participatory tool for enhancing the process of decision making in city development.

## ACKNOWLEDGEMENTS

Project MUVIS – Multidimensional urban visions – was supported from a structural grant scheme OPVaV-2008/4.2/01-SORO; ITMS 26240220009 in Slovak Republic. The authors of this paper would like to express sincere thanks to a project partner EUROSENSE Slovakia for aerial data acquisition and preprocessing. We thank to our colleagues at Comenius University for their support and fruitful discussions.

## References:

- [Aarh98] UNECE Aarhus Convention website. 1998. Online at (December 12, 2009.)
- [Adel12] Virtual Adelaide Portal. <http://www.adelaidecitycouncil.com/development/3d-city-model/>
- [Adzh10] ADZHIEV, V., OSSIPOV, A., PASKO, A. Multidimensional shape modeling in multimedia applications. KARMOUCH, A. ed. MultiMedia Modeling: Modeling Multimedia Information and Systems. ISBN 981-02-4146-1, pp.39-60. Singapore: World Scientific 1999.
- [Agar10] AGARWAL, S. et al. Reconstructing Rome. *Computer*, vol. 43, no. 6, pp. 40-47, 2010.
- [AMVH03] *Advanced Methods for Virtual Habitat*. 2003. Online at <http://www.sccg.sk/~projects/amvh> (December 12, 2009.)
- [Bang07] BANGS, H. 2007. *The Return of Sacred Architecture*. Czech translation. *Návrat posvátné architektury*. Cesky Tesin: Kma 2008.

- [Beha08] BEHAL, D. 2008. *Technológia streamingu pre virtuálne múzeum*. MSc. thesis. Bratislava: FMFI UK 2008.
- [Bern01] BERNERS-LEE, T. et al. 2001. The Semantic Web. *Scientific American*. Online at <http://www.sciam.com/article.cfm?articleID=00048144-10D2-1C70-84A9809EC588EF21>, May 2001. (December 12, 2009.)
- [Boro08] BOROVSKÝ, P. – SAMUELČÍK, M. – NOVOTNÝ, M. – STANEK, S. – LACKO, J. – FERKO, A. 2008. 3D Multimedia Historic Bratislava. *CORP 2008: Urban Planning and Regional Development in the Information Society*. Schwechat-Rannersdorf: Competence Center of Urban and Regional Planning, 2008. – ISBN 978-39502139-5-9. – pp. 525-530.
- [Came07] CAMERON, F. – KENDERDINE, S. eds. 2007. *Theorizing Digital Cultural Heritage*. ISBN 0-262-03353-4. Cambridge: MIT Press 2007.
- [Chan06] CHANG, F. et al. 2006. Bigtable: A Distributed Storage System for Structured Data. *OSDI'06: Seventh Symposium on Operating System Design and Implementation*. Seattle, WA, November, 2006.
- [City12] CityGML Portal Online at <http://www.citygml.org/index.php?id=1523>. (December 12, 2012.)
- [Čern06] ČERNEKOVA, Z. – PITAS, I. – NIKOU, C. 2006. Information theory-based shot cut/fade detection and video summarization. *IEEE Transactions on Circuits and Systems for Video Technology*, vol. 16, no.1, pages 82-91, January 2006.
- [Coop95] COOPER, A. 1995. *About Face. The Essentials of User Interface Design*. ISBN 1-56884-322-4. Foster City: IDG Books 1995.
- [Crof05] CROFTS, N. et al. eds. 2005. *Definition of the CIDOC Conceptual Reference Model*. Online at [http://cidoc.ics.forth.gr/official\\_release\\_cidoc.html](http://cidoc.ics.forth.gr/official_release_cidoc.html), June 2005. (December 12, 2009.)
- [Dušk09] DUŠKOVÁ, E. 2009. *Virtuálna Kremnica : Virtual city presentation*. Bratislava : FMFI UK, 2009. URL: <http://kremnica.duskova.sk/> [cit. 2009-08-27].
- [Euro09] Europeana Portal. 2009. Online at <http://www.europeana.eu/portal/>. (December 12, 2009.)
- [Feki07] FEKIAČOVÁ, M. 2007. *Múzeum bratislavských múzeí*. Bc. thesis. Bratislava: FMFI UK 2007.
- [Ferk04] FERKO, A. – MARTINKA, J. – SORMANN, M. – KARNER, K. – ZARA, J. – KRIVOGRAD, S. 2004. Virtual Heart of Central Europe. *CORP 2004*. Vienna: TU Wien 2004. [www.corp.at](http://www.corp.at).
- [Ferk09] FERKO, A. et al. 2009. *Narodny program virtualizacie muzei*. Banská Stiavnica: DMZ 2009.
- [Fers02] FERSCHIN, P. et al. 2002. The City as a Process in Time and Space. Online at <http://80.110.251.60/corp/archiv/papers/2002/>
- [Ftac04] FTACNIK, M. – Borovský, P. – Samuelčík, M. 2004. Low Cost High Quality 3D Virtual City Models. [www.corp.at](http://www.corp.at).
- [Ftac07] FTÁČNIK, M. et al. 2007. *Multimediálna historická Bratislava*. Projekt MDPT 456/131/2005. ISBN 978-80-89186-15-0. EAN 9788089186150. Bratislava: Knižničné a edičné centrum FMFI UK Bratislava 2007.
- [Gave98] GAVENTA, J. 1998. Towards Participatory Governance: Assessing the Transformative Possibilities. Pp. 25-42 in HICKEY, S. – MOHAN, G. eds. 2004. *From Tyranny to Transformation*. London: Zed Books 2004.
- [GooE09] *Google Earth*. Online at <http://earth.google.com/>. (December 12, 2009.)
- [Gron08] GRONEMAN, A. – ZLATANOVA, S. 2008. Toposcopy: A Modeling Tool for CityGML.
- [Grög08] GRÖGER, G. et al. 2008. OpenGIS CityGML Implementation Specification. URL: <http://www.opengeospatial.org/standards/citygml> (December 12, 2012.)
- [Guti08] GUTIÉRREZ, M. A. et al. 2008. *Stepping into Virtual Reality*. ISBN: 978-1-84800-116-9.
- [Huys05] HUYSEN, A. 2005. *Prítomnosť minulého. Urbánne palimpsesty a politika pamäti*. ISBN 80-968819-8-8. Slovak translation. Bratislava: Vydavateľstvo Ivan Štefánik 2005.



- [INSP09] *INSPIRE Infrastructure for Spatial Information in the European Community*. 2010. Online at (November 24, 2012.)
- [Jokl08] JOKLOVA, V. 2008. *E-learning a informačno-komunikačné technológie v urbanizme a architektúre*. Bratislava: FA STU 2008.
- [Kyem09] KYEM, P.A.K. – SAKU, J.C. 2009. Web-Based Gis and the Future of Participatory GIS Applications within Local and Indigenous Communities. *EJISDC* (2009) 38, 7, 1-16. *The Electronic Journal on Information Systems in Developing Countries*. Online at <http://www.ejisdsc.org>. (December 12, 2009.)
- [Lack09] LACKO J. – FERKO A. 2009. Techniques of Reconstruction of 3D Scenes. *Aplimat* 2009. ISBN 978-80-89313-31-0. – S. 431-437
- [Lack10] LACKO J. et al. 2009. *Innovating Multidimensional Urban Visions*. Vienna: Real Corp 2010.
- [Lebe00] LEBERL, F. W. et al. 2000. Urban site models: Accurate, detailed, rapid and inexpensive. Pp. 201-214 in [Leon00].
- [Lebe07] LEBERL, F. W. 2007. *Internet-inspired Urban Models*. Comenius University lecture. Bratislava 18. 10. 2007.
- [Lenh06] LENHART, Z. 2006. *Definice CIDOC CRM*. Czech translation of [Crof05]. Online at <http://www.snm.sk/cemuz/dokumenty/crm/Uvod.htm#terminology>. (December 12, 2009.)
- [Leon00] LEONARDIS, A. et al. 2000. *Confluence of Computer Vision and Computer Graphics*. NATO Science Series. Dordrecht: Kluwer Academic Publishers 2000.
- [Lync60] LYNCH, K. 1960. *Image of the City*. Cambridge: MIT Press 1960.
- [Klei00] KLEIN, R. et al. 2009. *Efficient Rendering of Landscapes*. Project page. Online at <http://cg.cs.uni-bonn.de/en/projects/efficient-rendering-of-landscapes/>. (December 12, 2009.)
- [Majo09] MAJOR, V. 2009. *Múzeum hodín*. Bakalárska práca. Bratislava: FMFI UK 2009. [online] At (September 15, 2009.)
- [Mars12] NOVOTNY, M. et al.: *Mars: Multi-Touch Augmented Reality System and Methods of Interaction with It*. In: *Aplikácie informačných technológií*. – ISSN 1338-6468. – Roč. 1, č. 2 (2012), s. 30-36.
- [Mesz06] MÉSZÁROSOVÁ, K. 2011. *Fraktály v krajinej štruktúre*. (Edition of scientific works; Book no.98). Bratislava: STU v Bratislave SvF, 2011. ISBN 978-80-227-3451-6.
- [Mose08] MOSER, S. et al. 2008. Context Aware Terrain Visualization for Wayfinding and Navigation. Vol 27 (2008), No 7. *Pacific Graphics* 2008. Online at <http://cg.cs.uni-bonn.de/docs/publications/2008/moeser-2008-context.pdf>. (December 12, 2009.)
- [Mits69] MITSCHERLICH, A. 1969. *Die Unwirtlichkeit unserer Städte. Anstiftung zum Unfrieden*. Suhrkamp 1969. Slovak translation. *Nehostinnosť miest. Pobádanie k nepokoju*. Bratislava: Pallas 1971.
- [Mrva07] MRVA, M. – FERKO, A. 2007. Považské múzeum 3D online. *Pamiatky a múzeá*, Č. 3 (2007), s. 30-33.
- [MSVE08] *Microsoft® Virtual Earth™*. Online at <http://msdn.microsoft.com/en-us/library/bb545001.aspx>. (December 12, 2009.)
- [Mus10] MUSILOVA, M. 2010. *Keltsky kniežaci palac. (Celtic Castle)*. Literarny tyzdennik. February 24, 2010. pp. 8-9. Bratislava: VSSS 2010.
- [Noci07] NOCIAR, M. 2007. *Taxonómia prístupov k úrovniam detailu*. Proceedings of Symposium on Computer Geometry, Vol. 16. – Bratislava : Slovak University of Technology, 2007. – ISBN 978-80-227-2734-1. – pp. 68-77
- [Norb81] NORBERG – SCHULZ, Ch. 1981. *Genius loci, k fenomenologii architektúry*. ISBN 80-207-0241-5. Czech translation from London 1981 edition by Academy Editions. Praha: Odeon 1994.
- [Nov07] NOVOTNY, M. 2007. *InfoVis*. PhD. thesis. Bratislava: FMFI UK 2006.



- [Ona07] ONAČILOVÁ, D. 2007. Urban reconstruction tutorials. In Slovak. [online]. [cit. 2009-09-14]. [online] <http://www.sprite.edi.fmph.uniba.sk/~dankao/>.
- [Pat10] PATOPRSTA, E. et al. 2010. LOD-stories for Virtual Museum. Submitted to Computational Aesthetics 2010.
- [PMZA08] Portal *Považské múzeum Žilina*. In Slovak. [online] [www.pmza.sk](http://www.pmza.sk) (September 15, 2009.)
- [Qvor01] QVORTRUP, L. ed. 2001. *Virtual Interaction: Interaction in Virtual Inhabited 3D Worlds*. ISBN 1-85233-331-6. London: Springer 2001.
- [Qvor02] QVORTRUP, L. ed. 2002. *Virtual Space: Spatiality in Virtual Inhabited 3D Worlds*. ISBN 1-85233-516-5. London: Springer 2002.
- [Renn95] RENN, O. et al. 1995. *Fairness and Competence in Citizen Participation, Evaluating Models for Environmental Discourse*. Dordrecht: Kluwer 1995.
- [Roth00] ROTH, G. 2000. Building Models from Sensor Data. Pp. 87-104 in [Leon00].
- [Sali03] SALINGAROS, N.A. 2003. Connecting the Fractal City. Keynote speech. 5th Biennial of towns and town planners in Europe. Barcelona 2003. Online at <http://zeta.math.utsa.edu/~yxk833/connecting.html>. (December 12, 2009.)
- [Samu08] SAMUELČÍK, M. et al. 2008. Princípy kvalitnej vizualizácie v reálnom čase. CD ROM. *MVPD 2008*. Bratislava: STU 2008.
- [SmHe08] SMOLEŇOVÁ, K., HEMMERLING, R., 2008. Growing virtual plants for virtual worlds. In *Proceedings of Spring Conference on Computer Graphics SCCG '2008*, vol. 24, p.77-84.
- [Stan09] STANEK, S. 2009. Simple user interface with empathy for virtual cultural heritage. *The 17-th International Conference on Computer Graphics, Visualization and Computer Vision 2009 (WSCG 2009)*. *The Journal of WSCG*. ISSN 1213-6972 (hardcopy), ISSN 1213-6964 (CD ROM version), ISSN 1213-6980 (on-line version) February 2-5, 2009, Pilsen, Czech Republic.
- [Šiku03] ŠIKUDOVÁ, E. – GAVRIELIDES, M. A. – PITAS, I. 2003. Automatic identification of portraits in art images databases. *DELOS-NSF workshop on multimedia contents in digital libraries*, 2003. Chania, Grécko.
- [Šiku06a] ŠIKUDOVÁ, E. – GAVRIELIDES, M. A. – PITAS, I. 2006. Extracting semantic information from art images. *Proceedings of the International Conference on Computer Vision and Graphics*. *Edícia Computational Imaging and Vision*, vol. 32, Springer-Verlag New York, Inc., 2006, pp. 394-399.
- [Šiku06b] ŠIKUDOVÁ, E. 2006. On some possibilities of automatic image data classification. PhD. thesis. Bratislava: FMFI UK 2006.
- [Toth06] TOTH, Z. 2006. Data-dependent Triangulation. *CESCG 2006*.
- [Varh09] VARHANÍKOVÁ, I. 2009. *Virtuálne Bánovce nad Bebravou*. MSc. thesis. Bratislava: FMFI UK 2009.
- [VirB09] *The 3D Model of Berlin on Google Earth*. Online at <http://www.virtual-berlin.de>. (December 12, 2009.)
- [VirC09] *Virtual Cities Directory*. Online at <http://www.intoronto.com/cities/home.html> (December 12, 2009.)
- [VirP09] *Virtual Old Prague*. Online at <http://sgi.felk.cvut.cz/vsp>. (December 12, 2009.)
- [Vitr09] VITRUVIUS, M.P. 2009. *The Ten Books on Architecture. De architectura*. Online at <http://penelope.uchicago.edu/Thayer/E/Roman/Texts/Vitruvius/home.html>. (December 12, 2009.)
- [VHCE09] *Virtual Heart of Central Europe*. Online at <http://www.vhce.info> (December 12, 2009.)
- [Wieg08] WIEGERS, K.E. 2008. *Software Requirements*. Redmond: Microsoft Press 2003. Czech translation. *Požadavky na software*. Brno: Computer Press 2008.
- [WiGE08] *Google Earth article*. Online at [http://en.wikipedia.org/wiki/Google\\_Earth](http://en.wikipedia.org/wiki/Google_Earth). (December 12, 2009.)

- [WiGM08] *Google Maps article*. Online at [http://en.wikipedia.org/wiki/Google\\_Maps](http://en.wikipedia.org/wiki/Google_Maps). (December 12, 2009.)
- [WiVE08] *Virtual Earth article*. Online at [http://en.wikipedia.org/wiki/Virtual\\_Earth](http://en.wikipedia.org/wiki/Virtual_Earth). (December 12, 2009.)
- [Zara02] ZARA J. 2002. On the Complexity of Web-based Presentations of Large Urban Scenes. *In: East-West-Vision 2002*. Wien: Österreichische Computer Gesellschaft, 2002, pp. 99-108. ISBN 3-85403-163-7.

---

**Matej Novotný**, mnovotny@sccg.sk, **David Behal**, behal@sccg.sk, **Peter Borovský**, borovsky@sccg.sk, **Zuzana Černeková**, cernekova@sccg.sk, **Andrej Ferko**, ferko@sccg.sk, **Martin Florek**, florek@sccg.sk, **Ján Lacko**, lacko@sccg.sk, **Martin Samuelčík**, samuelcik@sccg.sk, **Stanislav Stanek**, stanek@sccg.sk, **Elena Šikudová**, sikudova@sccg.sk

# Instructions for authors

---

- Articles submitted for publication will be accepted only as Word document (.doc or .docx) sent to e-mail address of managing editor (vvv.esr@gmail.com).
- Range: Articles and papers in 20 standard pages, essays in 10 standard pages, reviews and gleanings in 5 standard pages (on one page A4 is possible to type 1800 characters including spaces)
- Text should be written as plain text (text font Times New Roman, size 12, without hyphenation and justification).
- If you need you can use bold, italic or underline
- If you use notes in the text, place the note on the same page.
- Quote following general rules (STN ISO 690)
- The author is responsible for the formal and scientific side of the article.
- In our journal is not possible to public the article already published in other journal.
- The editorial board reserves the right to edit the headline of the contribution, to make stylistic, grammar, language and graphical emendations and decide on its inclusion into specific numbers, and rubrics
- The editorial board reserves the right to refuse the contribution.
- Structure of the paper as follow

## **TITLE OF THE ARTICLE in ENGLISH**

Title of the article in the other language

First and last name without academical degree; in the case of multiple authors, separate names with commas

**Abstract** in English (6-10 lines)

**Key words** in English (3-7 key words)

Key words in other language (optional)

## **The article**

If you want the pictures to be nice and readable, add the bigger and better quality pictures at the end of the articles with the same numbering as in the article.

Pictures, tables, math formulas will be centered. Please use Fig. 1, Tab. 1,..to label the objects in the article.

## **Citations and References**

In our journal we prefer to quote the citations by author (not by the reference number), so please try to follow this style (Editors, 2011).

Editors (2011). *How to create an article to publish it in ITA*. Retrieved July 19, 2011, from [http://www.v-v-v.sk/index.php?option=com\\_content&view=article&id=78&Itemid=497&lang=en](http://www.v-v-v.sk/index.php?option=com_content&view=article&id=78&Itemid=497&lang=en)

**About Author(s)** brief information about author (optional)

(Add name with academical degrees)

## **Contacts**

Name of the author with titles

Address of the institute

Email address:









May 28-30, 2014  
Smolenice castle  
Slovakia

#### CONFERENCE CHAIR

Diego Gutierrez  
Zaragoza

#### INVITED SPEAKERS

will be announced later

#### IMPORTANT DATES

Paper submission:  
March 2, 2014

Notification of acceptance:  
April 16, 2014

Camera ready:  
April 23, 2014

Posters:  
March 2, 2014

Notification of acceptance:  
April 16, 2014

Camera ready:  
April 23, 2014

[www.sccg.sk](http://www.sccg.sk)

[sccg2014@sccg.sk](mailto:sccg2014@sccg.sk)



CALL FOR PAPERS

[www.sccg.sk](http://www.sccg.sk)

# SPRING CONFERENCE ON COMPUTER GRAPHICS (SCCG 2014)

Comenius University Bratislava  
and  
The Slovak Society for Computer Science

invite you to probably the oldest regular meeting of computer graphics community in Central Europe.  
The SCCG attempts to cover all interesting projects from computer graphics, image processing and applications.

#### CONFERENCE TOPICS INCLUDE

- rendering
- geometry modeling
- natural phenomena
- visualization
- animation
- image processing
- computer vision
- computational photography
- applications
- fabrication

The philosophy of SCCG is to put together top experts with young researchers in CG and to support a good communication channel for East-West exchange of prospective ideas.

#### SUBMISSIONS

We welcome scientific papers to be printed in the proceedings. We welcome posters covering your recent research work, late-breaking technical results and work in progress. These will be printed in the posters proceedings. You also have a chance to present your recent research results on rendering (previously published in another venue) to the full rendering audience and gain more visibility. Note that these posters will not appear in the posters proceedings.

Post-conference proceedings will be published by ACM Digital Library.

Three best papers, as appointed by the IPC, will also be published in Computer Graphics Forum journal.

Organizers:



SLOVENSKÁ  
INFORMATICKÁ  
SPOLOČNOSŤ

In cooperation with:

